

https://dspace.org/

Flashover performance of a rod-rod gap containing a floating rod under switching impulses with critical and near critical times to crest

Viljoen, Ryan Andrew

2009-03-23T10:13:01Z
http://hdl.handle.net/10539/6775

Downloaded from a DSpace repository. https://dspace.org/

FLASHOVER PERFORMANCE OF A ROD-ROD GAP CONTAINING A FLOATING ROD UNDER SWITCHING IMPULSES WITH CRITICAL AND NEAR CRITICAL TIMES TO CREST

Ryan Andrew Viljoen

A dissertation submitted to the Faculty of Engineering and the Built Environment, University of the Witwatersrand, Johannesburg, in fulfilment of the requirements for the degree of Master of Science in Engineering.

Johannesburg, June 2008

Declaration

I declare that this dissertation is my own, unaided work, except where otherwise acknowledged. It is being submitted for the degree of Master of Science in Engineering in the University of the Witwatersrand, Johannesburg. It has not been submitted before for any degree or examination in any other university.

Signed this ____ day of _____ 20__

_____

Ryan Andrew Viljoen

Abstract

The U-curves of five different test objects, three of which contain a rod floating object at different positions within the gap, are characterised. During the testing, a high speed camera was used to photograph the discharges. The results are compared to Rizk's theoretical model for determining the flashover voltage of gaps with floating objects are presented. It is concluded that the position of the floating object within the gap affects which discharge mechanism exists in each of the gaps. The effect that each discharge mechanism has on the flashover voltage and time to crest of the gap is shown. Time interval photographs are presented showing the formation of a discharge channel due to the streamer mechanism. In evaluating the high speed photographs it is seen that the extent of the branching of the discharge channel is a function of the time to crest of the applied impulse, more branching is evident for shorter times to crest.

Acknowledgements

I would like to acknowledge Dr. Ken Nixon and Prof. Jan Reynders as two invaluable mentors. I would like to thank Ken for his continued support, enthusiasm and drive in pushing me to achieve more than I thought capable. I would also like to thank Prof. Reynders for providing me with this opportunity and for his continued support and interest in the work.

To my parents who ultimately made all this possible through everything that they have provided for me. To my family and friends for their continued encouragement and support.

I would gratefully like to acknowledge the following organisations for their funding and support:

- Eskom through the Tertiary Education Support Programme (TESP).
- The National Research Foundation (NRF) for supporting the High Voltage research programme at Wits.
- The Department of Trade and Industry (DTI) for Technology and Human Resources for Industry Programme (THRIP) funding.

I would also like to extend thanks to the team at the High Voltage Laboratory at SABS-NETFA for all their work and assistance during the testing, without them the testing would not have run so smoothly.

Contents

Declaration **i**

Abstract **ii**

Acknowledgements **iii**

Contents **iv**

List of Figures **x**

List of Tables **xiii**

List of Symbols **xiv**

Nomenclature **xvi**

1 Introduction **1**

2 Background **4**

2.1 Breakdown process and voltage 4

2.1.1 Breakdown process 4

2.1.2 Breakdown voltage 6

2.1.3 Assumptions 6

2.2 Continuous leader inception voltage 7

2.2.1 Previous work 7

2.2.2 Expressions 8

2.2.3 Assumptions and limitations 10

2.3 Presence of a floating object 11

2.4 Scope of dissertation 12

3 Approach taken **13**

3.1 Problem statement 13

3.2 Objective 13

3.3 Overall approach taken 14

3.3.1 Position of floating object 14

3.3.2 Large scale experiment 15

3.3.3 Simulated model 16

3.3.4 Critical time to crest 16

4 Experiment **18**

4.1 Test facility 19

4.2 Test Equipment 19

4.2.1 Impulse generator 19

4.2.2 Voltage measurement 20

4.2.3 High speed photography 20

4.2.4 Current measurement 21

4.3 Test object 22

4.4 Test Procedure 25

5 Model simulation **26**

5.1 Overview 26

5.2 Model implementation 27

5.3 Streamer breakdown of primary gap 31

5.4 Model assumptions 32

5.4.1 Leader inception voltage 32

5.4.2 Potential of the floating object 32

5.5 Model observations 33

6 Comparison of Results and Discussion **35**

6.1 Experimental Test Results 35

6.1.1 75% Floating object position 38

6.1.2 25% and 50% Floating object positions 39

6.1.3 Velocity and impulse front time 39

6.2 Model Verification 41

6.2.1 Discussion of model 42

6.2.2 Comparison between measured and predicted results 44

7 High Speed Photography **46**

7.1 Processing 47

7.1.1 Image Manipulation 47

7.1.2 Orientation 48

7.1.3 Scale 48

7.2 Exposure Time 50

7.3 Interaction with floating object 50

7.3.1 Typical discharges 50

7.3.2 Discharge on tips of floating object 54

7.4 Channel formation 59

7.4.1 Floating object at 25% position 59

7.4.2 Floating object at 50% position 64

7.5 Branching and impulse front time 66

8 Conclusion and Recommendations **70**

8.1 Recommendations 70

8.2 Conclusion 71

A Complete Results **73**

B Calculation of Rizk's constant using Electric field simulation **77**

B.1 Introduction 77

B.2 Approach 77

B.3 Electric field modelling package 78

B.3.1 Rotational 2-D models in electro 78

B.3.2 Balanced and unbalanced mode 78

B.3.3 Parametric simulation 79

B.4 Simulation model 79

B.4.1 Model setup 79

B.4.2 Model properties 80

B.5 Approach to simulation 80

B.6 Validity of results 82

B.7 Simulation results and conclusion 82

C Implementation of Rizk's Model **84**

D Discussion on Current Measurement **87**

D.1 Introduction 87

D.2 Current measurement setup 88

D.2.1 Approach Taken 88

D.2.2 Implementation 88

D.3 Results and analysis 91

D.3.1 Waveform analysis 91

D.3.2 Power frequency spectrum analysis 92

D.4 Associated difficulties and suggested solutions 96

D.4.1 Resolution and shunt resistor value 96

D.4.2 Coupled noise 96

D.5 Conclusion 97

E Published Paper **99**

References **106**

Bibliography **108**

List of Figures

2.1 Recorded voltage waveform of a breakdown event with the different stages defined by Carrara & Thione (1976) labelled. 5

3.1 Diagram showing the test configurations. 15

4.1 Layout of the indoor laboratory. 18

4.2 Photographs of the test configuration. 23

5.1 Algorithm of model used to determine the U_{50} flashover voltage of a gap with a floating object present. 28

5.2 Diagram of rod-rod gap as implemented in the model. 29

6.1 U-curves plotted from the measured results. 36

6.2 Approximate leader velocity and measured U_{50} flashover voltage for 3.36 m rod-rod gap plotted as a function of time to crest. 40

6.3 Predicted U_{50} Flashover voltage calculated using Rizk's model, plotted against the length of the primary gap. 41

6.4 Leader and streamer inception voltages plotted for primary and secondary gaps. 43

7.1 Processing steps applied to high speed photographs. 48

7.2 Photographs showing the test object with the floating object at the three different positions using a longer exposure time. 49

7.3 Photographs showing typical discharges for each position of floating object. 52

7.4 Photographs showing further typical discharges for each position of floating object. 53

7.5 Photographs of the floating object at 25%: 57 μs front time using 25 μs exposure time. 55

7.6 Photographs of the floating object at 25%: 57 μs front time using 25 μs exposure time. 56

7.7 Photographs of the floating object at 50%: 25 μs front time using 100 μs exposure time. 57

7.8 Photographs of the floating object at 50%: 25 μs front time using 50 μs exposure time. 58

7.9 Series of photographs showing the formation of a discharge channel. 62

7.10 Series of enhanced photographs showing the formation of a discharge channel. 63

7.11 Photographs of the floating object at 50%: 25 μs front time using 100 μs exposure time. 65

7.12 Photographs of discharges with different front times. The photographs are of the 3.36 m rod-rod gap. 68

7.13 Enhanced photographs of discharges of different front times. The photographs are of the 3.36 m rod-rod gap. 69

A.1 Summary of the test configurations. 74

A.2 Plots of temperature, pressure and humidity measurements. 76

B.1 Test configuration model used for electric field simulation. 81

B.2 Constant k_0 plotted as a function of the primary gap length. 83

D.1 Different shunt resistors used for current measurement. 88

D.2 Current measurement setup circuit diagram. 89

D.3 Current measurement setup. 90

D.4 High speed photograph of a 3.36 m rod-rod gap subjected to an impulse with a front time of 70 μs. 92

D.5 Voltage and current waveforms from both withstand and breakdown events. 93

D.6 Unitised power frequency spectrum of the current waveforms. 94

D.7 Normalised power frequency spectrum of the current waveforms, with associated noise due to the impulse generator set to zero. 95

List of Tables

4.1 Temperature, pressure and humidity ranges measured during testing. 19

4.2 Test configuration dimensions. 24

4.3 Primary and secondary gap lengths for each test object configuration. 24

5.1 List of the potentials used in Rizk's model with a description. Note: All units are in kV. 30

6.1 Summary of critical times to crest and CFO for each test object. . . 37

6.2 Leader and streamer inception voltages for different air-gap lengths. 37

6.3 Comparison between measured and predicted flashover voltages for each floating object position. 45

A.1 Summary of measured results. 75

B.1 Conductivity and permittivity's of materials used in model. 80

List of Symbols

The principal symbols used in this dissertation are summarised below. The units are shown in square brackets and the first equation where the symbol is used is given.

U_{50}	50% flashover voltage [kV] , *Equation (2.1)*
U_b	Applied voltage at the instant breakdown occurs [kV] , *Equation (2.1)*
σ	Standard deviation (typically 5%), *Equation (2.1)*
U_{lc}	Leader inception voltage [kV] , *Equation (2.2)*
$\frac{V_0}{E_{cr}}$	Dimension constant (3.891 m for rod-type gaps), *Equation (2.2)*
E_s	Streamer electric field gradient [kV/m] , *Equation (2.2)*
R	Geometric constant [m] , *Equation (2.2)*
d	Length of air gap [m] , *Equation (2.3)*
h	Length of ground rod electrode [m] , *Equation (2.4)*
h_f	Length of final jump [m] , *Equation (2.5)*
E_s	Streamer electric field gradient (500 kV/m for rod-rod gaps) [kV/m], *Equation (2.6)*
l_z	Length of leader channel [m] , *Equation (2.7)*
$\triangle U_{lc}$	Voltage drop across leader channel [kV] , *Equation (2.8)*
d	Length of gap between the high voltage and ground electrodes [m] , *Equation (5.0)*

d_0	Length of floating object [m] , *Equation (5.0)*
d_1	Length of primary gap [m] , *Equation (5.0)*
h	Length of ground rod electrode [m] , *Equation (5.0)*
E_s	Streamer electric field gradient [kV/m] , *Equation (5.0)*
k_0	Geometric potential factor, *Equation (5.0)*
σ	Standard deviation (typically 5%), *Equation (5.0)*
U_{app}	Applied voltage at the high voltage electrode [kV] , *Equation (5.1)*
v_{lz}	Velocity of the leader channel [cm/μs] , *Equation (6.1)*
l_z	Length of leader channel in gap [cm], *Equation (6.1)*
t_{bf}	Time to breakdown [μs], *Equation (6.1)*

Nomenclature

CIGRÉ	International Council on Large Electric Systems (Conseil International des Grands Réseaux Électriques)
IEC	International Electrotechnical Commission
SABS	South African Bureau of Standards
NETFA	National Electrical Testing Facility

Chapter 1

Introduction

Power utilities successfully implement live line working techniques to maintain transmission line networks. Typical maintenance includes the repair or replacement of broken insulator strings on support towers. The benefit of live line working is that down time associated with maintenance is reduced since the line remains live for the duration of the work.

Live line working is conducted on both transmission and distribution networks however work conducted on transmission networks is of greater interest as high voltages are involved. Numerous techniques are used during such work. The bare hand technique and stick technique are relevant as both involve introducing a floating object, be it an insulating rod, linesman wearing a conductive suit or other type of tool, into the gap. Furthermore the insulation strength of the gap may already be reduced due to the presence of broken insulator discs. Broken insulator discs are also seen as floating objects within the gap.

During live line working the safety of the linesman and team is of primary concern. For this reason a more indepth understanding of flashover of gaps with floating objects present helps lead to safer live line working conditions. Understanding the nature of the flashover mechanism allow for events that may endanger the live line team to be avoided. In addition suitable models for predicting flashover voltages greatly assist in assessing the associated safety of the work site.

This dissertation introduces further insight into flashover in gaps containing floating objects with the benefit of both theoretical, measured and visual results.

The structure of the dissertation is as follows:

Chapter 2: An outline of the different stages of the breakdown process is given.

A brief discussion on previous work relating to the prediction of the flashover voltage of air gaps is provided. The assumptions and limitations of the work are also highlighted and the scope of the dissertation is defined.

Chapter 3: The problem addressed by this dissertation is defined and the approach taken in solving the problem is discussed. The reason for the chosen test configuration and positions of the floating object is explained. The critical time to crest of the test configurations if defined and its importance discussed.

Chapter 4: The setup of the experiment is discussed. The relevance of the test object configuration is explained. The use of a high speed camera and voltage measurements is also outlined. The test procedure implemented during the testing is defined.

Chapter 5: Rizk's model for predicting the flashover voltage of air gaps with a floating object present is discussed. The model is presented in an algorithmic format. All the parameters, limitations, and assumptions are discussed along with additional observations. The model is used to predict the flashover voltage of each of the test objects.

Chapter 6: The measured results from the experiment and the predicted results from the model are presented. The measured results are analysed with regard to the critical time to crest and flashover voltage. The predicted results from the model are discussed and compared to the measured results.

Chapter 7: The photographs taken during the experiment using the high speed camera are presented. The steps taken in processing the photographs are outlined. The trends seen in the photographs are discussed with numerous examples of each given. A series of photographs showing the time progression of a discharge channel forming in a gap is presented. A link between the time to crest of the applied impulse and the extent of the branching of the discharge channel is identified and discussed.

Chapter 8: The findings of the dissertation are summarised and recommendations for future work are given.

Appendix A: The complete set of the measured results is presented in tabular format. This includes the atmospheric conditions measured during the tests.

Appendix B: The calculation of Rizk's constant used in his model is discussed. Electric field modelling is used to calculate its value. The aspects of the simulation

tool are discussed. The results are presented along with a discussion on the approach taken in implementing the simulation model.

Appendix C: The implementation of Rizk's model in Octave is listed. The code listing should be viewed in conjunction with **Chapter 5**.

Appendix D: An attempt was made to measure the pre-breakdown current during the application of an impulse. The measurement system is discussed and the associated difficulties with such a measurement are discussed as the results obtained were inconclusive.

Appendix E: A paper on the work presented in the dissertation is included. The paper was presented at the 15^{th} International Symposium on High Voltage Engineering.

In the following chapter, previous work relating to the breakdown of long air gaps is discussed.

Chapter 2

Background

The different stages of the breakdown process are outlined. Previous work on calculating the flashover voltage of long air gaps is discussed. The assumptions and limitations of the work are highlighted. The effect of the presence of the floating object in a long air gap is also discussed.

2.1 Breakdown process and voltage

Understanding the breakdown process or the different stages associated with the breakdown of a gap is necessary when establishing models for the breakdown voltage and hence the U_{50} flashover voltage. The following sections discusse this breakdown process.

2.1.1 Breakdown process

Carrara & Thione (1976) provided a simplified description for each stage of the breakdown process; Gallimberti (1979) however addressed each stage in greater detail. The stages are defined as follows with each stage marked on a voltage waveform recorded from a breakdown event in *Figure 2.1* :

1. **Voltage application** $[time = t_0, voltage = 0]$
   As the voltage increases the electric field at the electrode begins to increase giving rise to electron avalanches in the surrounding vicinity.
2. **Corona inception** $[t_i, U_i]$
   The electric field and voltage continue to increase to a point at which corona

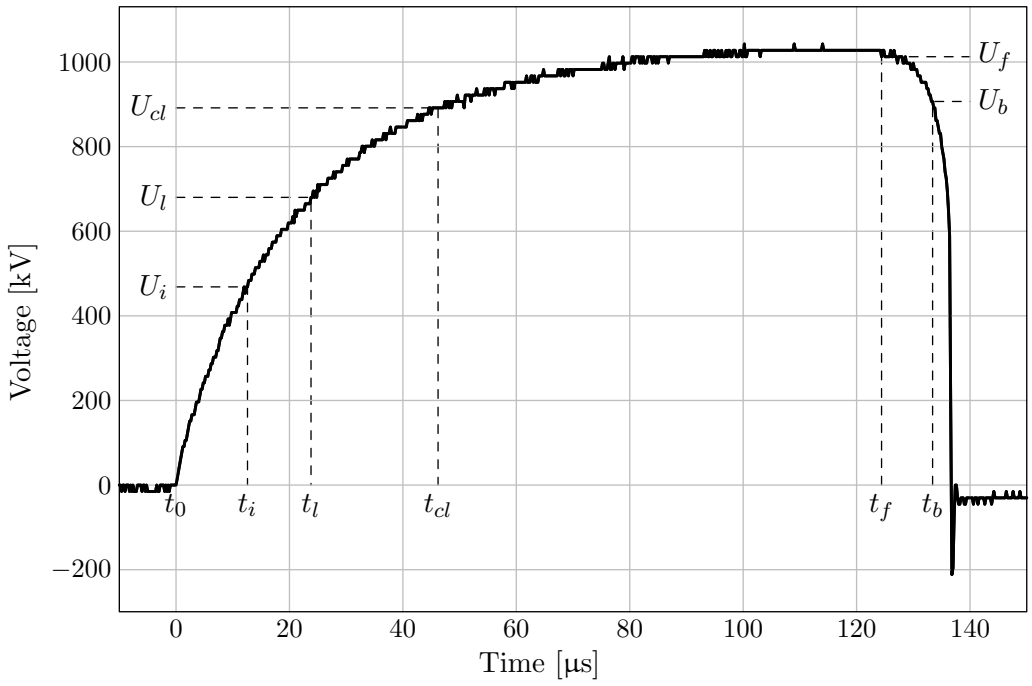


Figure 2.1: Recorded voltage waveform of a breakdown with the different stages labelled.

bursts are observed. After each corona burst a decrease in electric field strength is measured. This period is referred to as the the primary dark period. Nothing is visible in the gap during this period since the electric field decreases after each corona burst.

3. **Leader inception** $[t_l, U_l]$
   This period is referred to as the secondary dark period. During this period leader channels may form from corona filaments during corona bursts. The leader however is not yet self sustaining and does not continue to propagate into the gap. This process repeats as corona bursts occur.

4. **Continuous leader inception** $[t_{cl}, U_{cl}]$
   At some point the applied voltage is high enough to maintain a leader channel that is able to propagate into the gap. The voltage at which this occurs is known as the continuous leader inception voltage. The applied voltage continues to increase so as to maintain a constant leader tip potential.

5. **Final jump** $[t_f, U_f]$
   As the leader channel approaches the ground electrode or plane there exists a height at which the streamer zone preceding the leader tip reaches the ground

electrode or plane. At this instance the leader tip velocity increases exponentially. This length is known as the height of the final jump.

6. **Breakdown** $[t_b, U_b]$
   Breakdown occurs once the leader tip reaches the ground electrode or plane. The voltage begins to collapse as the current increases.

2.1.2 Breakdown voltage

Initial work conducted by Carrara & Thione (1976) suggested that the continuous leader inception voltage formed the largest component of the breakdown voltage of a gap. Using this, they presented an expression for calculating the minimum U_{50} flashover voltage, making use of an empirical formula for calculating the continuous leader inception voltage. They then applied this method leading to the development of expressions used to calculate the minimum U_{50} flashover voltage for different gap geometries such as rod-rod gaps and conductor-plane gaps.

The U_{50} voltage is calculated from the breakdown voltage using the following formula:

$$U_{50} = \frac{U_b}{1 - 3\sigma} \tag{2.1}$$

where

U_{50} = 50% flashover voltage [kV]
U_b = Applied voltage at the instant breakdown occurs [kV]
σ = Standard deviation (typically 5%)

2.1.3 Assumptions

On observing the breakdown process Carrara & Thione (1976) arrived at the following assumptions:

1. $\mathbf{t_c \leq t_{crit}}$
   For time to crests less than or equal to the critical time to crest, the leader inception stage coincides with the continuous leader inception stage such that:

$$[t_l, U_l] = [t_{cl}, U_{cl}]$$

2. $\mathbf{t_c = t_{crit}}$
   For time to crests equal to the critical time to crest the voltage at the instant of the final jump and the breakdown voltage are equal such that:

$$U_f = U_b$$

3. **Electrode size $\geq$ critical size**
   For electrode sizes typically greater than a critical size the corona inception stage coincides with the leader inception stage such that:

$$[t_i, U_i] = [t_l, U_l]$$

   In other words no primary dark period exists.

4. **Electrode size $\leq$ critical size**
   For electrode sizes less then the critical size the breakdown voltage remains the same as determined for the critical size.

5. **Shortest path**
   The leader progresses along the shortest path between the high voltage electrode and the ground electrode.

2.2 Continuous leader inception voltage

2.2.1 Previous work

Rizk (1989*a*) agreed with Carrara & Thione (1976) in that the continuous leader inception voltage is the dominant contributor to the breakdown voltage of the gap. In establishing an expression for the continuous leader inception voltage Rizk (1989*a*) made use of the following information established in previous work:

- The applied voltage increases such that a constant voltage is maintained at the leader tip as the leader channel propagates through the gap. This is assumed under critical conditions.
- Leader propagation is associated with charge injection into the gap at a rate of $40 - 50$ μC/m of axial leader length in rod-plane gaps. The charge density is lower for cylindrical conductors and higher for spherical conductors.

- The charge injection into the gap due to the propagating leader channel is modelled as a spacial cylindrical distribution with an equivalent radius. The equivalent radius is taken to be approximately 0.5 m. It should be noted that this represents the charge injection and not the actual leader channel which has a radius in the order of millimeters.

2.2.2 Expressions

In Rizk's work analytic expressions for the following were presented:

- Continuous leader inception voltage, *Equation (2.2)*
- Height of final jump, *Equation (2.5)*
- Voltage drop across leader channel, *Equation (2.8)*
- Approximate voltage drop across leader channel, *Equation (2.9)*

Each of these expressions will be explained in the following subsections.

Leader inception voltage

Rizk (1989*a*) initially determined the continuous leader inception voltage for a rod-plane configuration. All the parameters used by Rizk in the model are related to physical elements of the discharge process, as noted by Carrara et. al. when reviewing the work. Rizk (1989*b*) subsequently redefined the continuous leader inception voltage such that it could be applied to multiple gap configurations as shown in *Equation (2.2)*.

$$U_{lc} = \frac{\frac{V_0}{E_{cr}} \cdot E_s}{1 + 2\frac{V_0}{E_{cr}} \cdot \frac{1}{R}} \tag{2.2}$$

where

U_{lc} = Leader inception voltage [kV]
$\frac{V_0}{E_{cr}}$ = Dimension constant (3.891 m for rod-type gaps)
E_s = Streamer electric field gradient [kV/m]
R = Geometric constant [m]

The geometric constant R is a function of the gap spacing and the electrode configuration:

- For rod-plane gaps R is equal to:

$$R = 2d \tag{2.3}$$

where

d = Length of air gap [m]

- For rod-rod gaps R can be approximated to:

$$R \simeq 2(h + d) \tag{2.4}$$

where

h = Length of ground rod electrode [m]

This approximation is satisfactory for gaps of 4 m or more and for ground electrodes equal to or less than twice the gap spacing.

Height of final jump

The height of the final jump is the length at which the streamers that precede the leader channel reach the ground electrode. The height of final jump for rod-plane gaps is calculated as follows:

$$h_f = \frac{1}{\frac{V_0}{E_{cr}} + \frac{1}{d}} \tag{2.5}$$

where

h_f = Length of final jump [m]

For rod-rod gaps, the negative leader starts only after the positive leader corona reaches the ground rod. Rizk (1989*b*) therefore uses the the streamer inception criterion for calculating the height of the final jump for rod-rod gaps.

$$h_f = \frac{U_{lc}}{E_s} \tag{2.6}$$

where

E_s = Streamer electric field gradient (500 kV/m for rod-rod gaps) [kV/m]

The length of the leader channel at the point of the final jump is given by:

$$l_z = d - h_f \tag{2.7}$$

where

l_z = Length of leader channel [m]

Voltage drop across leader channel

Jones (1973) found there to be a resemblance between the leader channel and electric arc, such that the leader conductance per unit length can be assumed to be governed by Hochrainer (1970)'s dynamic equation. Rizk (1989*a*) uses this assumption while assuming a constant current flow and constant propagation velocity to form an analytic expression for the voltage drop across the leader channel. The expression for the voltage drop across the leader channel in a gap is shown in *Equation (2.8)*.

$$\triangle U_{lc} = \frac{50d}{1 + \dfrac{3.89}{d}} + 37.5 \ln \left[8 - 7 \exp \left(\frac{-1.33d}{1 + \dfrac{3.89}{d}} \right) \right] \tag{2.8}$$

where

$\triangle U_{lc}$ = Voltage drop across leader channel [kV]

Equation (2.8) can be approximated by *Equation (2.9)* when the length of the leader channel in question is greater than 2 m.

$$\triangle U_{lc} = \frac{50d}{1 + \dfrac{3.89}{d}} + 78 \qquad : \qquad l_z \geq 2 \text{ m} \tag{2.9}$$

2.2.3 Assumptions and limitations

The analytical expressions presented in **Section 2.2.2** are limited to impulses with critical time to crest resulting in a minimum flashover voltage. In addition they are limited to impulses of positive polarity. No expression exists currently that is capable of predicting the flashover voltage for impulses with non-critical times to crest as there is no linear dependence of the flashover voltage on time to crest.

The predicted flashover voltages are only valid at sea level as the expressions were validated against test results from experiments conducted at sea level.

The assumptions listed by Carrara & Thione (1976) relating to the electrode size and the time to crest of the applied impulse as discussed in **Section 2.1.3** are also applicable to Rizk's expressions.

2.3 Presence of a floating object

Research by Hutzler (1987) on gaps with floating objects present showed that:

- The presence of a perfectly smooth object (sphere) with no protrusions increased the flashover voltage of the gap.
- The presence of a small protrusion on the floating object present in the gap decreased the flashover voltage significantly.
- If the object is in a remote position from the gap axis its effect becomes negligible provided that the closest distance to the gap axis is greater than half of the gap length.

Hutzler (1987)'s work was however limited to a single impulse waveshape with a front time of 60 μs and a tail time of 900 μs.

Research conducted by Baldo (1989) showed that the minimum flashover voltage of a gap with a floating object present corresponds to a critical position of the floating object along the gap axis. Later research also showed the effect a floating object on the critical time crest. It is shown that the critical time to crest decreases for gaps with floating objects present compared to gaps without.

Research in the 1980's and early 1990's concentrated on the effects of floating objects and the use of models to predict the flashover voltage of gaps with floating objects present. One such notable model was proposed by Rizk (1994) for determining the U_{50} flashover voltage for different geometries with conducting floating objects present. The model is based on the forementioned work and is implemented and discussed further in **Chapter 5**.

It should also be noted that CIGRÉ's Working Group 07 Study Committee 33 was particularly focused on the effect of floating objects and its relevance to live line working.

2.4 Scope of dissertation

The scope of the dissertation is limited to obtaining measured results from large scale experimentation and obtaining predicted results from the implementation of Rizk (1994)'s model. The scope of the dissertation includes the analysis of the measured results and the validation of the model using photographic means and by comparison with the measured results. The dissertation does not address the implementation of any refinements to the model, but rather explains and validates the differences.

The following chapter defines the problem addressed in the dissertation. An outline of the work conducted is given. The choice of the position of the floating object in each test object is discussed.

Chapter 3

Approach taken

The problem addressed by this dissertation is defined and the approach taken in solving the problem is discussed. The reasons for the chosen test configuration and positions of the floating object are explained. The critical time to crest is defined and its importance discussed.

3.1 Problem statement

When setting safety guidelines for live line working, the guideline should be conservative and address the worst case scenario. Having an indepth understanding of mechanisms and the factors affecting flashovers in gaps with floating objects present assists in setting safer working guidelines. For example the effect of air density on the flashover parameters of a gap with a floating object present. Such effects, at present, are not clearly defined or understood. This makes it difficult to assess safety guidelines for performing live line work on insulator strings with broken discs at both high and low altitudes.

3.2 Objective

The objective of this dissertation is to broaden the knowledge on flashovers in gaps with floating objects present under reduced air densities (high altitudes). This is achieved through:

- Experimental work on various test test objects with a floating object present.

- The implementation of Rizk's model for calculating the flashover voltage of different geometries with a floating object present in the gap and providing an explanation thereof.
- Determining the suitability of the model for predicting flashover voltages at high altitudes.
- The comparison between measured results and theoretical results.
- Visual insight into discharges in gaps containing floating objects.
- A gap view of channel formation.

3.3 Overall approach taken

The approach taken is divided into two components, an experimental component and a theoretical component. The experimental component was completed first as certain aspects of the test object were defined by physical limitations. Such limitations included the dimensions of electrodes and the availability of material for the electrodes. The theoretical component however is flexible allowing for the results to be easily repeated to allow for unexpected changes to the test object. In addition due to the large amount of time required to complete each test only three positions for the floating object were selected for the experimental component.

In the theoretical component a model is implemented and used to predict the breakdown voltage of the given test configurations. The test object is chosen such that it can be applied to and used in both the experimental component and the theoretical component of the work. For this reason a rod-rod gap with a rod floating object is chosen as the test object. The specific relevance of the test object and its dimensions will be discussed further in the following sections.

3.3.1 Position of floating object

The positions of the floating object along the gap axis were selected based on Rizk's work discussed in **Chapter 2**. Rizk (1994) identified a transition point at which the first gap starts breaking down under the leader mechanism rather than under the streamer mechanism. This transition point is shown to be approximately a third of the gap length from the high voltage electrode however it is dependent on the gap length and other factors as discussed in the previous chapter.

The three positions chosen to be tested where at 25% of the gap length, 50% of the gap length and 75% of the gap length as measured from the high voltage electrode to the midpoint of the rod floating object. Each position is chosen to represent a unique situation occuring in the gap during an impulse. Two other configurations were tested without the floating object, the first a rod-rod gap as it is described above and the second a rod-rod gap with the length of the air gap reduced by the equivalent length of the rod floating object. The different configurations are shown in *Figure 3.1.*

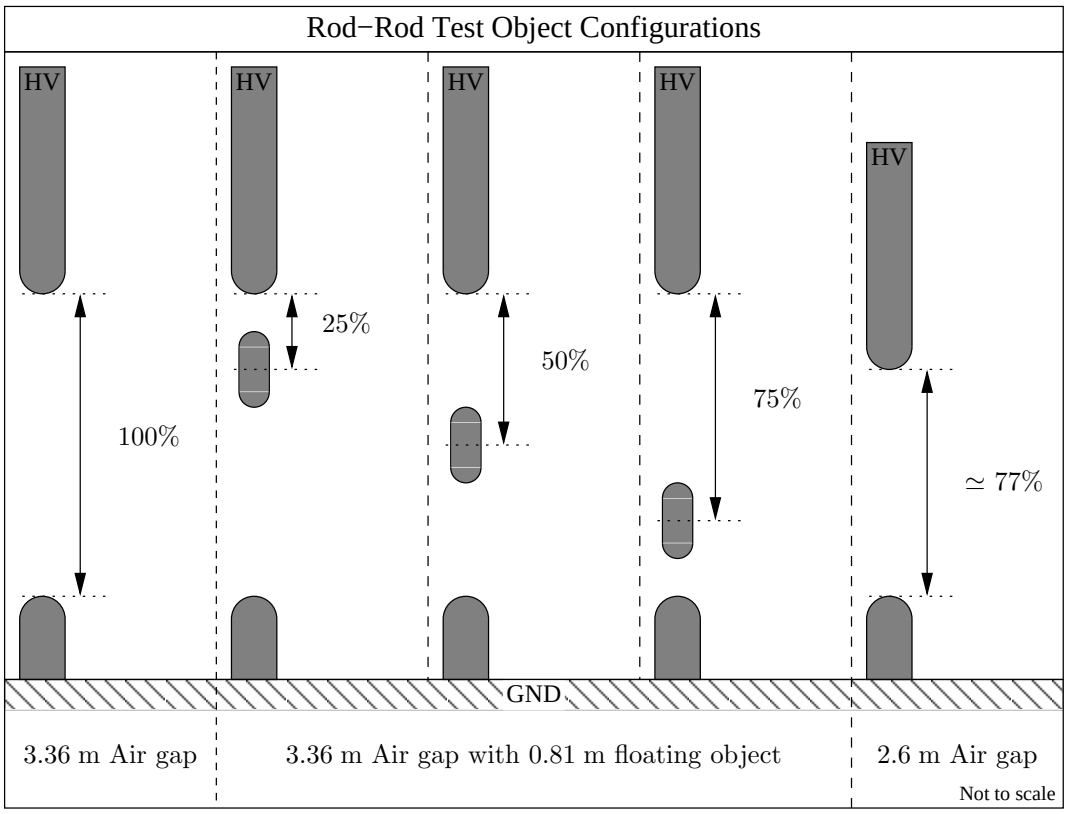


Figure 3.1: Diagram showing the test configurations.

3.3.2 Large scale experiment

The experiment was conducted at a high altitude test facility in an indoor laboratory. The objective of the experimental work was to determine the critical time to crest and hence the minimum breakdown voltage for the configurations. During the testing high speed photographs were taken of the activity in the gap during an applied impulse. In addition the voltage and current waveforms were recorded. The test setup will be discussed further in **Section 4**.

3.3.3 Simulated model

The model proposed by Rizk for determining the minimum flashover voltage of a gap with a floating object along the gap axis is implemented. The model is then used to plot the breakdown voltage of the test object as a function of the position of the floating object within the gap. The U_{50} flashover voltages calculated are for impulses with critical times to crest for each position of the floating object. The model and its implementation is discussed further in **Chapter 5**.

3.3.4 Critical time to crest

The critical time to crest of the test object is determined by characterising its U-curve. A range of front times (time to crest) is selected and the U_{50} flashover voltage is determined for each waveshape. The U_{50} breakdown voltage is determined using the up-down test method. A series of 30 applied voltage impulses were used instead of 20 as suggested by IEC 60060–1 (1989), allowing for better accuracy. The resulting U_{50} flashover voltages are then plotted as a function of the time to crest of the applied impulse resulting in a U-shaped curve, aptly named the U-curve.

The critical time to crest is the front time of the impulse that results in the lowest flashover voltage and can be identified on the U-curve by locating it minimum. The average time to breakdown (t_b) for the given waveshape can be compared to the time to crest (t_c) of the applied impulse. This gives insight into the location of the minimum breakdown voltage and hence the critical time to crest (t_{crit}) as well as aiding in the selection of the impulse waveshapes. In then follows that for:

- $\mathbf{t_b > t_c}$
  If the time to breakdown is longer than the time to crest of the impulse then breakdown is occurring on the tail of the impulse. In other words the current time to crest is greater than of the critical time to crest if looking at the U-curve.
- $\mathbf{t_b = t_c}$
  If the time to breakdown is equal to the time to crest of the impulse then it is referred to the critical time to crest. The critical time to crest results in the lowest breakdown voltage.
- $\mathbf{t_b < t_c}$
  If the time to breakdown is shorter than the time to crest of the impulse then

breakdown is occurring on the front of the impulse. In other words the current time to crest is less than of the critical time to crest if looking at the U-curve.

In the following chapter, the experimental aspect of the work is discussed.

Chapter 4

Experiment

The experimental setup is discussed. The relevance of the test object configuration is explained. The use of a high speed camera and voltage measurements is also discussed. The test procedure implemented during the testing is outlined.

The following section describes the facility where the tests were conducted and the equipment and test objects and configurations used. The layout of the test facility and position equipment is shown in *Figure 4.1*.

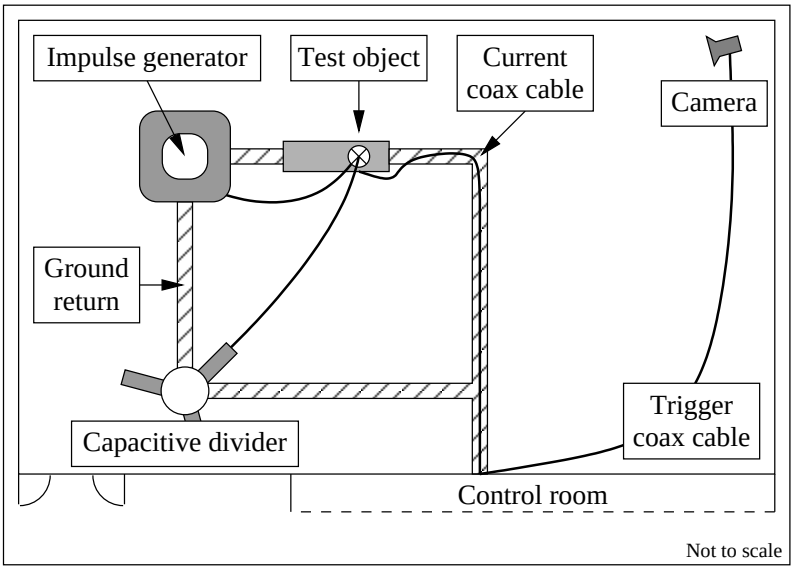


Figure 4.1: The layout of the indoor laboratory during testing.

4.1 Test facility

The tests were conducted at the SABS-NETFA high voltage test facility in the indoor laboratory. The laboratory is at an altitude of 1539 m above sea level.

The indoor laboratory can be treated as a closed system in which the temperature, pressure and humidity are not subject to large fluctuations as expected with an outdoor laboratory. The temperature, pressure and humidity ranges are shown in *Table 4.1* and the standard deviation for each parameter is given. It is therefore assumed that all testing was conducted under the same conditions even though it spanned a five week period. Small changes in the atmospheric conditions were observed through the day and also from day to day. These changes were considered negligible, however some tests were repeated if the atmospheric conditions deviated substantially.

Table 4.1: Temperature, pressure and humidity ranges measured during testing.

	Temperature [°C]	**Pressure** [kPa]	**Humidity** [%]
Maximum	19.0	86.2	34.0
Minimum	11.0	84.3	14.0
Average	14.3	85.5	27.7
Standard Deviation	2.0 %	0.4 %	6.3 %

4.2 Test Equipment

4.2.1 Impulse generator

Seventeen stages of a Haefly 18-stage 3.6 MV impulse generator capable of supplying 25 kJ per stage was used. This was more than sufficient as the maximum impulse peak voltage required is below 1.5 MV. The impulse generator uses a distributed network of front and tail resistors. This allows for the generator to be easily configured using parallel and series configurations of existing resistors to achieve the desired rise times without the use of additional external resistors. For the duration of the testing the tail resistor was fixed at 16.8 kΩ.

A range of front times from 20 µs to 250 µs (standard switching impulse) was used to characterise the U-curve's for each test configuration. The approximate waveshapes used during testing are as follows:

- 25/2500 µs
- 40/2500 µs
- 60/2500 µs
- 70/2500 µs
- 90/2500 µs
- 120/2500 µs
- 140/2500 µs
- 160/2500 µs
- 190/2500 µs
- 250/2500 µs

4.2.2 Voltage measurement

A 5-stage, 2.1 nF per stage, capacitor divider was for the voltage measurements. The capacitive divider was connected to a TDA544 Tektronics Digital Storage oscilloscope via a 75 Ω coaxial cable run through cable ducts below the ground plane. The oscilloscope was set to trigger on the rising edge of the voltage waveform. The 75 Ω cable was terminated in a 50 Ω characteristic impedance.

4.2.3 High speed photography

A high speed camera manufactured by `Cooke` is used to photograph any discharge or channel formation in the air gap during an applied impulse. The camera has the following specifications:

- Shutter speed range from 1 µs to 1 ms
- 8-bit resolution (256 grey-scale colours)

- 752 by 286 pixel image size
- Adjustable gain setting
- Triggered by TTL falling edge

The ambient light intensity within the laboratory was kept constant. This is important from a photography aspect as the intensity of the ambient light effects the level of detail captured by the high speed camera. The high speed camera was also fixed in one position without the concern of the position of the sun or other moving light sources effecting its operation.

A 1:4.5/150 lens was fitted to the camera so as to maximise the field of view of the camera. In addition the camera was positioned in the furthest position from the test object again in order to further increase the field of view. The field of view of the camera is approximately 1.9 m by 0.75 m in size, capturing roughly half of the test object. The location of the camera with respect to the test object and the control room is shown in *Figure 4.1.*

A 50 Ω coaxial cable was run from the control room to the camera. The falling edge TTL output trigger from the oscilloscope was used to trigger the camera based on the rising voltage waveform. After the camera is triggered the frame is stored by the camera. A laptop computer was then used to connect to the camera, using a parallel cable, to download the stored frame. Interface to the camera was through a custom application running on the the computer. The application gives the option to store the frame as a binary array or as an image in the `png`[1] file format.

4.2.4 Current measurement

A 1 Ω shunt resistor in series with the ground electrode was used to measure the pre-breakdown current. The shunt resistor was connected in parallel with a gas arrestor and a transient voltage suppression diode in order to protect the oscilloscope from over voltages. The protection circuit was then connected to the oscilloscope via a coaxial cable. The differential voltage across the shunt resistor was measured by the oscilloscope. The shunt current measurement was successful however the results were inconclusive. The details relating to the current measurement is presented in **Appendix D** where a set of measurements from a withstand and breakdown event are given, and the difficulties associated with the current measurement are discussed.

[1] png is a bitmap image file format, available at http://www.libpng.org/pub/png/.

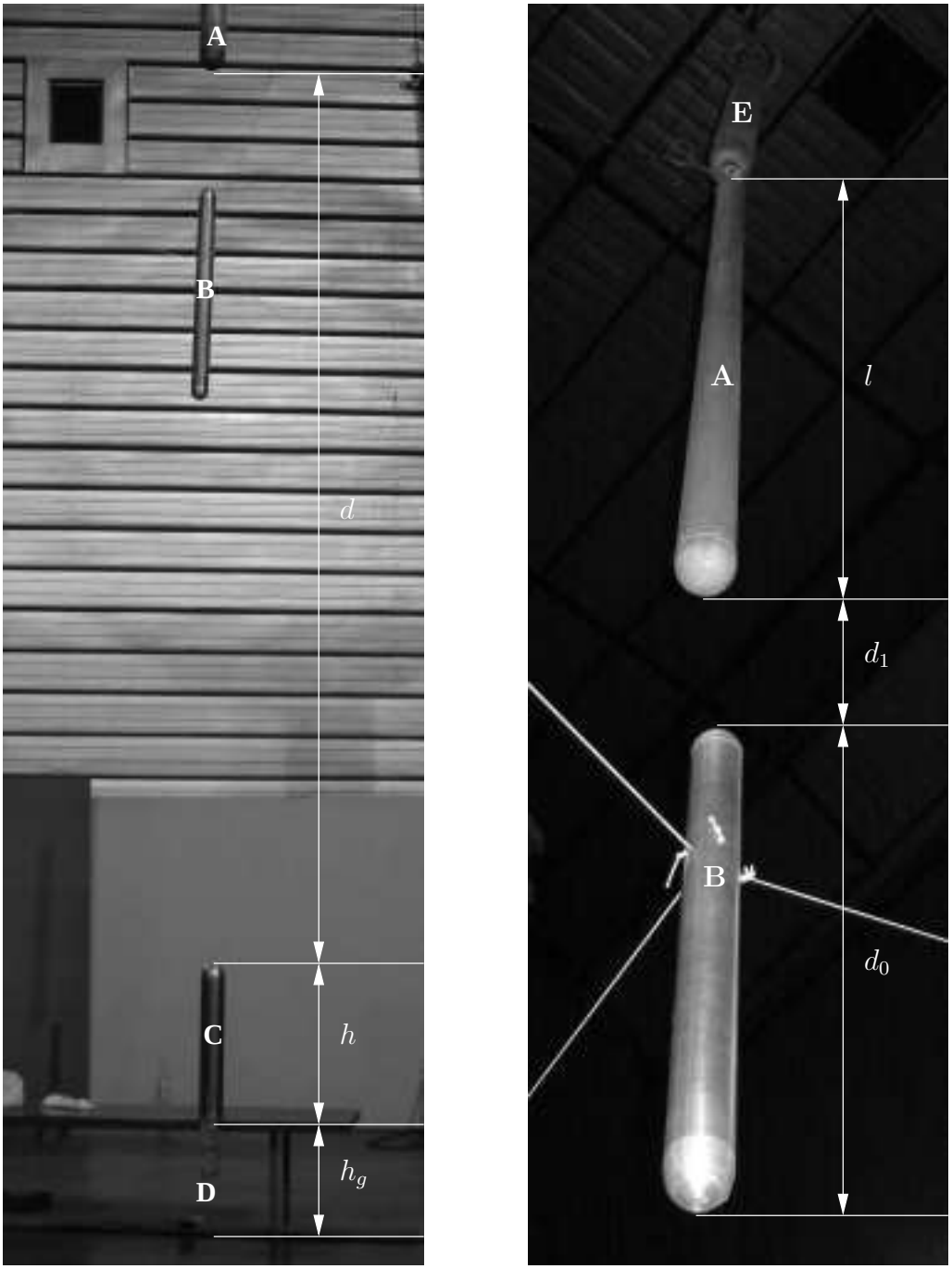
4.3 Test object

A 3 m rod suspended via a composite insulator from a service crane formed the high voltage electrode. The ground electrode consisted of a 0.5 m rod positioned on a wooden table to isolate it from the ground plane. The electrode was then connected via a shunt resistor to the earth return path of the impulse generator. Connections from the impulse generator and the capacitive divider were made to the top of the suspended rod using copper wire. *Figure 4.2* shows photographs of the test object.

The rod floating object was suspended along the gap axis via three diagonal guy lines attached just above the midway point of the rod. Polyethylene rope of 3 mm diameter where used for the guy lines.

The air gap length between the high voltage and the ground electrode was based on the length of a 23-disc cap and pin insulator string. The electrodes construction was based on the availability of materials resulting in the given radii. The dimensions of the rod floating object were based on the dimensions of a broken cap and pin insulator disc. The radius of the floating rod is equivalent to the maximum radius of the cap. The length of the floating rod was chosen such that the rod would represent a series of five broken cap and pin insulator discs. The floating rod is seen to represent five shorted broken discs. *Tables 4.2* and *4.3* list all the lengths and dimensions of the electrodes used. All electrodes were fitted with spherical caps to avoid any sharp edges hence areas of higher electric field stress.

The motivation for the selection of the above described dimensions is based on assumption that the results will form a suitable comparison for any future results from tests with cap and pin insulator strings with broken discs.



(a) Complete test setup. *(b)* High voltage electrode and floating object.

Figure 4.2: Photographs of the test configuration with dimensions shown.

A - High voltage rod electrode with radius r_{hv}.

B - Floating object, suspended with poly-ethylene guy ropes, with radius r_{fo}.

C - Ground rod electrode with radius r_{gnd}.

D - 1 Ω Shunt resistor.

E - Composite insulator suspended from service crane.

Table 4.2: Test configuration dimensions.

Parameter	**Description**	**Length** [mm]
d	Air gap length between electrodes	3360
h	Length of ground electrode	500
h_g	Height above ground plane	430
l	Length of high voltage electrode	3000
d_0	Length of floating rod electrode	810
d_1	Length of primary air gap	varied
d_2	Length of secondary air gap	varied
r_{hv}	Radius of high voltage electrode	50
r_{fo}	Radius of floating rod electrode	35
r_{gnd}	Radius of ground electrode	45

Table 4.3: Lengths of the primary (d_1) and secondary (d_2) gaps for each test configuration.

Test Object	$\mathbf{d}_1$ [mm]	$\mathbf{d}_2$ [mm]
3.36 m rod-rod gap with 25% floating object	435	2115
3.36 m rod-rod gap with 50% floating object	1275	1275
3.36 m rod-rod gap with 75% floating object	2115	435

4.4 Test Procedure

In preparation for the testing, a 3 m rod-plane gap was used to confirm the correct operation of the test setup and measurements circuits. The 3 m rod-plane gap was characterised and the results compared to values from previous tests conducted at SABS-NETFA. This initial testing allowed for confidence to be built in the experimental results acquired. The following test procedure outlines the steps implemented while conducting the testing.

1. Set up the test configuration.
2. Select the waveshape and reconfigure the impulse generator.
3. Check the waveshape by firing three to five impulses that result in a withstand event.
4. Identify starting voltage for the U_{50} tests.
5. Record temperature, pressure and humidity values.
6. Complete 30-shot U_{50} for the given waveshape.
    - If a withstand occurs discharge floating object using earth stick.
7. Record temperature, pressure and humidity values.
8. Check that impulse generator efficiency is consistent throughout the test.

After each shot during the U_{50} test the voltage and current waveforms were saved. If the test object withstood the applied impulse the photograph from the high speed camera was saved.

In the following chapter, Rizk's model for predicting the flashover voltage of gaps with floating objects present is introduced. The results predicted by the model will be used in subsequent chapters for comparison with the measured results from the experiment discussed in this chapter.

Chapter 5

Model simulation

Rizk's model for calculating the flashover voltage of different test configurations with a floating object present is discussed. The model is presented in an algorithm format with the parameters and associated stages discussed. All assumptions and limitations of the model are presented. Additional observations of the model are also included.

5.1 Overview

The model presented by Rizk (1994) for determining the critical flashover voltage of an air gap with a floating object present in the gap, along the gap axis, is used to determine the flashover voltages for the given test objects.

Rizk (1994) applied the model to numerous test configurations namely rod-plane, conductor-plane and conductor tower leg gaps in his own work. Tests objects with different shaped floating objects namely rod and sphere floating objects were also tested. Rizk (1994) showed that the model had good correlation with the experimental results from other testing conducted.

As mentioned in **Chapter 2**, Rizk (1989*a*,*b*) presented analytic expressions for calculating the leader inception voltage of different gap configurations, the relevant gap configurations being rod-plane gaps and rod-rod gaps. Analytical expressions for the voltage drop across the leader channel and the length of the final jump when the leader channel bridges the gap are also presented. These expressions are used in the model. The model implementation is specifically based on the rod-rod test configuration however it can easily be adapted for other configurations.

The model takes the dimensions of the test object and gap as inputs. The model follows the chronological progression as breakdown occurs. Firstly the breakdown voltages of the primary gap under leader mechanism and streamer mechanism are calculated and compared. Rizk's expression for calculating the leader inception voltage is used.

The lowest breakdown voltage of the primary gap is then used to calculate the potential of the floating object once the primary gap is bridged. This then becomes the criterion for breakdown in the secondary gap. Again the breakdown voltages for the leader mechanism and streamer mechanism are calculated for the secondary gap. If the potential of the floating object is higher then either of the calculated breakdown voltages it is possible that a discharge channel exists in the secondary gap prior to the primary gap being bridged.

If the potential of the floating object is lower then that of either the breakdown voltages a higher applied voltage is then required to breakdown the secondary gap.

5.2 Model implementation

The model is presented in algorithm format in *Figure 5.1.* The model is based on a rod-rod gap shown in *Figure 5.2. Table 5.1* lists the variables of different potentials and breakdown voltages with a description of each used in algorithm.

- *Inputs and Output*
  The model requires the following inputs:

$$d; d_0; d_1; h; E_s; k_0; \sigma$$

where

d = Length of gap between the high voltage and ground electrodes [m]
d_0 = Length of floating object [m]
d_1 = Length of primary gap [m]
h = Length of ground rod electrode [m]
E_s = Streamer electric field gradient [kV/m]
k_0 = Geometric potential factor
σ = Standard deviation (typically 5%)

Input: d, d_0, d_1, h, E_s and k_0
Output: U_{50}

1: $d_2 \Leftarrow d - d0 - d1$ {determine length of secondary gap}

$\boxed{A}$ *Gap 1*

2: $U_{s1} \Leftarrow \dfrac{E_s d_1}{1 - k_0}$ {streamer breakdown criterion}

3: $U_{lc1} \Leftarrow \dfrac{1556}{1 + \dfrac{3.89}{h + d}}$ {positive leader inception voltage, *Equation (2.2)*}

4: **if** $U_{s1} \geq U_{lc1}$ **then** {determine under which mechanism gap 1 breaks down}

5: $U_{b1} \Leftarrow U_{s1}$ {$\therefore$ streamer breakdown}

6: **else**

7: $U_{b1} \Leftarrow U_{lc1}$ {$\therefore$ leader breakdown}

8: **end if**

$\boxed{B}$ *Instant gap 1 is bridged*

9: $\triangle U_{lc1} \Leftarrow \dfrac{50 d_1}{1 + \frac{3.89}{d}} + 37.5 \ln \left[8 - 7 \exp \left(\dfrac{-1.33 d_1}{1 + \frac{3.89}{d_1}} \right) \right]$ {determine volt drop across channel, *Equation (2.8)*}

10: $U_{ss} \Leftarrow U_{b1} - \triangle U_{lc1}$ {determine potential of floating object}

$\boxed{C}$ *Gap 2*

11: $U_{s2} \Leftarrow E_s d_2$ {streamer breakdown criterion}

12: $U_{lc2} \Leftarrow \dfrac{1556}{1 + \dfrac{3.89}{h + d_2}}$ {positive leader inception voltage, *Equation (2.2)*}

13: **if** $U_{s2} \leq U_{lc2}$ **then** {determine under which mechanism gap 2 breaks down}

14: $U_{b2} \Leftarrow U_{s2}$ {$\therefore$ streamer breakdown}

15: **else**

16: $U_{b2} \Leftarrow U_{lc2}$ {$\therefore$ leader breakdown}

17: **end if**

18: $U_{b2} \Leftarrow U_{b2} + \triangle U_{lc1}$ {Relate breakdown voltage to applied voltage}

$\boxed{D}$ U_{50} *Flashover voltage*

19: **if** $U_{b1} > U_{b2}$ **then** {determine dominant breakdown voltage}

20: $U_b = U_{b1}$ {$\therefore$ gap 1 dominates}

21: **else**

22: $U_b = U_{b2}$ {$\therefore$ gap 2 dominates}

23: **end if**

24: $U_{50} = \dfrac{U_b}{1 - (3 \cdot \sigma)}$ {determine U_{50} flashover voltage, *Equation (2.1)*}

Figure 5.1: Algorithm of model used to determine the U_{50} flashover voltage of a gap with a floating object present. Comments are included in braces {}. Different sections are marked by $\boxed{\mathbf{X}}$.

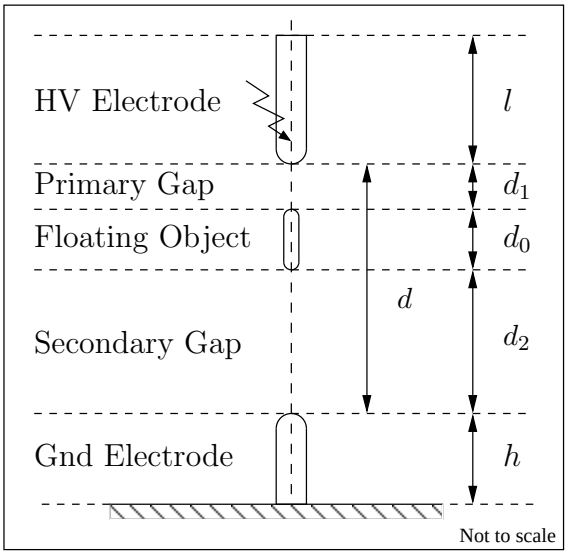


Figure 5.2: Diagram of rod-rod gap showing dimension parameters as implemented in the model.

- The electric field gradient E_s is typically taken as 400 kV/m however Rizk (1994) suggests using a value of 500 kV/m for rod-rod gaps.
- The constant k_0 is determined using electric field modelling and is discussed further in **Section 5.3**.

The model output is the U_{50} flashover voltage. It is suggested that a sigma of 5% be used. Given the results of the tests conducted, the average standard deviation calculated showed a sigma of 2.5%.

- $\boxed{A}$ *Primary gap (Gap 1)*
  - *Line 2*

    The streamer breakdown voltage of the primary gap is calculated using the minimum streamer electric field gradient (E_s) and the length of the primary gap (d_1). A geometric constant is included in the expression to account for the potential of the floating object, this is discussed further in **Section 5.3**.
  - *Line 3*

    The leader inception voltage is calculated using Rizk's analytical expression for rod-rod gaps. The total gap length (d) is used in the expression for determining the leader inception voltage of the primary gap. It is assumed that the leader formation is not affected by the presence of the floating object. The reason leading to this assumption is that the leader mechanism is a self-sustaining process and is strongly dependent on the

Table 5.1: List of the potentials used in Rizk's model with a description. Note: All units are in kV.

Parameter	**Description**
U_{app}	Applied voltage at high voltage electrode
U_{s1}	Streamer breakdown voltage for primary gap
U_{lc1}	Leader inception voltage for primary gap
U_{b1}	Lowest voltage required for breakdown of primary gap
$\triangle U_{lc1}$	Voltage drop across discharge channel in primary gap
U_{ss}	Potential of floating object at instant primary gap is bridged
U_{s2}	Streamer breakdown voltage for secondary gap
U_{lc2}	Leader inception voltage for secondary gap
U_{b2}	Lowest voltage required for breakdown of secondary gap
U_b	Breakdown voltage of test object

applied voltage and the localised electric field at the leader tip rather then the electric field due to the applied voltage over the entire gap as is with the streamer mechanism.

- *Lines 4–8*
  The breakdown voltage of the primary gap is determined by comparing the leader inception voltage to the streamer breakdown voltage. This voltage is the minimum applied voltage required to breakdown the primary gap.

- $\boxed{B}$ *Instant the primary gap is bridged*

  - *Line 9*
    The voltage drop across the discharge channel bridging the primary gap is calculated using the expression presented by Rizk. This value is used to relate the breakdown voltage of the secondary gap to the applied voltage at the high voltage electrode.
  - *Line 10*
    The potential of the floating object can be calculated at the instant at which the primary gap is bridged. This gives insight into simultaneous discharges and is discussed further in **Section 5.5**.

- $\boxed{C}$ *Secondary gap (Gap 2)*

  - *Line 11*

    As with the primary gap, for a sustainable streamer to develop, a minimum electric field gradient (E_s) is required. As the primary gap is bridged, the primary gap and the floating object can now be considered part of the high voltage rod electrode. The streamer channel will be initiated from the bottom tip of the floating object propagating towards the ground electrode. The required applied voltage can therefore be calculated by multiplying the gap distance (d_2) by the streamer electric field gradient (E_s).

  - *Line 12*

    Similarly for the leader inception voltage the length of the secondary gap (d_2) can be inserted into Rizk's leader inception voltage expression for a rod-rod gap to determine the required applied voltage.

  - *Lines 13–18*

    The breakdown voltage of the secondary gap is determined by comparing the leader inception voltage to the streamer breakdown voltage. As with the primary gap inception voltage this breakdown voltage is related to the applied voltage at the high voltage rod electrode. For this reason the voltage drop along the discharge channel bridging the primary gap is added to the breakdown voltage for the secondary gap.

- $\boxed{D}$ U_{50} *Flashover voltage*

  - *Lines 19–23*

    The final breakdown voltage of the test object is equal to the highest breakdown voltage of either the primary or secondary gap.

  - *Line 24*

    The final U_{50} flashover voltage is calculated using the above determined breakdown voltage taking into account the standard deviation.

5.3 Streamer breakdown of primary gap

For a sustainable streamer to develop, a minimum electric field gradient of E_s is required in the gap. Normally the required applied voltage would be calculated by multiplying the gap distance by the minimum streamer electric field gradient. The electric field gradient is typically chosen to be between 400 kV/m and 500 kV/m depending on the gap configuration.

In the presence of a floating object within the gap the streamer criterion can no longer be applied to determine the voltage required for streamer breakdown as the floating object has a floating potential and not at ground potential. This floating potential is a function of the geometric position of the floating object within the gap amongst other factors which are discussed further in **Section 5.4**. For the streamer breakdown voltage of the primary gap to be calculated the potential of the floating object needs to be related to the applied voltage. The geometric constant k_0 is therefore used to relate the potential of the floating object to the applied voltage. The applied voltage can then be calculated using the expression in *Equation (5.1)*.

$$U_{app} - k_0 U_{app} = E_s d_1 \tag{5.1}$$

where

U_{app} = Applied voltage at the high voltage electrode [kV]

Rizk (1994) suggests that the constant be determined using charge simulation. The calculation of this constant for the given test configuration is detailed in **Appendix B**.

5.4 Model assumptions

5.4.1 Leader inception voltage

The model inherits the assumptions and criteria from the expressions as the model makes use of Rizk's expressions for the leader inception voltage and the voltage drop across the leader channel.

5.4.2 Potential of the floating object

As discussed in **Section 5.3** the geometric factor is used to calculate the potential of the floating object in the model. This assumes that the potential of the floating object is solely based on the geometric position of the floating object. Rizk (1994) shows that the potential of the floating object consists of three components, namely:

- The potential due to the geometric position of the floating object within the gap.

- The potential induced due to the space charge in the gap (the charge associated with the leader channel in the primary gap). This value can be calculated if the values and positions of the space charge are known.
- The potential due to accumulated free charge on the floating object. This value cannot be calculated as the value of accumulated charge on the floating object is unknown. Rizk (1994) states that the presence of a protrusion on the bottom of the floating object reduces the effect of this component.

The model only considers the first component as a simplification due to the difficulty of calculating the other two contributing components.

5.5 Model observations

For the case where the floating object is positioned in the vicinity of the ground electrode it is clear that the primary gap will breakdown under the leader mechanism due to the high applied voltage required to achieve the streamer electric field gradient necessary for the streamer mechanism.

As the leader propagates into the gap the potential of the floating object will begin to rise gradually as a result of the space charge due to the leader channel. As the leader channel nears the floating object the potential induced on the floating object may be sufficient to sustain either breakdown mechanism in the secondary gap. The model can be used to predict whether simultaneous discharges occur by determining if the potential of the floating object when the primary gap is bridged exceeds the predicted breakdown voltage of either mechanism for the secondary gap:

$$U_{ss} > U_{b2}$$

If this is true then the breakdown voltage of the secondary gap will be reached before the primary gap is bridged. Electric field simulations of the test setup with the progressing leader channel modelled can be used to determine the voltage and the length of the leader channel in the primary gap at the point at which the floating object reaches a voltage high enough for either a leader or streamer discharge to develop in the secondary gap.

In the following chapter, the measured results from the experiment and the predicted results from the model are presented, compared and discussed.

Chapter 6

Comparison of Results and Discussion

The experimental test results and predicted results are presented. The experimental test results are analysed and explained with regard to the critical time to crest and flashover voltage. A discussion on the results from Rizk's model is presented. The predicted and experimental test results are compared and the suitability of the model is discussed.

6.1 Experimental Test Results

The U-curve of each test object is plotted in *Figure 6.1*, and the critical flashover (CFO) voltage and critical time to crest (t_{crit}) are listed in *Table 6.1* for each test object. It is seen that the measured critical time to crest does not occur at the same point as the minimum or critical flashover voltage occurs. For this reason the closest time to crest (t_1) to the critical time to crest (t_{crit}) is listed. Similarly, the time to crest (t_2) at which the CFO voltage occurs is also listed.

For the discussion of the experimental test results the critical time to crest will be assumed to be the time to crest at which the minimum U_{50} flashover voltage or CFO voltage occurs namely t_2.

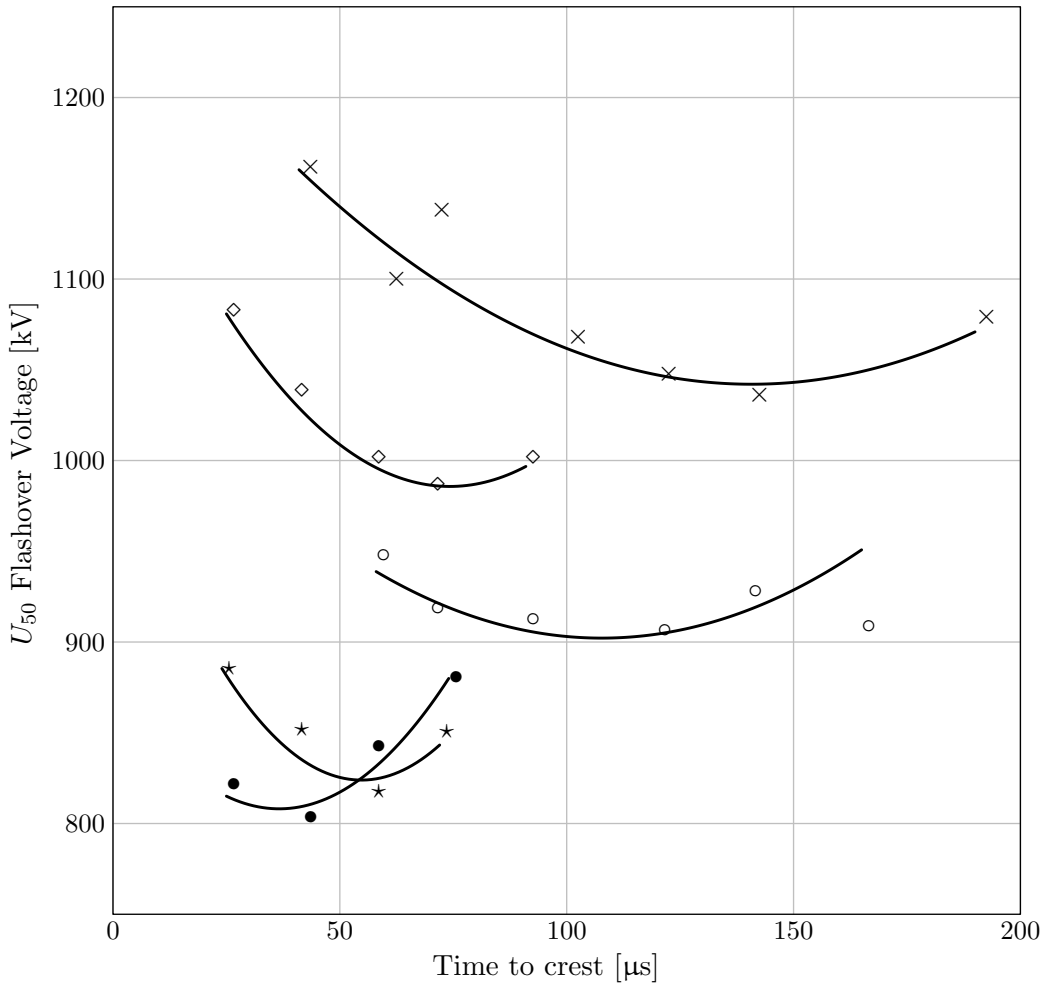


Figure 6.1: U-curves plotted from the measured results.

Legend:

× - 3.36 m rod-rod gap

• - 3.36 m rod-rod gap with 25% floating object

⋆ - 3.36 m rod-rod gap with 50% floating object

◇ - 3.36 m rod-rod gap with 75% floating object

○ - 2.6 m rod-rod gap

The experimental test results show that:

- The 3.36 m rod-rod gap resulted in the highest CFO voltage in comparison to the other test objects.
- The test object with the floating object positioned at the 25% position results in the lowest flashover voltage.
- The test object with floating object positioned at the 50% position had a similarly low flashover voltage.
- In contrast, for the floating object at the 75% position the CFO is significantly higher than that of the 2.6 m rod-rod gap.
- Test objects with the floating object along the gap show shorter critical times to crest than that of both the rod-rod test objects.

Table 6.1: Summary of critical times to crest (t_{crit}) with corresponding front time (t_{c1}) and CFO with corresponding front time (t_{c2}) for each test object.

Test Object	$\mathbf{t}_{c1}$ [µs]	$\mathbf{t}_{crit}$ [µs]	$\mathbf{t}_{c2}$ [µs]	**CFO** [kV]
3.36 m rod-rod gap	120	124	140	1032
3.36 m rod-rod gap with 25% floating object	42	45	42	800
3.36 m rod-rod gap with 50% floating object	72	79	57	814
3.36 m rod-rod gap with 75% floating object	70	66	70	983
2.6 m rod-rod gap	70	70	120	903

Table 6.2: Leader and streamer inception voltages for a 2.12 m, 2.6 m and 3.36 m rod-plane air-gap which represent the primary, equivalent and the total air-gap of the 75% floating object position respectively.

Breakdown Mechanism	2.12 m **Air-gap** [kV]	2.6 m **Air-gap** [kV]	3.36 m **Air-gap** [kV]
Streamer inception voltage	848	1040	1440
Leader inception voltage	549	623	748

6.1.1 75% Floating object position

Flashover voltage

Table 6.2 shows the inception voltages for 2.12 m, 2.6 m and 3.36 m air-gaps which represent the primary, equivalent and the total air-gap of the 75% floating object position respectively.

The calculation of the inception voltages is made simpler by equating the primary gap to a rod-plane gap of equivalent length. This is valid as the predicted flashover voltages for the equivalent rod-rod gap will be slightly higher then those calculated for the rod-plane gap.

The plotted U-curves in *Figure 6.1* show that the 2.6 m rod-rod gap has a lower flashover voltage compared to that of the floating object positioned at 75% in the gap. The 2.6 m rod-rod gap breaks down under the leader mechanism as the streamer inception voltage far exceeds that of the leader inception voltage for the given gap length (2.6 m air-gap) as shown in *Table 6.2*. Similarly, the primary gap of floating object positioned at 75% breaks down under the leader mechanism (2.12 m air-gap).

In comparing the measured flashover voltage for the floating object positioned at 75% to the calculated leader inception voltages it is clear that it is closer to the 3.36 m air-gap leader inception voltage.

Both the measured and the calculated results show that initiation and early propagation of the leader channel is not substantially affected by the remote floating object but more so by the total length of the gap (the length of the gap as measured from the high voltage electrode to the ground electrode).

Critical time to crest

While the 75% floating object position has a higher CFO, its critical time to crest is lower than that of the 2.6 m rod-rod gap. The lower critical time to crest can be explained due to the presence of the streamer mechanism in the secondary gap. The streamer mechanism propagates at roughly the drift velocity of electrons ($\sim 10^5$ m/s) compared to that of leader. Carrara & Thione (1976) suggested that the propagation rate of a leader is in the order of centimeters per second. The streamer mechanism will be present in the secondary gap due to the short gap length and the high

potential of the floating object once the primary gap is bridged.

6.1.2 25% and 50% Floating object positions

The 25% and 50% positions show very similar characteristics in that their CFOs are almost identical and both exhibit very short critical times to crest (t_{c2}). In contrast the 75% position has a substantially higher CFO and a longer critical time to crest (t_{c2}). The shorter critical time to crest (t_{c2}) and lower CFOs suggests that the streamer mechanism dominates breakdown in the 25% and 50% positions whereas the leader mechanism dominates in the 75% position.

This can be explained for the 25% test object since the short primary gap breaks down under the streamer mechanism. According to Rizk (1994)'s model, once the primary gap is bridged, the effective applied voltage minus the volt drop across the channel appears at the bottom of the floating object. This results in an effective shorter rod-rod gap. Given the length of the secondary gap (2.12 m), it will breakdown under the leader mechanism but will require a lower leader inception voltage due to it being shorter than the total gap length (3.36 m).

6.1.3 Velocity and impulse front time

Gallimberti (1979) showed that a relationship exists between the ratio of applied impulse voltage to the U_{50} flashover voltage and the velocity of the leader. The leader velocity is seen to increase for higher overvoltages.

The velocity of the leader is calculated for each unique time to crest for the 3.36 m gap. The velocity and the U_{50} flashover voltage are plotted as a function of the time to crest in *Figure 6.2*.

The leader velocity using the average time to breakdown recorded from the U_{50} up-down test and the leader channel length.

$$v_{lc} = \frac{l_z}{t_{bd}} \tag{6.1}$$

where

v_{lz} = Velocity of the leader channel [cm/µs]
l_z = Length of leader channel in gap [cm]
t_{bf} = Time to breakdown [µs]

Recalling that the leader channel length within the gap is calculated using *Equations (2.6)* and *(2.7)*. The leader channel length for a 3.36 m rod-rod gap is calculated as 1.728 m using a leader inception voltage of 816 kV (*Equation (2.2)*).

The results show that the leader velocity decreases as the time to crest increases. This is expected as the time to breakdown is directly proportional to the time to crest resulting in the velocity being inversely proportional to the time to crest.

The leader velocity for the given range of front times is $1.2 - 2.4$ cm/µs. This range is consistent with range of $1 - 2$ cm/µs quoted by Carrara & Thione (1976), Rizk (1989*a*) and Gallimberti (1979) respectively.

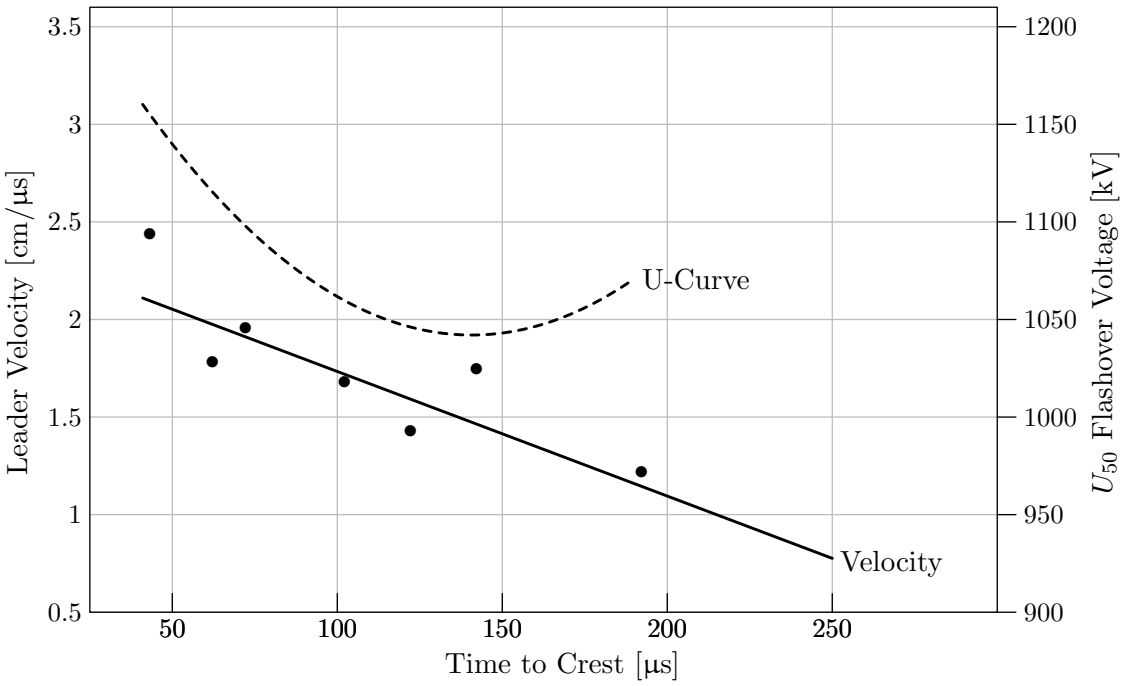


Figure 6.2: Approximate leader velocity and measured U_{50} flashover voltage for 3.36 m rod-rod gap plotted as a function of time to crest.

6.2 Model Verification

The predicted flashover voltage is plotted as a function of the primary gap length in *Figure 6.3* as determined by Rizk's model. In addition the measured values from the testing are also plotted on the same set of axes.

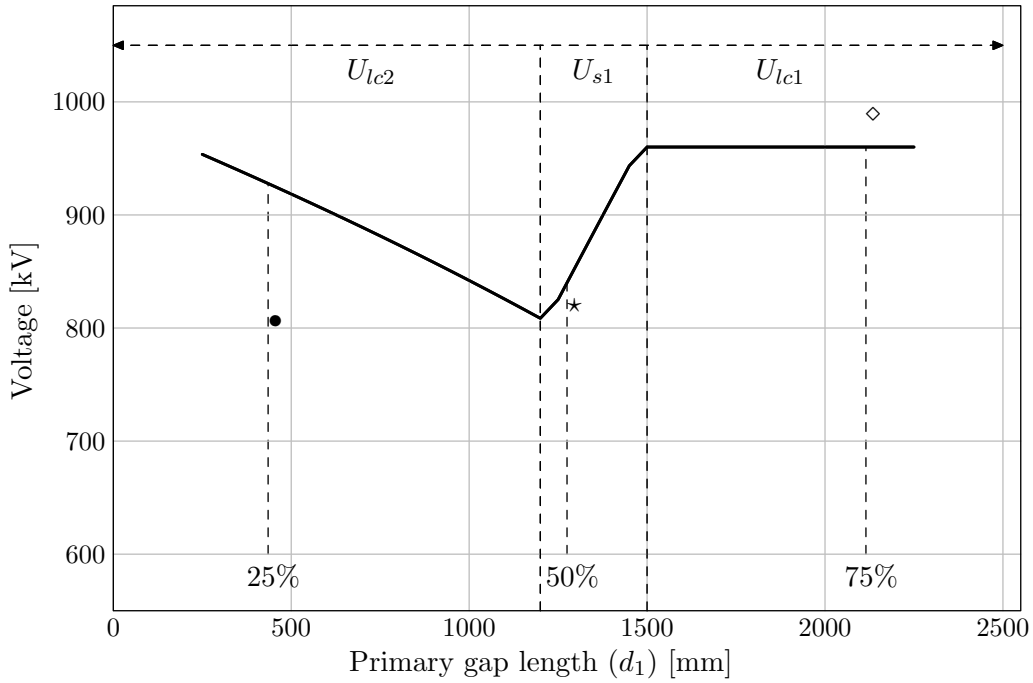


Figure 6.3: Predicted U_{50} Flashover voltage plotted against the length of the primary gap, calculated using Rizk's model.

Legend:

• - 3.36 m rod-rod gap with 25% floating object

⋆ - 3.36 m rod-rod gap with 50% floating object

◇ - 3.36 m rod-rod gap with 75% floating object

Dominant gap:

U_{lc2} - Gap 2: leader inception voltage ($x - 1200$ mm)

U_{s1} - Gap 1: streamer inception voltage ($1200 - 1500$ mm)

U_{lc1} - Gap 1: leader inception voltage ($1500 - y$ mm)

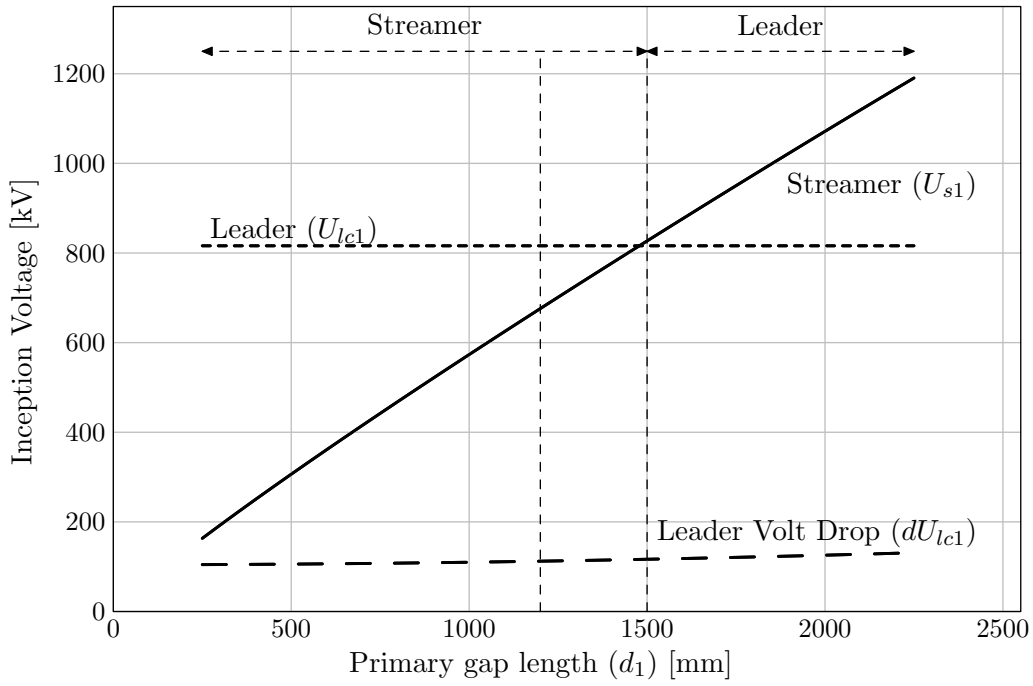
6.2.1 Discussion of model

The model can be divided into three distinct sections. These sections are labelled in *Figure 6.3*. The sections show which breakdown mechanism (in primary or secondary gap) dominates the flashover voltage plotted as a function of the primary gap length. *Figure 6.4* show the required applied voltage for the inception of each breakdown mechanism for both the primary and secondary gaps as a function of the primary gap length. The sections are as follows:

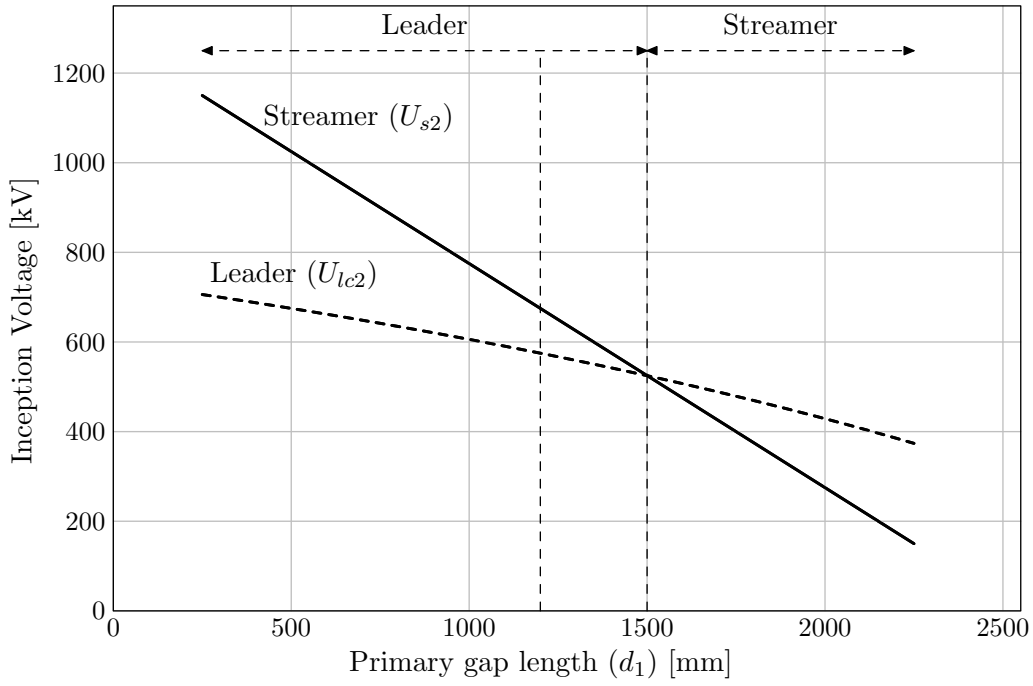
1. **Primary gap length between** $x - 1200$ mm
   The model predicts that the leader inception voltage of the secondary gap (U_{lc2}) will dominate the flashover voltage as the secondary gap requires a higher applied voltage to break down the gap compared to that of the primary gap. The leader mechanism will be responsible for the secondary gap breaking down as it requires a lower inception voltage than the streamer mechanism as seen in *Figure 6.4b*.

2. **Primary gap length between** $1200 - 1500$ mm
   The model predicts that the streamer inception voltage of the primary gap (U_{s1}) will dominate the flashover voltage as the primary gap required a higher applied voltage to break down the gap in comparison to that required by the secondary gap. In this instance the streamer mechanism requires a lower applied voltage than the leader mechanism to break down the primary gap as seen in *Figure 6.4a*.

3. **Primary gap length between** $1500 - y$ mm
   The model predicts that the leader inception voltage of the primary gap (U_{lc1}) will dominate the flashover voltage whereas before the primary gap requires a higher applied voltage to break down the gap. Here the leader inception voltage is lower than that of the inception voltage of the streamer mechanism hence it will be responsible for the primary gap breaking down as seen in *Figure 6.4a*. The flat nature of this section of the model will be discussed further in the following subsection.



(a) Primary gap



(b) Secondary gap

Figure 6.4: Leader and streamer inception voltages plotted for the primary and secondary gaps as a function of the primary gap length. The voltage drop across the leader channel in the primary gap is also plotted. All values were obtained using the model.

Flat section in predicted results

The flat section in the plot of the predicted flashover voltage from $1500 - y$ mm is due to the leader inception voltage of the primary gap as mentioned above. As discussed in **Chapter 5**, this leader inception voltage is calculated using the total length of the gap as opposed to just the length of the primary gap. As the total gap length is a constant the inception voltage will not change as a function of the primary gap length.

The use of the total length of the gap is based on the assumption that the floating object has little effect on the leader inception voltage when located near to the ground electrode and or plane. This assumption is discussed in **Section 6.1** and is shown to be acceptable by experimental validation.

Discontinuities in predicted results

The two discontinuities seen in the plot of the predicted flashover voltage at each turning point (just after 1200 mm and just before 1500 mm) are not characteristics of the model. They are glitches due to the incremental interval of the primary gap length. A 50 mm interval is used for the primary gap as the constant k_0 is calculated for 50 mm intervals in the electric field simulations as discussed in **Chapter 5** and **Appendix B**

6.2.2 Comparison between measured and predicted results

The measured and predicted flashover voltages are shown in *Table 6.3*. In comparing the two flashover voltages the following is observed:

- The floating object positioned at 50% has a lower measured flashover voltage than the predicted flashover voltage.
- The model predicts a lower flashover voltage for the 50% floating object position than the 25% floating object position when the measured values show that they are approximately equal.
- The flashover voltage of the 75% floating object position is substantially higher than the predicted value recalling that the leader inception voltage for the

primary gap is equivalent to the inception voltage calculated for a 3.36 m rod-rod gap.

Table 6.3: Comparison between measured and predicted flashover voltages for each floating object position.

Test Object	**Measured** [kV]	**Predicted** [kV]	**Difference** [%]
3.36 m rod-rod gap with 25% floating object	800	928	13.77
3.36 m rod-rod gap with 50% floating object	814	840	3.10
3.36 m rod-rod gap with 75% floating object	983	960	2.39

The model shows that the 50% position of the floating object is dominated by streamer breakdown of the primary gap, however the breakdown mechanism in the other gap still has an effect.

An increase in humidity or an increase in air density leads to an increase of the minimum electric field required to initiate and sustain the streamer mechanism as stated by Baldo et al. (1992). The testing was conducted at altitude, hence under lower air density conditions. Given that the results of the model are calculated for standard atmospheric conditions, a decrease in the streamer inception voltage would be expected. This is true of the floating object positioned at 25% as the measured flashover voltage is approximately 13% lower than the predicted value. However the floating object at 50% only showed an approximately 3% lower measured flashover voltage than predicted by the model.

In the following chapter, the photographs taken using the high speed camera are presented and discussed. The conclusions drawn in this chapter assist in the explanation of the photographs.

Chapter 7

High Speed Photography

The processed photographs from the high speed camera are presented. The trends seen in the photography are discussed with numerous examples given. A series of photographs showing the time progression of a channel forming in the primary gap is presented and discussed. A link between the time to crest of the applied impulse and the extent of branching of the discharge channel is discussed.

High speed photographs of the discharges within the gap are presented in this chapter. The photographs have been processed to enhance the discharge activity captured by the high speed camera. The high speed photography allowed for different stages of the discharge process to be captured. This adds a new dimension to understanding the measured results. The photographs showing the nature of the dischargess are correlated with the measured results providing further insight into the discharge process and the effect of the floating object.

Qualitative discussions are presented on the photographs under the following headings:

- **Section 7.1: Processing**
  The steps taken in processing the raw high speed photographs are discussed. This includes calculating the scale shown in the photographs and the effect of the high speed camera's exposure time used.
- **Section 7.3: Interaction with floating object**
  The interaction of the discharge channel with the floating object is discussed. Aspects include typical discharges seen for each floating object position and then the discharges off the tips of the floating object.

- **Section 7.4: Channel formation**
  The formation of a discharge channel due to the streamer mechanism is discussed. A series of photographs shows the progression of the channel through the primary gap.
- **Section 7.5: Branching and impulse front time**
  A relationship between the impulse front time and the observed branching of the main discharge channel is presented.

The camera specifications and setup details are discussed in detail in **Chapter 4**.

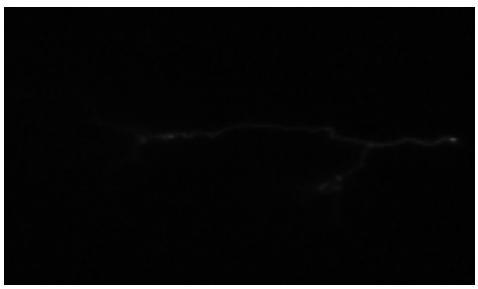
7.1 Processing

7.1.1 Image Manipulation

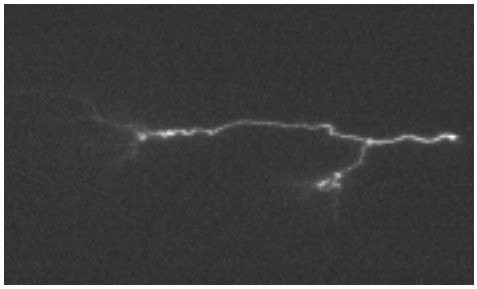
The high speed photographs presented in this chapter have been processed using `Gimp`[1]. *Figure 7.1a* shows part of an unprocessed photograph as downloaded from the high speed camera. As can be seen the discharge channel captured by the camera in the photograph is not clearly visible. The brightness and contrast of the photograph can be adjusted to improve the visibility of the discharge channel in the photograph as seen in *Figure 7.1b*. This can automatically be adjusted but best results are achieved by manually adjusting the brightness and contrast levels as each photographs differs.

While increasing the brightness and contrast of the photographs enhances the discharge channel, there is still information in the photographs that is not apparent. The equalise function is used to over enhance the photographs revealing more about the discharge channels. Before the equalise function can be applied, the image is inverted as seen in *Figure 7.1c*. The equalise function attempts to flatten the histogram of the image. In doing so the colours that appear frequently are stretched further apart in the histogram than those that do not. This over enhances the image as seen in *Figure 7.1d*.

[1] Gimp is an open source graphics editor, available at http://www.gimp.org.

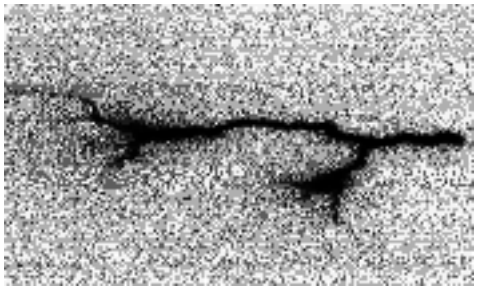


(a) Raw photograph.



(b) Processed photograph.

(c) Inverted photograph.



(d) Enhanced photograph.

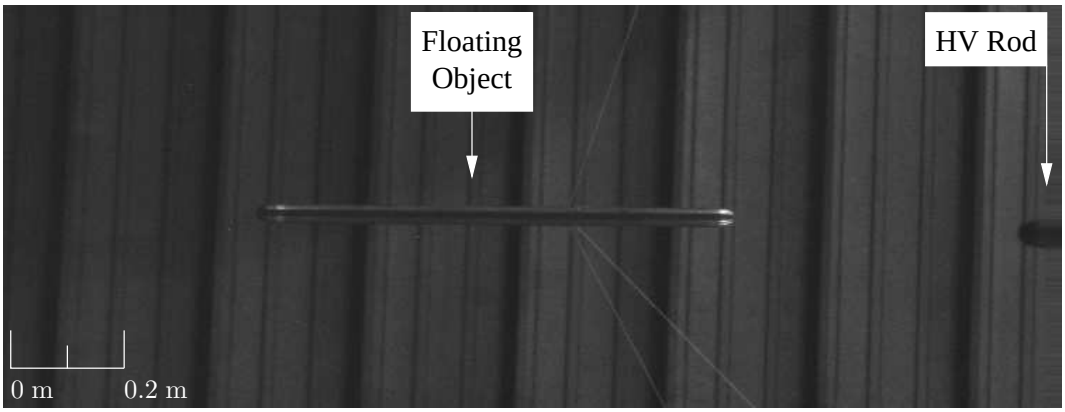
Figure 7.1: Processing steps applied to the high speed photographs. Such steps include increasing the brightness and contrast of normal photograph resulting in a processed photograph. Other steps include inverting the normal photograph and then equalising the photograph resulting in an enhanced photograph.

7.1.2 Orientation

The high speed photographs are oriented using photographs of the test object taken by the high speed camera with a longer exposure time before each U_{50} test begins. These photographs or setup photographs are used to identify the location of the high voltage electrode and if applicable the location of the floating object in the high speed photographs, as seen in *Figure 7.2*. The photographs also aid in visualising the scale of the electrodes and discharges.

7.1.3 Scale

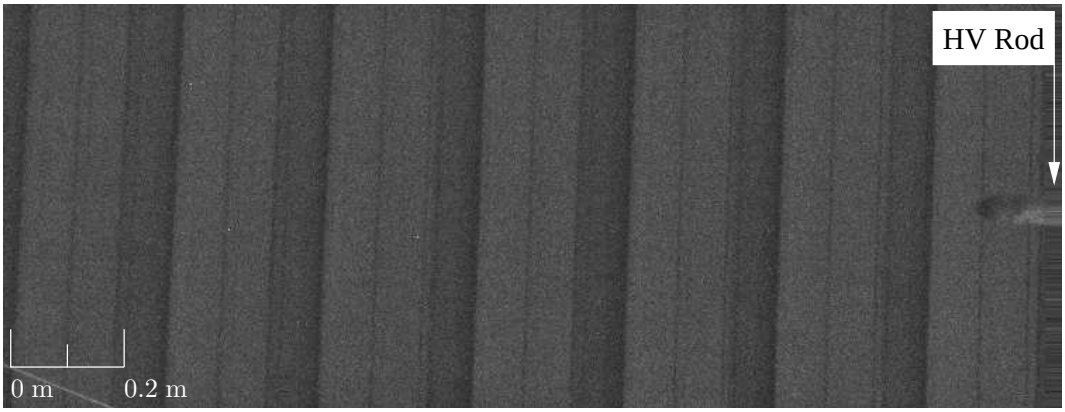
The camera is able to photograph an area roughly 1.9 m by 0.75 m in size. The scale in the photographs is determined by placing a pole with markings every 200 mm next to the test object and photographing it. The scale shown in the processed photographs can be applied in both the horizontal and vertical directions, allowing



(a) Floating object at 25% of the gap length.



(b) Floating object at 50% of the gap length.



(c) Floating object at 75% of the gap length.

Figure 7.2: Photographs showing the test object with the floating object at the three different positions using a longer exposure time.

for the length of the discharges to be measured and the radius of discharge channels or areas of ionisation to be estimated.

7.2 Exposure Time

The exposure time and the front time of the applied impulse determines the extent of the discharge activity within the gap that the photograph captures. It is likely that the photograph will capture any discharges propagating in the gap for exposure times less than that of the front time of the applied impulse.

If the front time is less than or equal to the exposure time the photograph captures all discharge activity in the gap for the duration that the applied voltage rises. It is assumed that little or no discharge development continues once the applied voltage has reached its peak and has begun to decay. This only applies to withstand events as during a breakdown event the discharge channel continues to propagate until it has bridged the gap. This can be before or after the impulse voltage peak.

7.3 Interaction with floating object

The effect of the applied impulse and the interaction of the discharge channel on the floating object is discussed for each position of the floating object.

7.3.1 Typical discharges

In characterising the U-curves for each of the positions photographs were taken of discharges. A trend is seen in the shape and size of the discharge for each position. The typical discharges observed for each position of the floating object is shown in *Figures 7.3* and *7.4*. The photographs in these figures were taken using an exposure time longer than the applied front time hence assumed to be longer than the duration of discharge progression.

Photographic evidence is consistent with the leader inception stage discussed in **Section 2.1**. During this stage leader channels develop from corona filaments during corona bursts. The difference between this stage and the previous is that a definite channel can be seen. This process is repeated. A number of definite discharge channels (leader channels) may be seen in the photographs due to this. This stage

is the final stage of development during a withstand event as a self-sustaining leader does not develop. If it did, breakdown of the gap would occur as it would successfully propagate the entire gap.

Floating object position at 25%

Figures 7.3a and *7.4a* show two typical photographs for the floating object positioned at 25%. It is clear that the primary gap is bridged. The direct nature of the channel seen in the photographs and the length of the primary gap (430 mm) suggest that the primary gap breaks down under the streamer mechanism each time. This channel formation will be discussed further in **Section 7.4**. Both photographs are taken with exposure times equal to or exceeding that of the time to crest of the applied impulses. It can be assumed that what is seen is the extent of the discharge for the given withstand event.

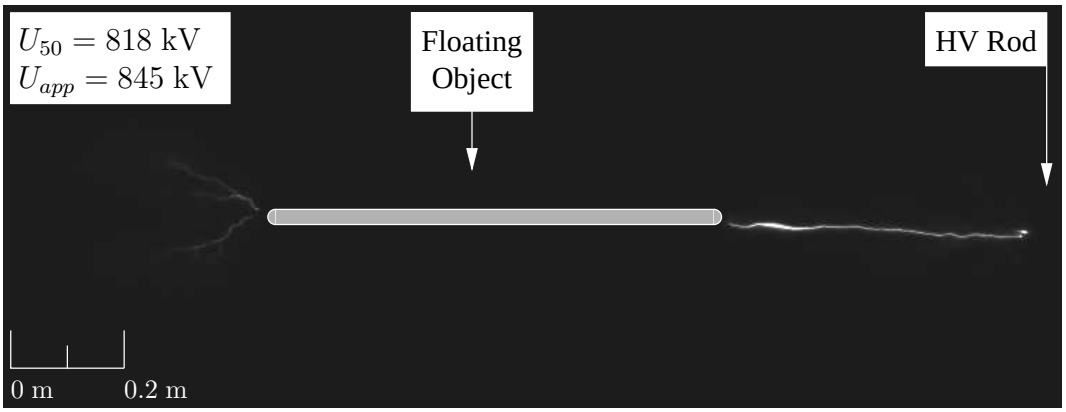
When the floating object is positioned at 25% complete breakdown of the primary gap occurs, however the breakdown process in the secondary gap never progresses to the continuous leader stage during a withstand event.

Floating object position at 50%

Figures 7.3b and *7.4b* both show typical photographs of discharges occurring in the primary gap of the floating object positioned at 50%. The primary gap is not seen to breakdown during the withstand events photographed. However discharge channels are seen to extend at least a third of the way into the primary gap. The mechanisms leading to the breakdown of the primary gap will be discussed further in **Section 7.4**. More than one channel is seen to have formed and started to propogate into the gap. It is not possible to determined whether the channels co-existed.

Floating object position at 75%

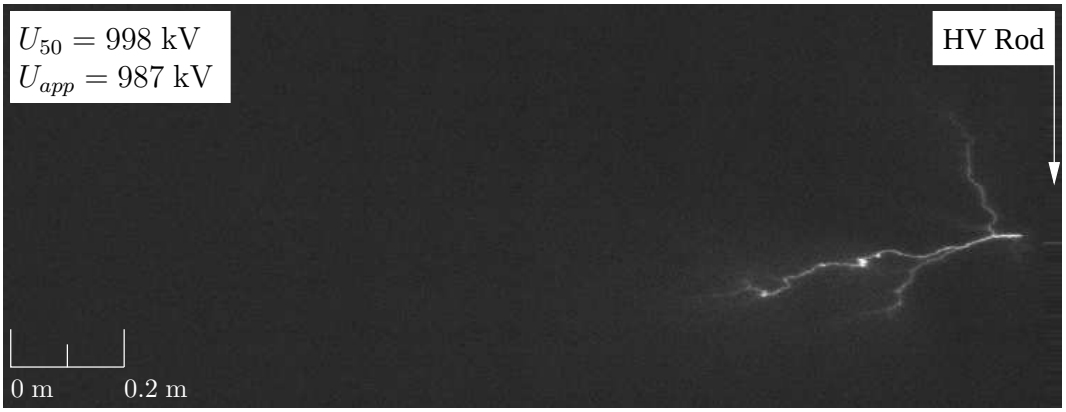
The photographs in *Figures 7.3c* and *7.4c* differ. A typical example of a discharge for the 75% floating object position is seen in *Figure 7.3c*. A longer dominant discharge channel is seen to propagate into the gap for impulses with magnitudes equal to or exceeding that of the U_{50} flashover voltage, during a withstand event.



(a) 25 µs front time, 25 µs exposure time.

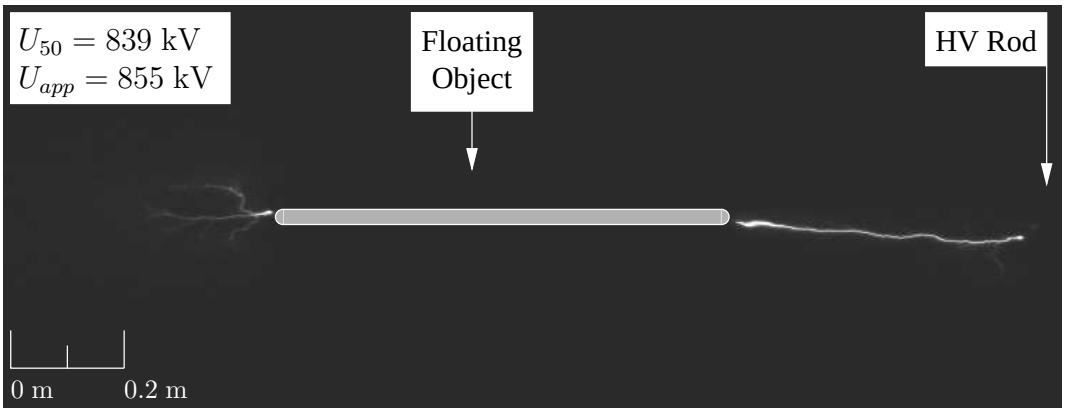


(b) 25 µs front time, 100 µs exposure time.



(c) 90 µs front time, 200 µs exposure time.

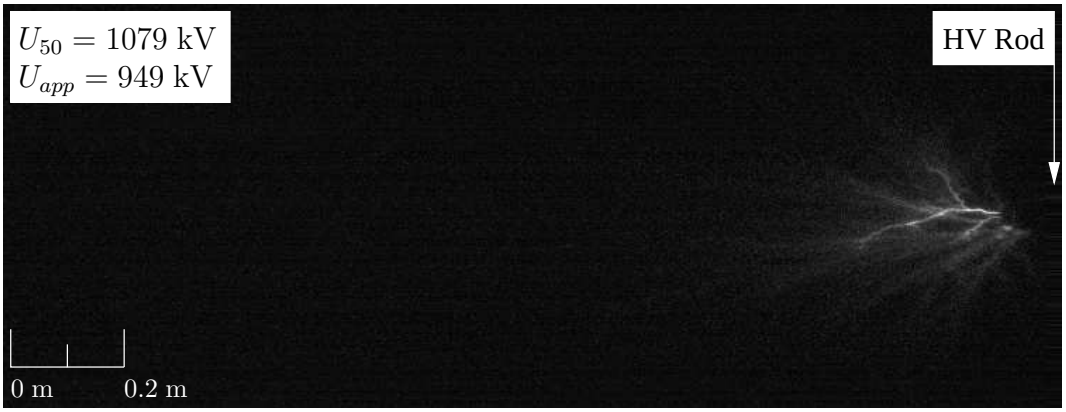
Figure 7.3: Photographs showing typical discharges for each position of floating object.



(a) 57 µs front time, 40 µs exposure time.



(b) 57 µs front time, 100 µs exposure time.



(c) 25 µs front time, 25 µs exposure time.

Figure 7.4: Photographs showing further typical discharges for each position of floating object.

The discharge seen in *Figure 7.4c* differs from the typical dominant channel in that there are a number of faint filaments originating from the high voltage electrode and no clearly dominant discharge channel extending into the gap. Furthermore it can be assumed that the extent of the discharge within the gap is shown in the photograph as the applied impulse front time is the same as the exposure time. The nature of the discharge can be explained by taking cognisance of the final U_{50} flashover voltage of 1079 kV and comparing it to the applied voltage of 949 kV. The applied voltage is significantly lower than the measured U_{50} flashover voltage. In addition the short front time of the applied impulse may also be responsible.

7.3.2 Discharge on tips of floating object

This section discusses the occurrence of discharges off the tips of the floating object. The presence of the floating object in the gap alters the electric field in the gap. There is an intensification of the electric field at the tips of the floating object. The electric field is due to the presence of space charge in the gap and the applied voltage on the high voltage electrode. Photographic evidence shows that discharge activity is present on the tips of the floating object for the 25% and 50% positions. This occurs when the electric field is high enough to cause the surrounding air to ionise.

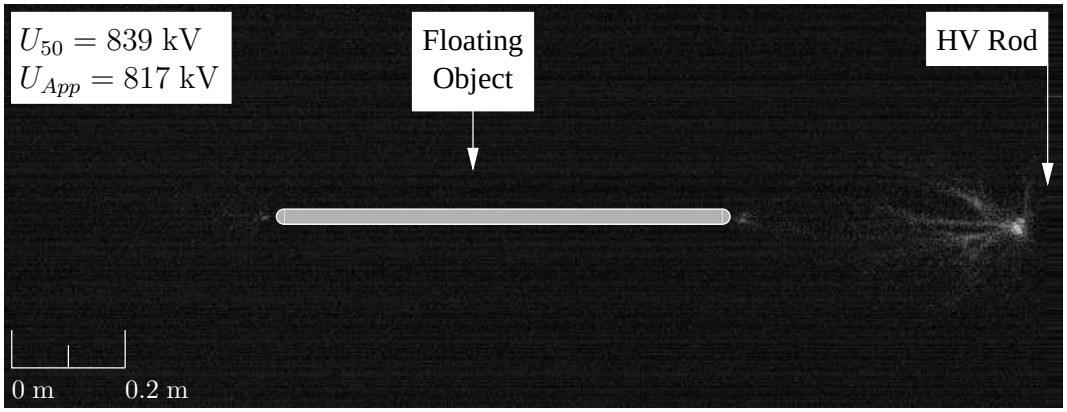
Floating object position at 25%

Examples of the discharge activity on both ends of the floating object are seen in *Figures 7.5* and *7.6*. Both the processed and enhanced photographs are shown.

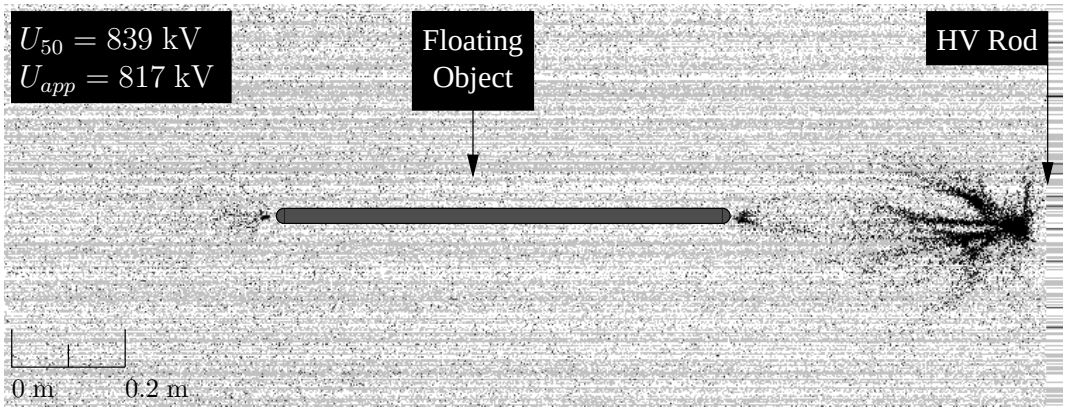
It is clear in both photographs that the primary gap is not bridged, however, the potential of the floating object is high enough to lead to to areas of high electric field stress. The air in these areas as seen around the tips of the floating object begins to ionise. The potential of the floating object is due to its geometric position and the space charge in the gap.

In *Figure 7.5* thin filaments of ionised air can be seen extending from the high voltage electrode. No clear channel formation can be seen and it is unclear as to whether these filaments co-existed. The air at the top tip of the floating object is seen to be ionising and extending in the direction of the filaments. There is also a hint of ionisation occurring at the bottom tip of the floating object.

This is consistent with the corona inception stage discussed in **Section 2.1**. During



(a) Processed photograph.



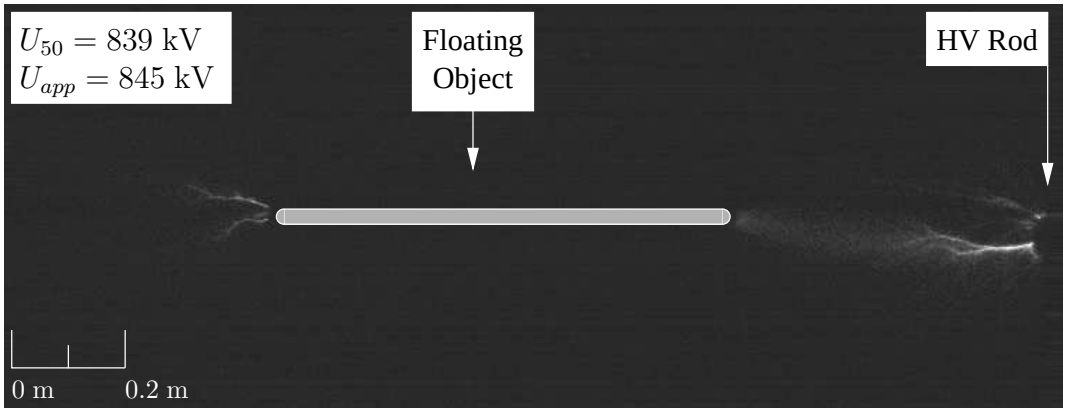
(b) Enhanced photograph.

Figure 7.5: Photographs of the floating object at 25%: 57 µs front time using 25 µs exposure time.

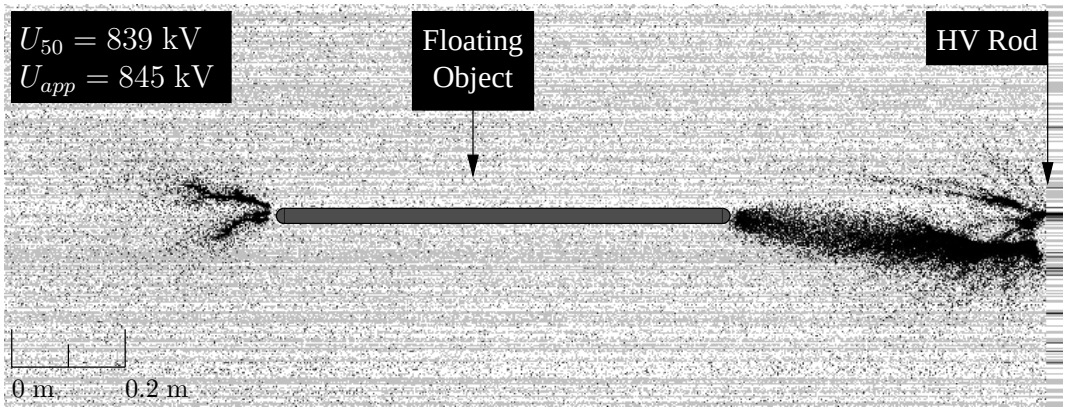
this stage corona bursts occur more than once as the voltage increases above a given level. This process repeats itself after each burst the electric field decreases and builds up again. During this stage nothing is visible to the naked eye.

Figure 7.6 is similar to that of *Figure 7.5* in that there are some faint filaments however a dominant discharge channel can be see extending into the gap. The air in between the tip of the discharge channel and the top tip of the floating object is completely ionised. The area around the tip of the floating object is denser suggesting that the air began ionising at the floating object tip as well as at the high voltage electrode.

At this point a clear channel has formed on the bottom tip of the floating object and has begun to propagate into the secondary gap. This channel would have initially started as an area of ionised air and will continue to propagate until the point at which it is no longer self sustaining.



(a) Processed photograph.



(b) Enhanced photograph.

Figure 7.6: Photographs of the floating object at 25%: 57 µs front time using 25 µs exposure time.

Floating object position at 50%

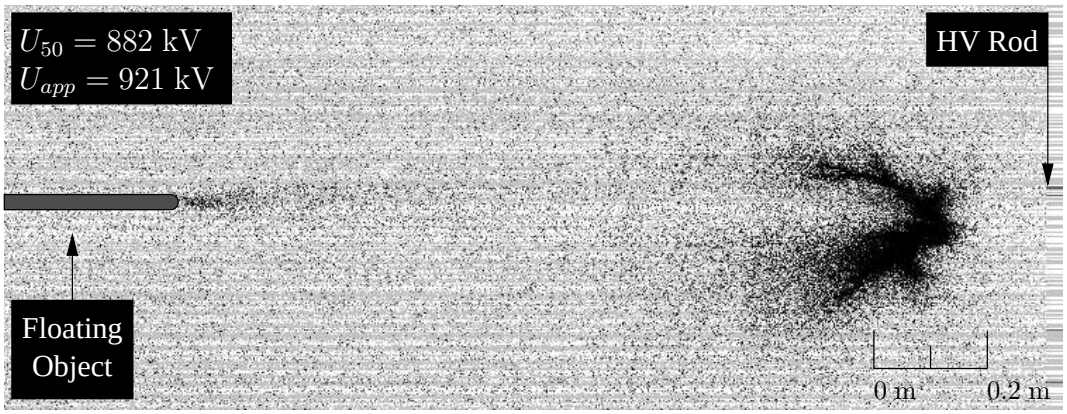
At the 50% position the floating object has less effect on the electric field as the electric field decreases in magnitude as it gets closer to the ground electrode and ground plane. Due to this no extensive discharge activity is expected on the tips of the floating object.

Very slight ionisation is evident on the top tip of the floating object in both the enhanced photographs shown in *Figure 7.7b*. *Figure 7.8b* shows ionisation at the top tip of the floating object and slight ionisation along the full extent of the primary gap. As with the floating object positioned at the 25% areas of more concentrated ionisation occur at the tip of the floating object and at the tip of the propogating discharge channel. This is because of the high local electric field stresses.

The bottom tip of the floating object is not visible in both the photographs shown



(a) Processed photograph.



(b) Enhanced photograph.

Figure 7.7: Photographs of the floating object at 50%: 25 µs front time using 100 µs exposure time.

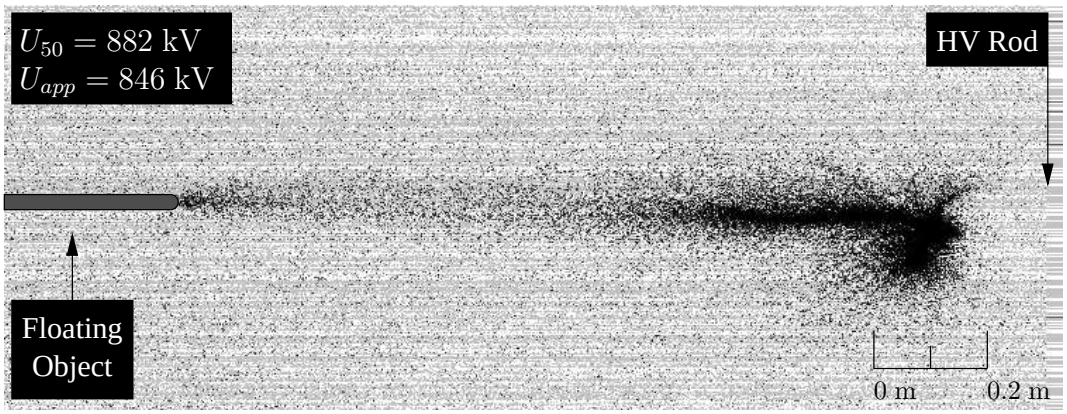
in *Figures 7.7* and *7.8*. Separate photographs taken of the bottom tip of the floating object showed no visible signs of ionisation occurring.

More activity would be evident on the tips of the floating object should the discharge channel initiated from the high voltage electrode continue to propagate further into the gap. As the channel gets closer the potential of the floating object will begin to rise leading to areas of high electric field stress.

In both *Figures 7.7* and *7.8* the exposure time is longer than the applied front time. It can be assumed that no further channel formation or ionisation had occurred thereafter.



(a) Processed photograph.



(b) Enhanced photograph.

Figure 7.8: Photographs of the floating object at 50%: 25 µs front time using 50 µs exposure time.

Floating object position at 75%

There was no photographic evidence to suggest that any ionisation activity occurred near the tips of the floating object when located at 75% during a withstand event. This is expected as the floating object is located at a greater distance from the high voltage electrode and in close proximity to the ground electrode and plane and hence is subject to a weaker electric field. The electric field strength surrounding the tips of the floating object is therefore below the threshold required for initiation of the ionisation of the air.

7.4 Channel formation

7.4.1 Floating object at 25% position

The floating object positioned at 25% was photographed during the application of impulses with a front time of 25 µs. All the photographs show the tip of the high voltage electrode, the complete view of the primary gap, the floating object and a section of the secondary gap, as seen in *Figure 7.2a*.

By changing the exposure time and repeatedly applying impulses of the same front time a stage of events can be identified for the formation and propagation of the discharge channel. In the following instance the stages of the formation of a streamer channel in the primary gap is described.

It should be noted that each photograph represents a unique withstand event as the high speed camera is not capable of capturing individual multiple frames.

Four different photographs are presented each taken with increasing exposure times ranging from 5 µs to 50 µs.

1. **Exposure time**: 5 µs (*Figures 7.9a* and *7.10a*)

   The applied voltage begins to rise and initially corona bursts will be expected on the tip of the high voltage electrode. The air in the vicinity of the electrode will begin to ionise when the electric field reaches a given value, assumed to be just below the critical streamer electric field gradient.

   A discharge channel has formed from the high voltage electrode due to the ionised air in the vicinity of the electrode, as seen in *Figure 7.9a*. A cone shape is seen at the tip of the channel. It extends roughly 150 mm ahead of the channel tip and its ending diameter is roughly 10 mm. This is attributed to the high localised electric field at the tip causing air proceeding the channel to ionise.

   No ionisation of the air between the high voltage electrode and the floating object is visible in *Figure 7.9a*. However the enhanced photograph in *Figure 7.10a* shows very slight ionisation starting to occur. This will increase as the applied potential continues to rise leading to an increase in the electric field in the gap.

   There is evidence of slight ionisation occurring on the bottom tip of the floating object, again in the form of a cone shape.

2. **Exposure time**: 10 µs (*Figures 7.9b* and *7.10b*)

   As the voltage of the applied impulse continues to rise the air between the floating object and the high voltage electrode will continue to ionise further. *Figures 7.9b* and *7.10b* show that the air in the primary gap has ionised. As this occurs the initiated channel will continue to propagate along the path of ionised air towards the floating object.

   The diameter of the column of ionised air as seen in the photographs is roughly $50 - 70$ mm. In comparison Carrara & Thione (1976) modelled the area of charge injection into the gap due to a discharge channel as a cylinder with an equivalent radius of 500 mm, as discussed in **Section 2.2**.

   Figure 7.10b shows that there is more ionisation occurring at the top tip of the floating object. The discharge activity off the bottom tip of the floating object continues to become more pronounced.

   Other filaments can be seen extending into the gap from the high voltage electrode. These filaments are possibly remnants from the corona inception stage. One of these filaments would lead to the formation of the channel seen in the photograph.

3. **Exposure Time**: 15 µs (*Figures 7.9c* and *7.10c*)

   The channel is seen to be continually propagating along the ionised air toward the floating object. An area of concentrated ionised air is seen to precede the channel tip. The potential of the floating object will continue to increase further facilitating discharge activity on the bottom tip.

   As seen in *Figure 7.9c*, the potential of the floating object is now high enough and leads to the formation of a discharge channel. In this case the leader inception voltage has been reached. As the applied voltage continues to rise the channel will propagate further into the gap. The leader will cease to propagate further after the voltage peak is reached unless it becomes self-sustaining. This process will more then likely be repeated as the applied voltage may not be high enough to sustain continuous leader inception. Two definite leader channels are seen to have formed even though the primary gap is not bridged. Once again it is unclear as to whether these channels co-existed, however it is unlikely.

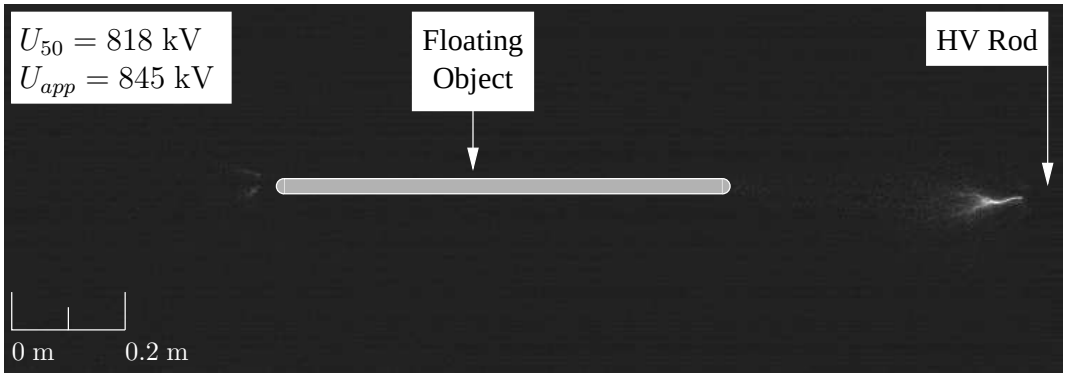
   The area of ionised air preceding the channel has become more developed due to the increased electric field between the floating object tip and the tip of the channel. This is clearer in the enhanced photograph in *Figure 7.10c*.

4. **Exposure time**: 50 µs (*Figures 7.9d* and *7.10d*)

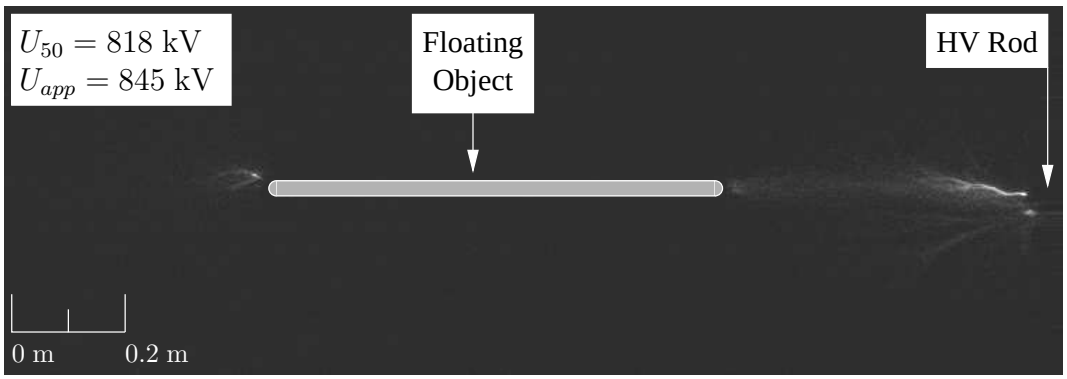
   The primary gap has been bridged by the advancing streamer channel. The potential of the floating object is now the same as the applied impulse voltage minus the volt drop across the channel.

   The photograph shows the extent of the discharge activity in the gap for the given withstand event. Leader channels are seen to have developed off the bottom tip of the floating object however only penetrated approximately 200 mm into the secondary gap.

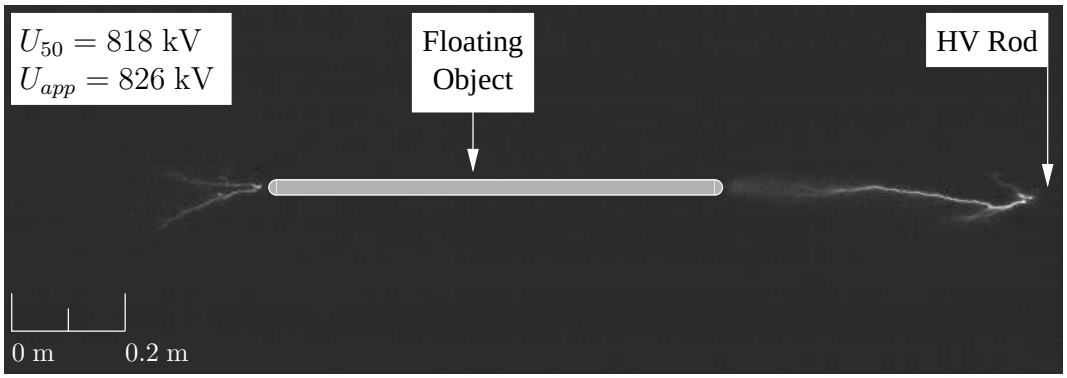
   The enhanced photograph shows the area of ionisation around the bottom tip of the electrode has greatly extended. This is attributed to an increase in the potential of the floating object as the primary gap is now bridged.



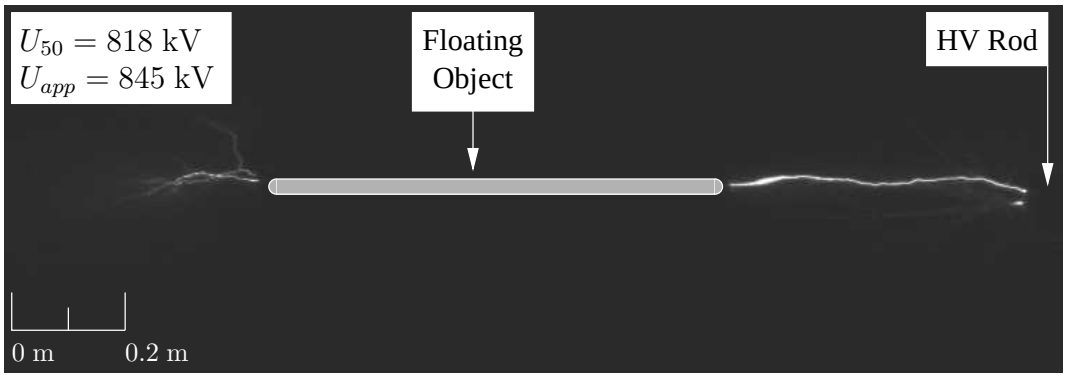
(a) 25 µs front time, 5 µs exposure time.



(b) 25 µs front time, 10 µs exposure time.

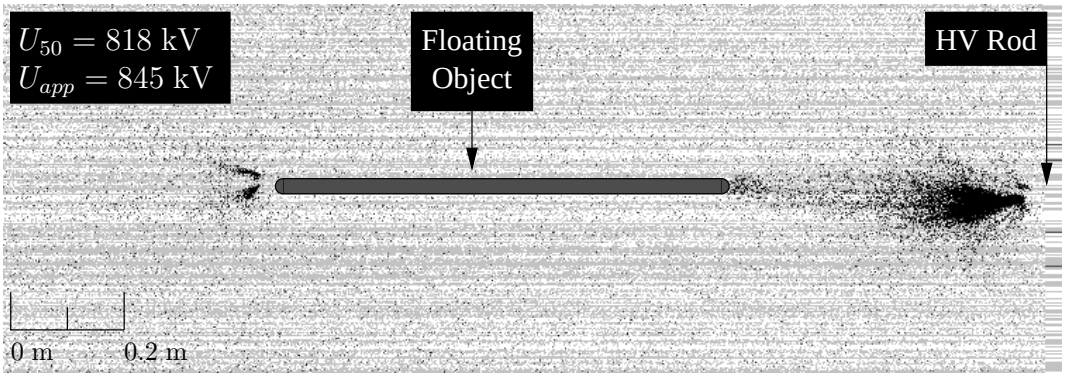


(c) 25 µs front time, 15 µs exposure time.

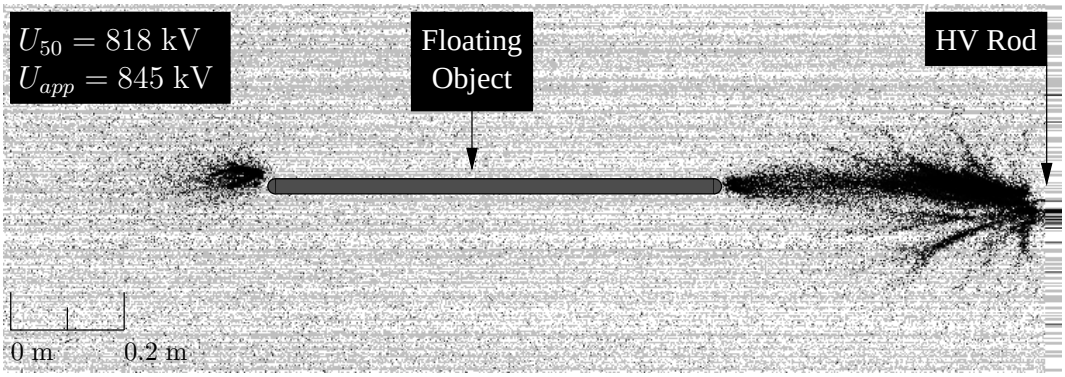


(d) 25 µs front time, 50 µs exposure time.

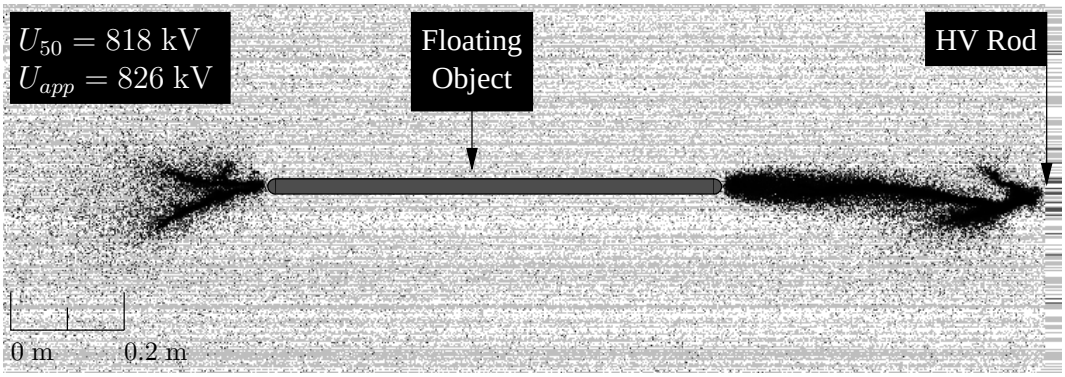
Figure 7.9: Series of photographs showing the formation of a streamer channel in the primary gap of the floating object positioned at 25% test object. **NOTE:** Each photograph was taken during a different applied voltage impulse.



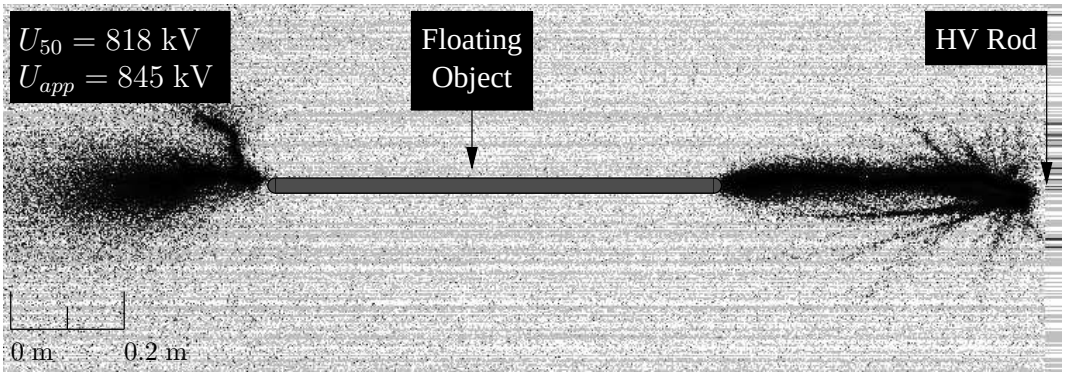
(a) 25 µs front time, 5 µs exposure time.



(b) 25 µs front time, 10 µs exposure time.



(c) 25 µs front time, 15 µs exposure time.



(d) 25 µs front time, 50 µs exposure time.

Figure 7.10: Series of enhanced photographs showing the formation of a streamer channel in the primary gap of the floating object positioned at 25% test object. **NOTE:** Each photograph was taken during a different applied voltage impulse.

7.4.2 Floating object at 50% position

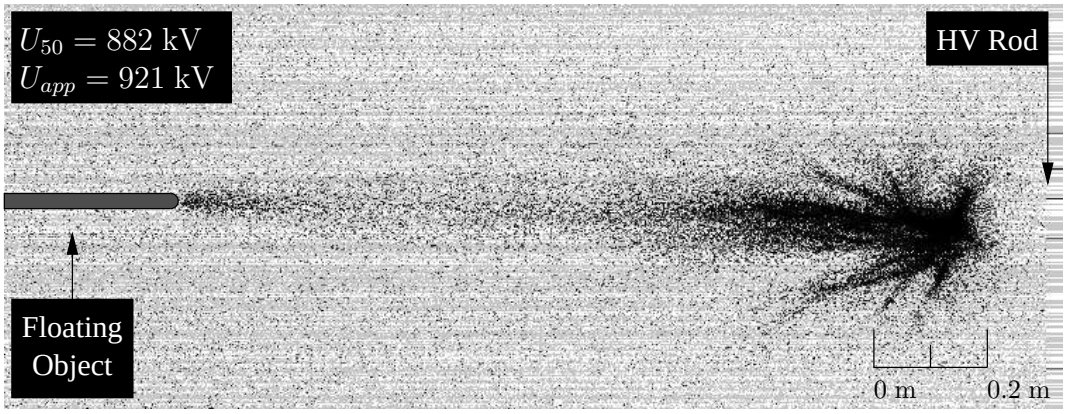
The photographs in *Figures 7.11a* and *7.11b* are of the floating object positioned at 50% during a withstand event. The photographs show the tip of the high voltage electrode, the full extent of the primary gap and the top tip of the floating object. The discharge activity seen is very similar to that discussed in **Section 7.4**, for the floating object positioned at the 25% position, in that both showed:

- An area of ionisation extending along the length of the primary gap.
- A direct, straight discharge channel propagating along the area of ionisation toward the floating object.

This suggests that the primary gap breaks down under the same mechanism as the primary gap of the floating object at the 25% position, namely under the streamer mechanism. Furthermore, this is consistent with the measured results presented in **Section 6.1**. Recalling that both the 50% and 25% position show very similar characteristics in that their CFOs are almost identical and both exhibit very short critical times to crest. The model also predicts that the primary gap of the floating object positioned at 50% will break down under the streamer mechanism as seen in *Figure 6.4a* in **Section 6.2**.



(a) Processed photograph.



(b) Enhanced photograph.

Figure 7.11: Photographs of the floating object at 50%: 25 µs front time using 100 µs exposure time.

7.5 Branching and impulse front time

Figure 7.12 shows a series of photographs taken of the 3.36 m rod-rod gap under applied impulses of different times to crest. It is noticeable in the photographs that the extent of the branching of the leader channel is a function of the time to crest of the applied impulse. The enhanced photographs are shown in *Figure 7.13*. The branching in the enhanced photographs is more evident.

It is observed that for shorter times to crest more branching along the main channel occurs. *Figures 7.12a* and *7.13a* shows the leader channels formed during the application of a 40 µs time to crest impulse in comparison to *Figures 7.12c* and *7.13c* which shows the leader channels formed during the application of a 190 µs time to crest impulse.

This can be explained by the rate of the voltage rise which is dependent on the time to crest and the extent of the overvoltage applied. A high rate of voltage rise is conducive to channel formation because the local electric fields are higher. However due to the high rate of rise they are of shorter duration. The higher electric fields lead to ionisation of the air hence allowing for more channels to form.

Observing *Figure 7.13* it is also noticeable that the branching occurs closer to the high voltage electrode. As the leader channel grows in length either the volt drop associated across the leader channel becomes a limiting factor in the growth and branching of the channel, or the duration of the impulse or magnitude of the impulse is not long enough to support the channel growth and further branching. For longer times to crest the lower rate of voltage rise is suited to continuous channel development of the main channel up to a point as seen by the U-shaped nature of the U_{50} flashover voltages when plotted.

This can be confirmed by photographing breakdown events and determining to what extent the branching occurs along the channel. If the branching is consistent along the entire channel through the gap then the impulse magnitude is the limiting factor. If the branching is localised near the higher voltage electrode then it can be assumed that leader channel volt drop is the limiting factor.

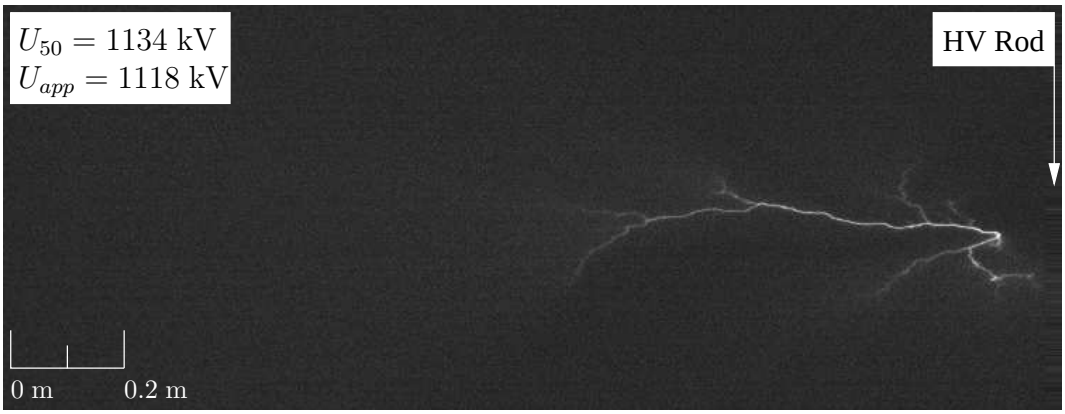
The difference between the applied voltage and the calculated U_{50} flashover voltage is considered small and hence the applied voltages are considered approximately equal to that U_{50} flashover voltage. This results in an overvoltage ratio of 1. Furthermore it is assumed that the photographs shows the extent of the discharge activity as the

exposure times are greater than the times to crest. The breakdown process in each photograph shows numerous leader channels. These channels are possibly formed during the leader inception stage.

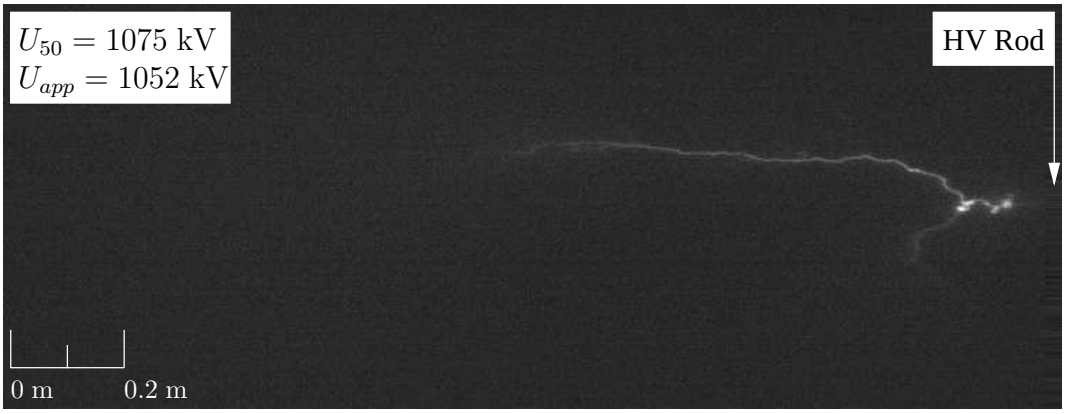
In the following chapter, the findings of the dissertation are summarised and recommendations for furthering the work outlined.



(a) 40 µs front time, 200 µs exposure time.

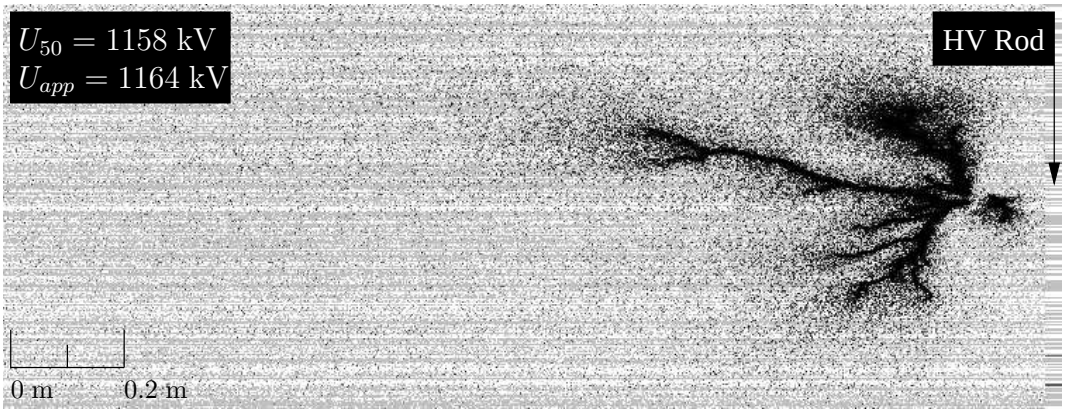


(b) 70 µs front time, 200 µs exposure time.

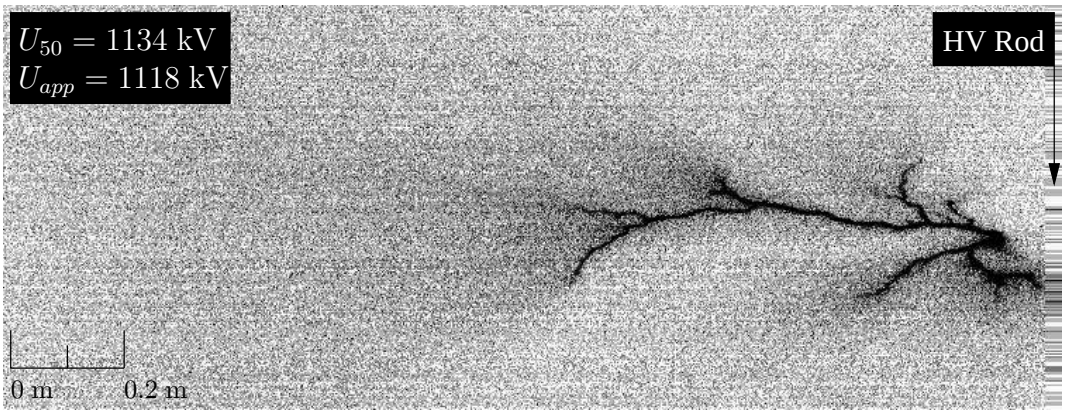


(c) 190 µs front time, 200 µs exposure time.

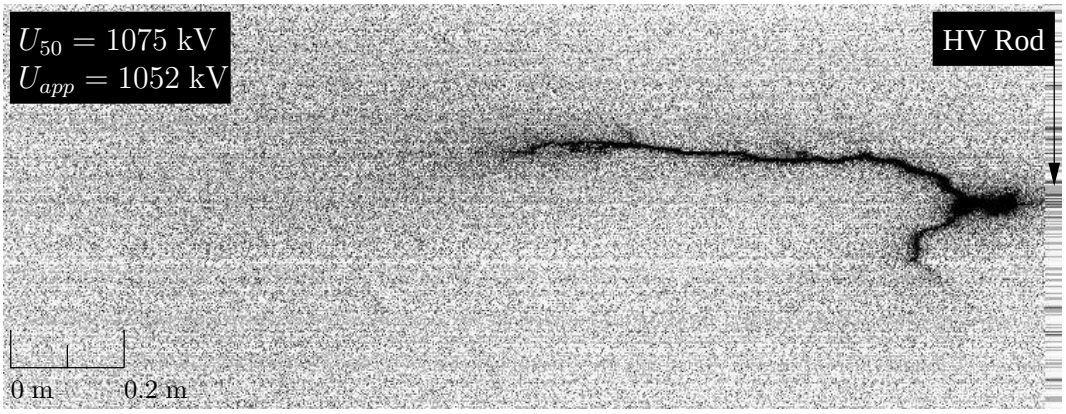
Figure 7.12: Photographs of discharges with different front times. The photographs are of the 3.36 m rod-rod gap.



(a) 40 µs front time, 200 µs exposure time.



(b) 70 µs front time, 200 µs exposure time.



(c) 190 µs front time, 200 µs exposure time.

Figure 7.13: Enhanced photographs of discharges of different front times. The photographs are of the 3.36 m rod-rod gap.

Chapter 8

Conclusion and Recommendations

The findings of the dissertation are summarised and recommendations for future work are given.

8.1 Recommendations

The following recommendations are suggested to build on the work and results presented. All the recommendations are based on the fact that all tests were conducted at altitude (reduced air density). It is therefore suggested that the above defined tests be repeated at sea level allowing for direct comparisons to be made.

1. The results will allow Rizk's model to be adapted and built on in conjunction with his work on air density effects.
2. High speed photography may identify changes in the channel formation or interaction with the floating object due to different altitudes and hence different air densities. If this were to be proven true further insight will be gained in understanding flashovers at different air densities.

Additional recommendations are suggested as follows:

1. Verify the proposed relationship between the impulse front time and the branching of the discharge channel. Further testing should include applying the same ratio of overvoltages for each of the front times. The results will confirm the relationships between front time and the extent of branching and the effect

of overvoltage on branching. The factor limiting branching should also be established, as discussed in **Section 7.5**.

2. The above results can be used for comparative purposes when performing similar up-down tests on glass insulator strings with broken discs present. The aim would be to determine whether the insulator string and broken discs have any similarities to that of a rod-rod gap with a floating object present.

8.2 Conclusion

The culmination of the results allows for a number of conclusions to be drawn of which all lead to a better understanding of both the theoretical model and actual discharge phenomenon in gaps with floating objects present, more specifically rod-rod gaps with a rod floating object. To surmise, the following conclusions are drawn:

1. In long air gaps with floating objects both streamer and leader mechanisms may be present. When the floating object is on the high voltage side of the gap, streamer breakdown will be present in the primary gap and leader in the secondary gap. When the floating object is close to earth potential, leader is present in the primary gap and streamer in the secondary gap.

2. The presence of streamer breakdown reduces the critical time to crest (t_{c2}). This means that t_{c2} for a gap with an object floating will be shorter than t_{c2} in a single air gap of equivalent air gap length.

3. The initiation and early propagation of a leader is largely dependent on the total gap length, particularly when the floating object is positioned close to the earth electrode. For this reason the breakdown voltage for a gap with a floating object in the vicinity of the earth is significantly greater than the breakdown voltage of an equivalent air gap without a floating object.

The following conclusions are drawn from the analysis of the high speed photography:

1. When the streamer mechanism is present in a gap, ionisation of the air is seen to occur prior to the channel formation. The ionisation continues to occur as the channel propagates until the entire gap has ionised allowing the streamer channel to bridge the gap. This is seen in both primary gaps of the floating object positioned at 25% and 50% respectively.

2. The extent of branching of a leader channel in a gap without a floating object present is a function of the applied impulses time to crest. The photographic evidence presented shows that more branching is apparent for short times to crest.

Appendix A

Complete Results

A figure summarising the different test configurations is presented in support of the complete set of the experimental test results, presented in tabular format. The atmospheric conditions measured during the tests are included.

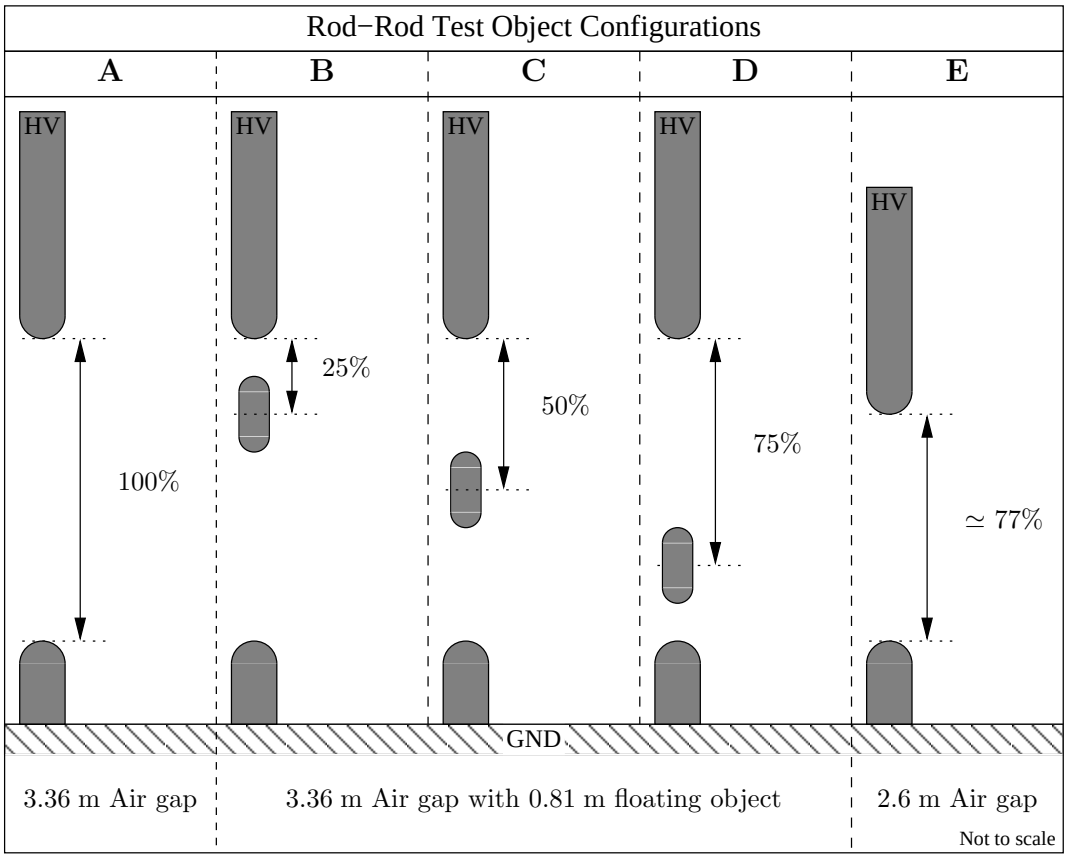
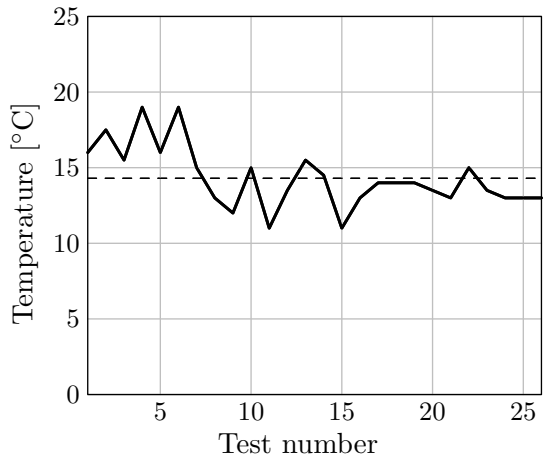


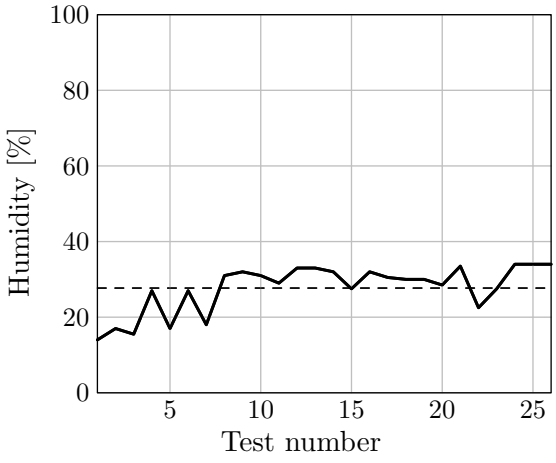
Figure A.1: Summary of the test configurations.

Table A.1: Summary of measured results for the different gap configurations tested, shown in *Figure A.1.*

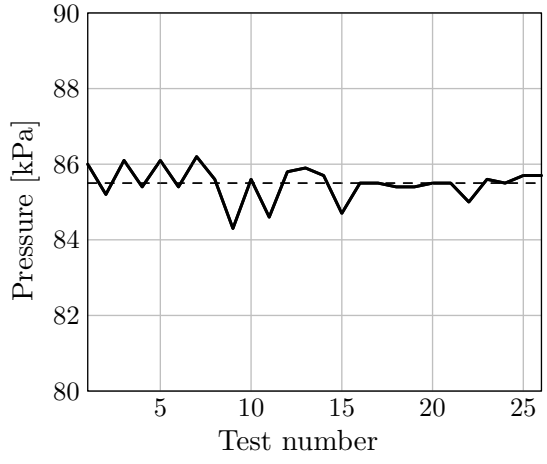
	Test No.	**Configuration**	$\mathbf{t}_c$ [µs]	$\mathbf{t}_{bd}$ [µs]	$\mathbf{U}_{50}$ [kV]	**STD** [%]	**T** [°C]	**P** [kPa]	**H** [%]
A	1	3.36 m Rod-Rod	41	72	1158	2.7	16.0	86.0	14
	2		60	99	1096	2.5	17.5	85.2	17
	3		70	90	1134	2.0	15.5	86.1	16
	4		100	105	1064	2.4	19.0	85.4	27
	5		120	124	1044	1.9	16.0	86.1	17
	6		140	101	1032	2.1	19.0	85.4	27
	7		190	146	1075	1.2	15.0	86.2	18
B	8	Rod-Rod with FO	25	45	818	2.0	13.0	85.6	31
	9	at 25% from HV	42	45	800	2.9	12.0	84.3	32
	10		74	78	877	2.2	15.0	85.6	31
	11		57	52	839	1.9	11.0	84.6	29
C	12	Rod-Rod with FO	72	79	847	3.1	13.5	85.8	33
	13	at 50% from HV	40	71	848	2.4	15.5	85.9	33
	14		24	57	882	2.6	14.5	85.7	32
	15		57	74	814	2.0	11.0	84.7	28
D	16	Rod-Rod with FO	25	40	1079	1.4	13.0	85.5	32
	17	at 75% from HV	40	51	1035	2.4	14.0	85.5	31
	18		57	62	998	2.0	14.0	85.4	30
	19		70	66	983	1.8	14.0	85.4	30
	20		91	72	998	1.9	13.5	85.5	29
E	21	2.6 m Rod-Rod	58	64	944	1.9	13.0	85.5	34
	22		70	70	915	1.7	15.0	85.0	23
	23		91	79	909	2.0	13.5	85.6	28
	24		120	108	903	1.9	13.0	85.5	34
	25		140	101	924	1.5	13.0	85.7	34
	26		165	125	905	1.9	13.0	85.7	34



(a) Temperature



(b) Humidity



(c) Pressure

Figure A.2: Temperature, pressure and humidity plotted against the test number to show variations in atmospheric conditions during testing.

Appendix B

Calculation of Rizk's constant using Electric field simulation

The calculation of Rizk's constant, using electric field modelling, for use in Rizk's model is discussed. The aspects of Electro, the simulation tool, are discussed. The approach taken in implementing the simulation model is discussed and the results presented.

B.1 Introduction

In Rizk (1994)'s model for determining the flashover voltage of a gap with a floating object present, Rizk makes use of a constant that relates the potential of the floating object to the applied voltage on the high voltage electrode. This constant is then used in determining the streamer inception voltage for the primary gap of the given gap. The following chapter discussing the steps taken in calculating the value of the constant for the given test setup discussed in **Chapter 4**.

B.2 Approach

Rizk (1994) suggests using the charge simulation method in determining the numerical value of constant k_0. There are numerous numerical techniques that exist for solving electrostatic field problems. The methods are divided into two categories based on the approach taken. The boundary element method and the charge simulation method techniques are in the same category. Both of which are suited for solving problems with large or infinite boundary conditions.

B.3 Electric field modelling package

`Electro` by `IES Software` is used as the simulation application. `Electro` is a 2-dimensional electric field simulation program that uses the boundary element method. `Electro` is capable of 2-dimensional simulations and rotational 2-dimensional simulations.

B.3.1 Rotational 2-D models in electro

`Electro` supports both x and y rotational simulations. Rotational simulations extend themselves to symmetric models where an axis of symmetry can be clearly defined. In defining a rotational simulation the model is simulated as if it were swept through a 360° arc tracing out a solid.

B.3.2 Balanced and unbalanced mode

Most geometries modelled in high voltage engineering tend to have a large ground plane in the vicinity such as the earth. This ground plane needs to be accounted for. Normally it would need to be modelled and given a 0 V boundary condition as stated in `Electro`'s online help. This inherently increases the problem complexity and size and results in a needless waste of computing time. It is because of this that `Electro` offers the option of changing how the boundary conditions of the model or the voltage at infinity are defined.

The two options are termed *Balanced mode* and *Unbalanced mode*:

- Balanced mode assumes the voltage at infinity to be the average of the maximum and minimum system voltages. This ensures a charge balance.
- Unbalanced mode assumes the presence of a near infinite ground plane in model space hence the voltage at infinity to be zero.

The unbalanced mode is useful when simulating a rotational symmetrical object in the presence of a ground object such as an insulator string attached to a tower. The tower is not rotationally symmetrical as is the insulator. It is therefore impossible to model the effect of the tower of the electric field surrounding the insulator due to

the nature of the simulation. The unbalanced mode can be used to account for the presence of the tower geometry.

It should be noted that balanced and unbalanced modes are not limited to just rotational simulations but can be used in normal 2-D model simulations.

B.3.3 Parametric simulation

`Electro` provides the user with a parametric tool that allows the user to change different parameters in the model without having to generate a new unique model each time. The user is required to define parameters in the existing model and specify loops that dictate how the parameter should be changed. The parametric tool also allows for nested loops providing further benefit. An example of such parameters include displacement, rotation and stretching of objects within the model as well as increasing or decreasing the magnitudes of charges or voltages set. The user is also able to specify linear or non-linear discrete steps or intervals for the given parameters.

B.4 Simulation model

B.4.1 Model setup

The model used in the simulation is representative of the configuration used during the testing. In the experimental configuration the ground rod electrode is placed on a table in order to isolate it from the ground. It is then connected to ground using copper tape in series with a shunt resistor. For the purpose of the simulation the copper tape and shunt are treated as if the ground electrode where extended to the ground plane.

The ground plane is modelled as roughly twice the length of the air gap. There is no exact definition as to what the ratio of the length of the ground plane to the length of the air gap and electrodes should be. Increasing the ground plane further would have little effect on increasing the accuracy. It would also not be representative of the actual configuration as there is equipment and other objects in the the surround vicinity that would need to be modelled.

A 2-D y-rotational model is defined as the configuration is symmetrical through the gap axis. The simulation model is shown in *Figure B.1.*

B.4.2 Model properties

The electrodes and floating object are modelled as solid copper pieces however this is of little consequence as the current will flow on the surface due to skin effect. The medium surrounding the electrodes is modelled as having the same conductivity and permittivity as air at standard atmospheric conditions. *Table B.1* lists the conductivities and permittivity's used for each material in the model.

Table B.1: Conductivity and permittivity's of materials used in model.

Material	**Conductivity** [S/m]	**Permittivity** [F/m]
Air	0	1.0006
Copper	59.6×10^6	0

B.5 Approach to simulation

The aim of the simulation is to plot the value of k_0 as a function of the length of the primary gap where the primary gap is defined as the distance from the bottom of the high voltage electrode to the tip of the floating object. As mentioned previously k_0 is used to relate the voltage induced on the floating object to the voltage applied to the high voltage electrode.

k_0 is calculated by dividing the voltage induced on the floating object by the measured voltage on the high voltage electrode. In a sense k_0 is the voltage of the floating object unitised, for this reason the voltage applied to the high voltage electrode is set to 1 V with respect to the ground electrode.

Once the model was setup the parametric tool was used to create a loop with the position of the floating object as the parameter. The floating object is initially positioned 50 mm from the tip of the high voltage electrode as seen in in *Figure B.1.* The loop is set to displace the floating object by 50 mm along the gap axis after

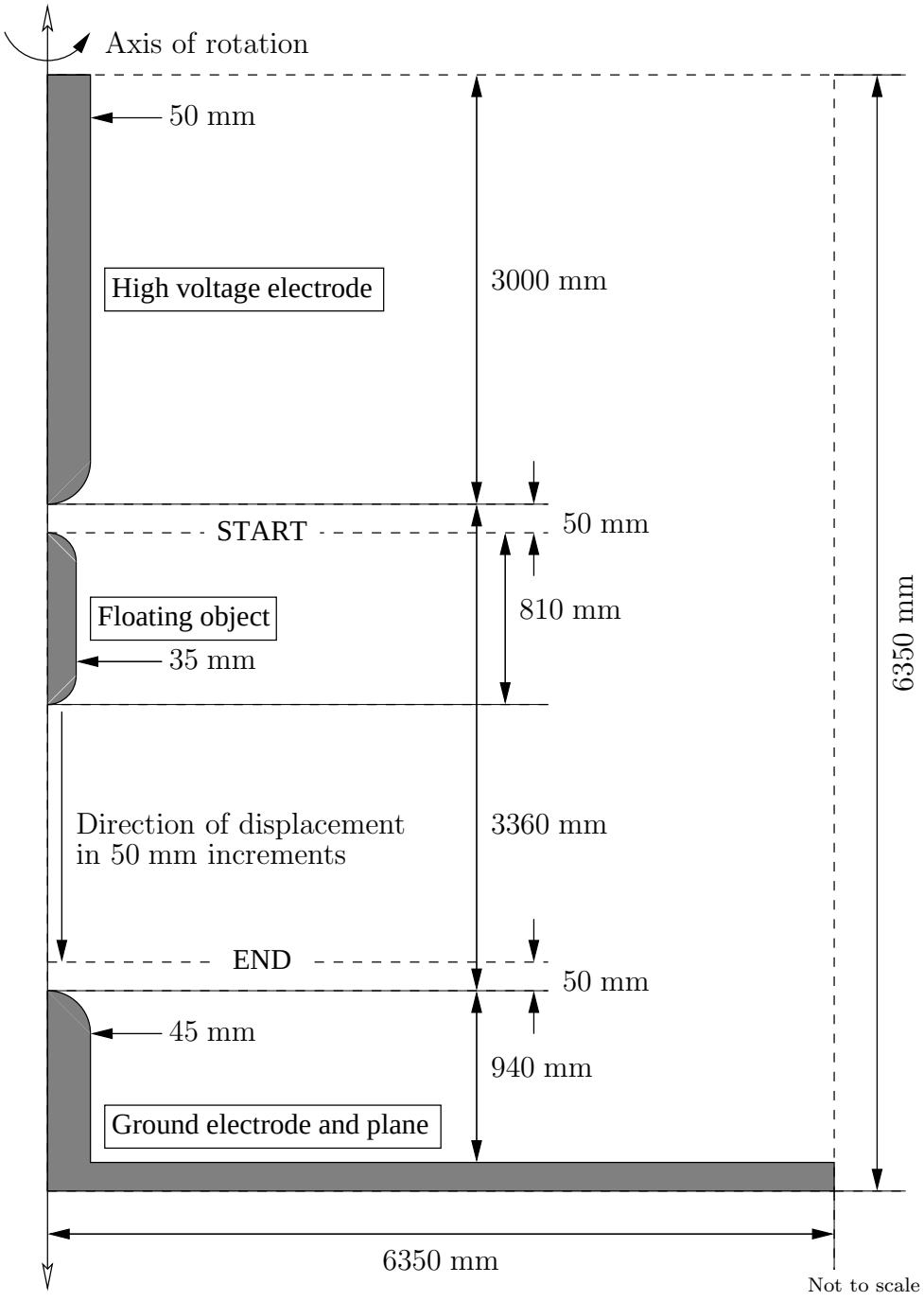


Figure B.1: Test configuration model used for electric field simulation.

each iteration. The loop terminates after the bottom of the floating object is within 50 mm of the tip of the ground electrode.

The voltages as measured along the gap axis at 50 mm intervals for each position of the floating object are output to a file when the simulation is run. GNUOctave [1] is then used for processing of the results.

B.6 Validity of results

Electro is only capable of running simulations under steady state conditions. It requires that the user defines the simulation frequency of the model with the default set to 50 Hz. The constant k_0 is used in calculating the voltage induced on the floating object at an instant in time during the rising front of an applied impulse. The frequency of the induced voltage is unknown, for this reason the simulation frequency is set to 0.001 Hz or near DC. The effect of changing the simulation frequency has little effect on the induced voltage or the constant k_0.

B.7 Simulation results and conclusion

The results from the simulation is plotted in *Figure B.2*, showing the constant k_0 as a function of the primary gap. The results are expected as k_0 decreases exponentially as the floating object is moved further away from the high voltage electrode. The decrease in k_0 becomes less evident as the floating object gets closer to the ground electrode and plane. k_0 tends to 1.0 as it approaches the high voltage electrode and tends to 0.0 as it approaches the ground electrode.

[1] GNU Octave is an open source program used for computing numerical problems. It is part of the GNU project and is available at http://www.octave.org.

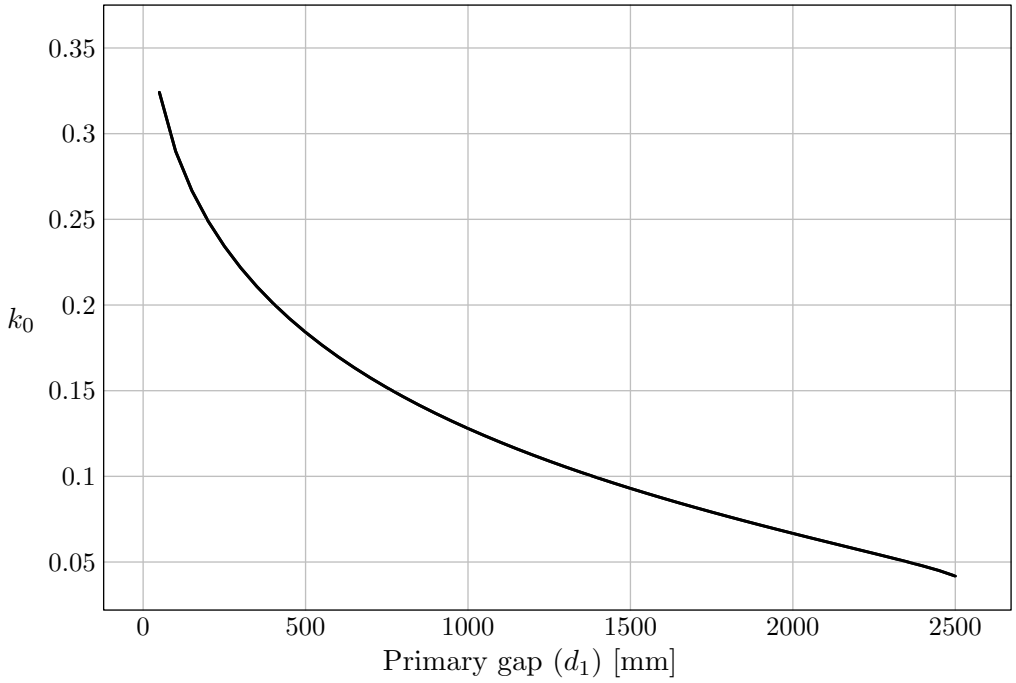


Figure B.2: Constant k_0 plotted as a function of gap sizing.

Appendix C

Implementation of Rizk's Model

Rizk's model is implemented using Octave. The code for the model is included and can be viewed in conjunction with **Chapter 5**.

GNU Octave is an open source program used for computing numerical problems. It is part of the GNU project and is available at http://www.octave.org. GNU Octave is for the most part compatible with MATLAB by Mathworks.

```
% Calculate Ub for rod-rod gap with rod floating object using
% Rizk's work
%       d  - length of gap
%       h  - length of ground rod
%       d0 - length of floating object
%       d1 - length of gap 1
%       k0 - geometric potential factor
%       Es - minimum streamer gradient
%       o  - Sigma (standard deviation)

function [U50,Us1,Ulc1,Ub1,Us2,Ulc2,Ub2,Uss,dUlc1] = RizkFO(d,h,d0,d1,k0,Es,o)

% Calculate length of gap 2.
        d2 = d-d0-d1;

% Gap 1
        % Streamer breakdown
        Us1 = (Es*d1)/(1-k0);

        % Positive leader inception voltage
        Ulc1 = 1556/(1+(3.89/(h+d)));

        % Leader volt drop in gap 1
        A = (50*d1/(1+(3.89/d1)));
        B = 38.5*log(8+(7*exp(-1.33*d1/(1+(3.89/d1)))));
        dUlc1 = A+B;

        % Approximation for leader volt drop in gap 1
        % dUlc1 = (50*d1/(1+(3.89/d1)))+78;

% Instant gap 1 is bridged

        % Determine which mechanism gap 1 breaks down under
        if ( Ulc1 > Us1 )
                Ub1 = Us1;
                % Potential of floating object
                Uss = Us1 - dUlc1;
        else
                Ub1 = Ulc1;
                % Potential of floating object
                Uss = Ulc1 - dUlc1;
        endif

% Gap 2
        % Streamer breakdown
        Us2 = Es*d2;

        % Positive leader inception voltage
        Ulc2 = 1556/(1+(3.89/(h+d2)));

% Breakdown voltage

        if ( Us2 < Ulc2 )
                Ub2 = Us2;
```

```
54          else
                    Ub2 = Ulc2;
56          endif

58          Ub2 = Ub2 + dUlc1;

60  % Determine U50
            if ( Ub1 > Ub2 )
62                  Ub = Ub1;
                    U50 = Ub1/(1-(3*o));
64          else
                    Ub = Ub2;
66                  U50 = Ub2/(1-(3*o));
            endif
68  end
```

Appendix D

Discussion on Current Measurement

An attempt was made to measure the pre-breakdown current of the test objects tested. The measurement system is discussed and the associated difficulties with such a measurement are discussed. Current measurements were obtained however the analysis results were inconclusive.

D.1 Introduction

The aim of measuring the pre-breakdown current is to determine whether it is possible to identify any characteristics on the current waveform, during a withstand or breakdown event, that are specific to either the leader or streamer mechanism. There characteristics could either be evident in the shape of the current waveform or appear on it's frequency spectrum.

On identifying any characteristics relating to the streamer or leader mechanisms, it is envisaged that these characteristics could be used to identify the mechanisms present in flashovers of gaps with floating objects.

Given the above aims, obtaining the shape of the current waveform was a priority and less so obtaining maximum accuracy. The initial current measurements were successful in that current waveforms where obtained for rod-rod gaps. However current measurements taken during the testing of rod-rod gaps with floating objects present were inconclusive. The difficulties associated with the given measurement is discussed.

D.2 Current measurement setup

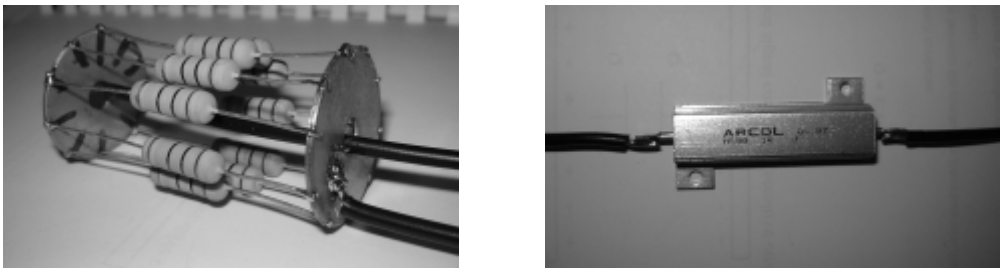
D.2.1 Approach Taken

Initially a pearson coil was thought to be the best method of measuring pre-breakdown currents however acquiring a coil for the given current range with a suitable resolution on the output was difficult.

A shunt resistor connected in series with the ground electrode and the ground return path was then used for the current measurement. The differential voltage developed across the shunt resistor due to the current flow from the ground electrode to the ground return path is then measured using an oscilloscope.

D.2.2 Implementation

A shunt resistor with the following specifications 1 Ω 50 W was used. Two types of resistors where available, the first, a single manufactured resistor meeting the above specifications while the second was constructed from 10-off 10 Ω 1 W resistors. The two resistors are shown in *Figure D.1.* The constructed resistor makes use of a low inductive design by feeding the conductor back through the center of the resistors. The value of the shunt resistor was chosen so as to give a 1 : 1 current to voltage relationship, ignoring any attenuation existing in the protection and measurement system.



(a) Constructed shunt resistor. *(b)* Manufactured shunt resistor.

Figure D.1: Two types of 1 Ω 50 W shunt resistor used for the current measurement.

As a precautionary measure a gas arrestor is connected in parallel with the shunt resistor. A transient voltage suppression diode (Transorb) is also added in parallel

after the gas arrestor. The transorb has a reaction time in the order of picoseconds while the gas arrestor is orders of magnitude slower. For this reason an impedance (5 Ω resistor) is connected in series between the gas arrestor and the transorb. The resistor limits the current through the transorb until the gas arrestor becomes active.

A 50 Ω resistor is also connected in parallel so as to terminate the connected coaxial cable in its characteristic impedance. *Figure D.2* shows the circuit diagram. The protection circuit is housed in a tin box that is bonded to the ground return path to shield it. *Figure D.3* shows the current measurement setup.

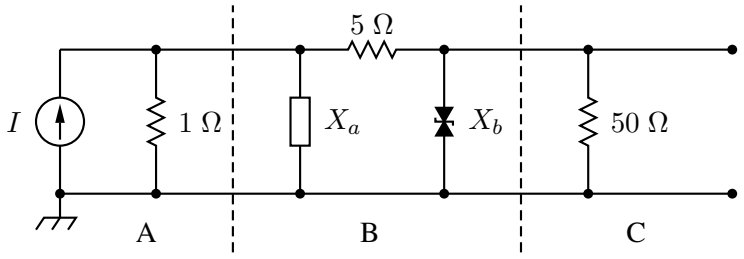
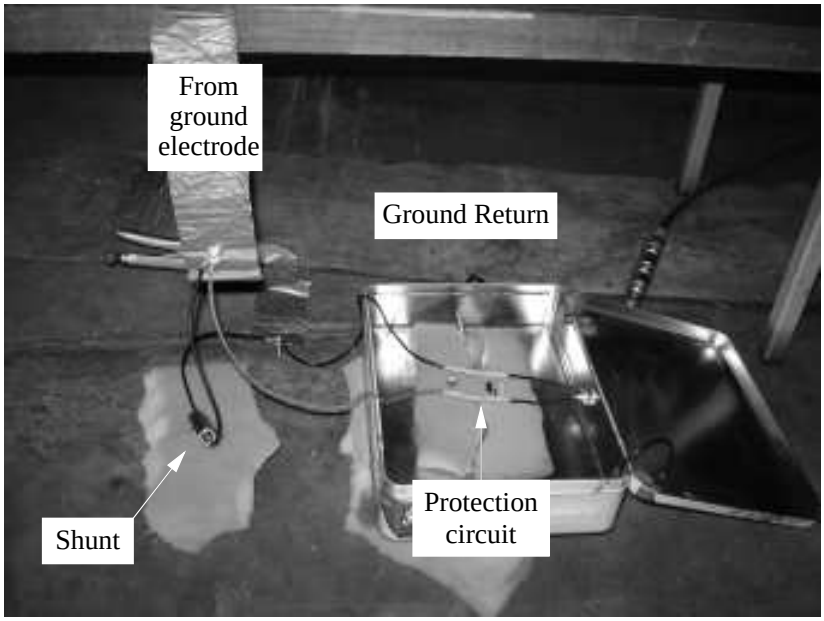
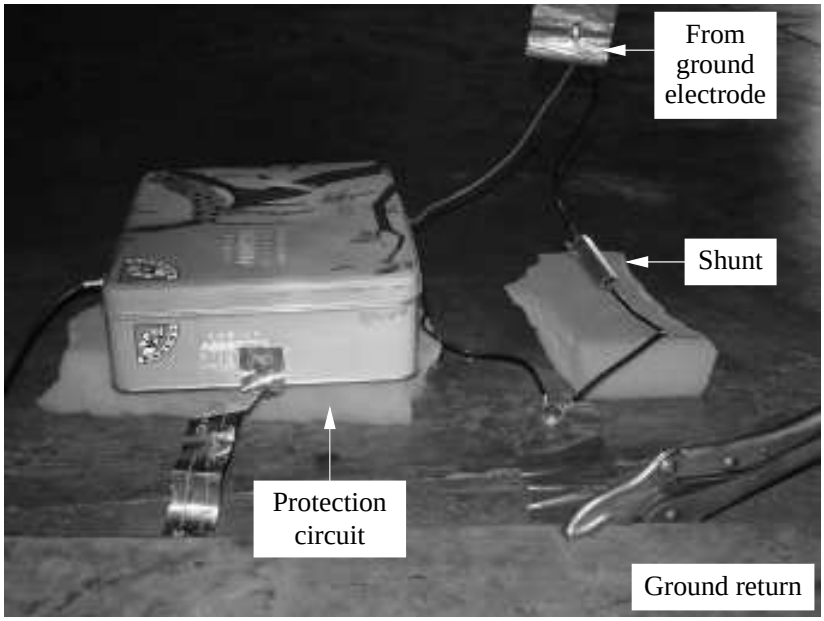


Figure D.2: Circuit diagram of shunt resistor and protection circuitry.
X_a - Gas arrestor.
X_b - Transient voltage suppression diode (Transorb).
A - Shunt resistor.
B - Protection circuit.
C - Circuit connected to oscilloscope via coaxial cable.



(a) Front view of measurement circuit.



(b) Rear view of measurement circuit.

Figure D.3: Shunt resistor installed between the ground return path of the ground electrode used for current measurement.

D.3 Results and analysis

D.3.1 Waveform analysis

The current and voltage waveforms of both a withstand and breakdown event due to the application of an impulse with time to crest of 70 µs is shown in *Figure D.5*. The impulse is applied to a 3.36 m rod-rod gap. The current is measured as the potential across the series shunt resistor. The current waveforms can be broken into three stages:

1. **Period prior to the impulse generator firing through to approximately** 10 µs**.**
   What is seen to be clipped noise is associated with the spark gaps on the impulse generator firing. For different front times the duration of this noise varies however consistently exceeds the magnitude of any current measured there after, excluding the breakdown current. This period is marked in *Figure D.5b* as "Imp Gen Noise".

2. **Period during which the voltage rises up until the peak is reached or breakdown occurs.**
   Bursts or current impulses are seen during this phase and is consistent in both withstand and breakdown events. *Figure D.4* shows a high speed photograph of the discharge activity occurring in the gap during the first 50 µs of voltage rise. A number of developed leader channels are seen to have formed. It is not possible to associate the leader channel developement with the current waveform as no time line exists for the photograph exists. The exposure period of the high speed camera is labelled in *Figure D.5a*.

3. **Period during which the current ramps up preceding the collapse of the voltage and breakdown occurring.**
   This period is only associated with breakdown events. The point at which the final jump occurs can be clearly seen on the breakdown current waveform. The current begins to rise steadily at approximately 60 µs. This is associated with the streamers preceding the leader channel reaching the ground electrode. The rise in the measured current causes the voltage waveform to start collapsing.

   This breakdown current is labelled as "Breakdown Current" in *Figure D.5b*. The current waveform is clipped as the current magnitude exceeds the range of the oscilloscope used to make the measurements. The current measurement this period is not of importance given the above discussed aims.

The current waveforms both show the current flow as measured at the ground electrode to occur in bursts rather then as a continued flow as shown by Baldo et al. (1992). It is possible that the current bursts measured at the ground electrodes represent changes in the electric field rather then actual current flow.

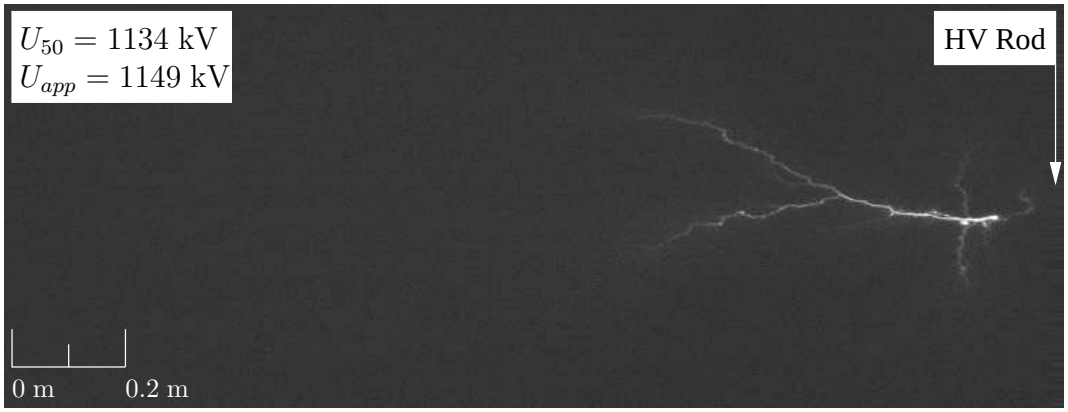


Figure D.4: High speed photograph of a 3.36 m rod-rod gap subjected to an impulse with a front time of 70 μs. An exposure period of 50 μs is used.

D.3.2 Power frequency spectrum analysis

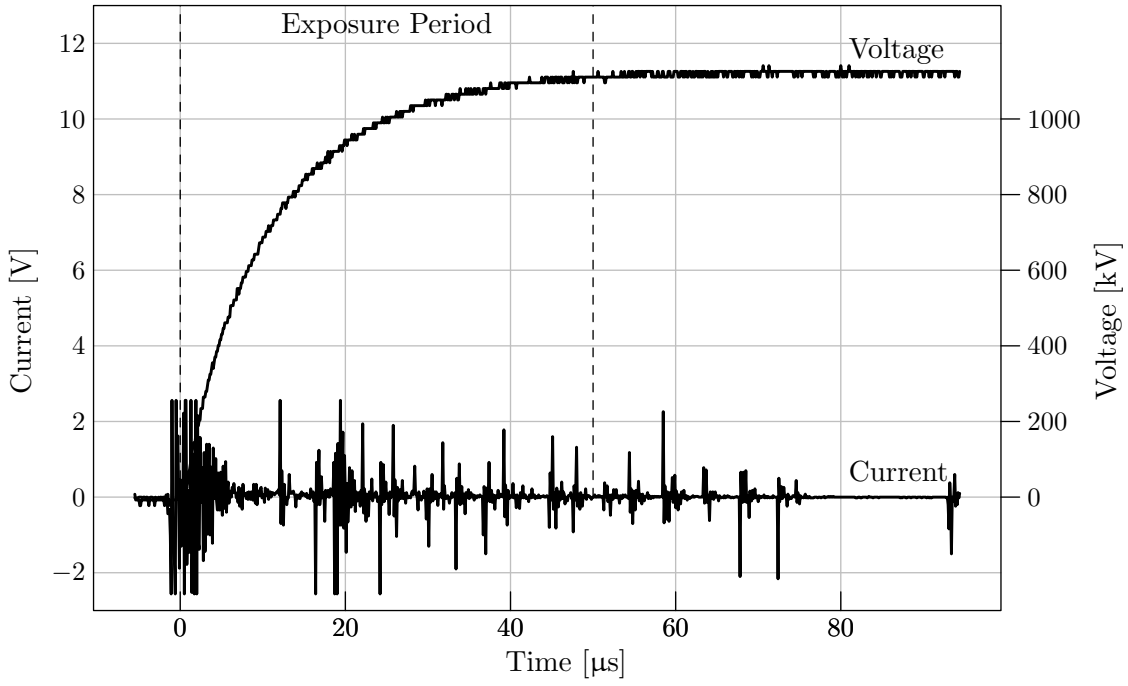
The power frequency spectrum's for each current waveform are calculated. The power frequency spectrum shows the power distribution of the frequency range. The frequency range is dependent on the sampling frequency of the oscilloscope. A sampling frequency of 10 MHz is used.

Both power frequency spectrum's in *Figure D.6* show peaks at approximately 750 kHz and 3.5 MHz. The power frequency spectrum's were calculated with the impulse generator noise included.

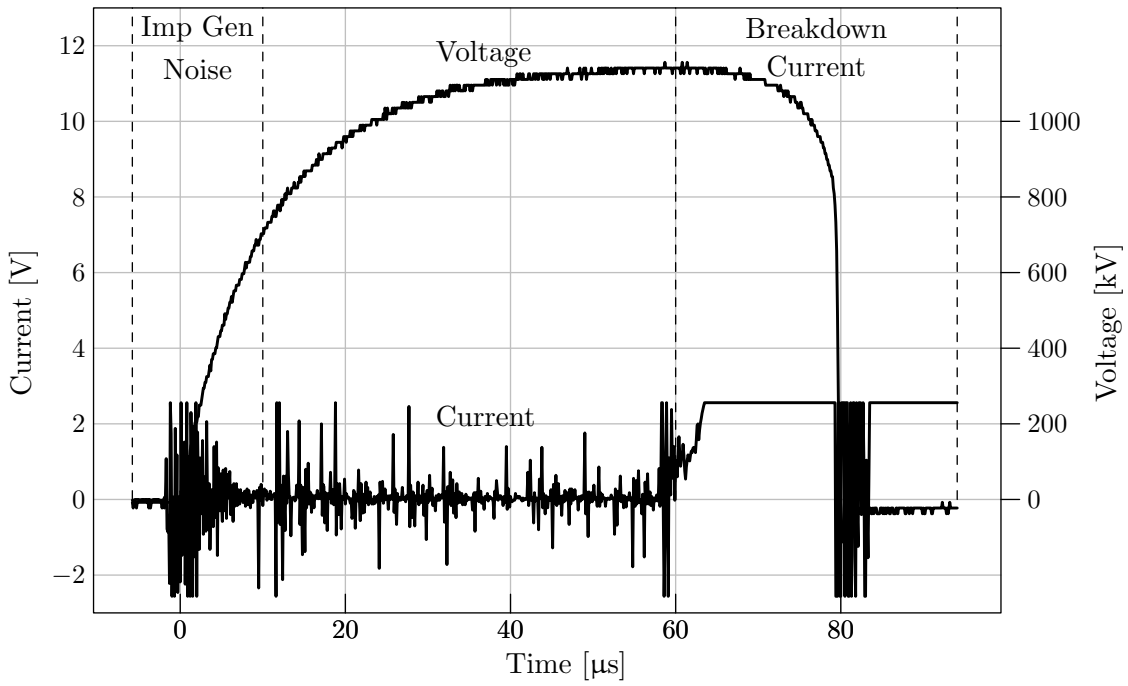
Figure D.7 show the power frequency spectrum's of the current waveforms where the initial noise due to the impulse generator is set to zero.

The power frequency spectrum's for each event in *Figures D.6* and *D.7* have been unitised respectively. The factor used to unitise the plots is given for each event.

A considerable decrease in the magnitudes of across the measured frequency range is seen in *Figure D.7*. The peaks at approximately 750 kHz and 3.5 MHz are still present.

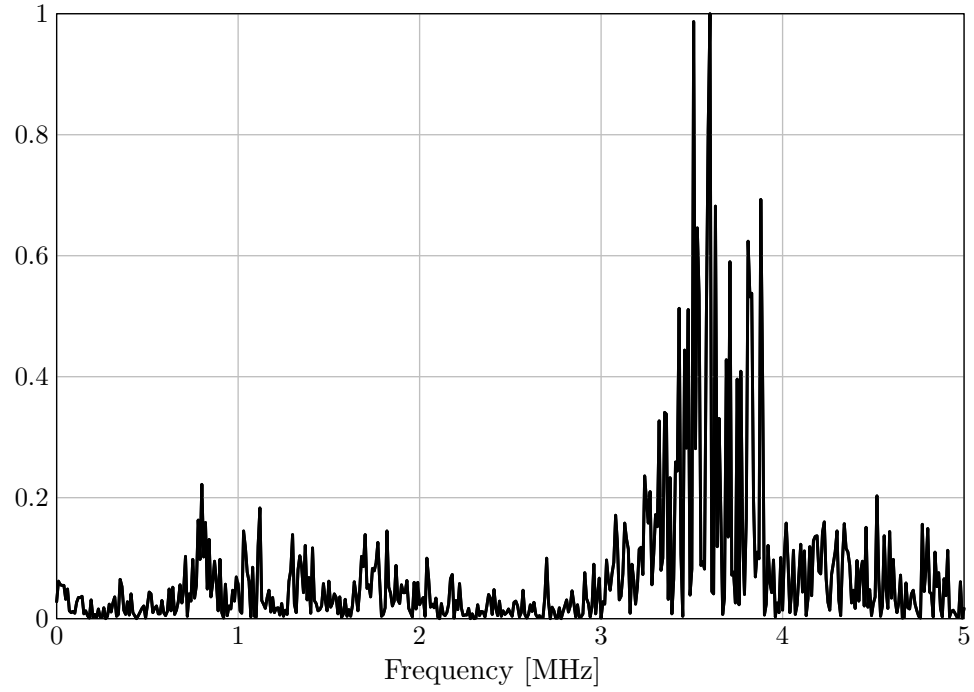


(a) Withstand event.

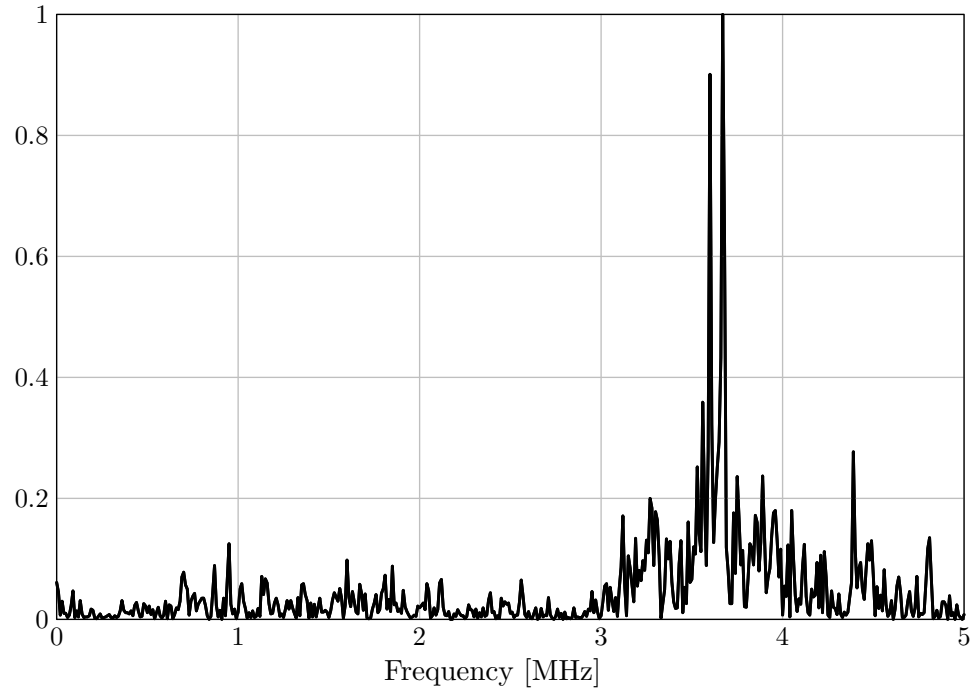


(b) Breakdown event.

Figure D.5: Voltage and current waveforms. The camera's exposure period is marked on the withstand event's graph. **NOTE:** The period of current rise ($60 - y$ µs) on the current breakdown waveform is set to zero to give a more accurate representation of the pre-breakdown currents when calculating the power frequency spectrums (labelled as "Breakdown Current").

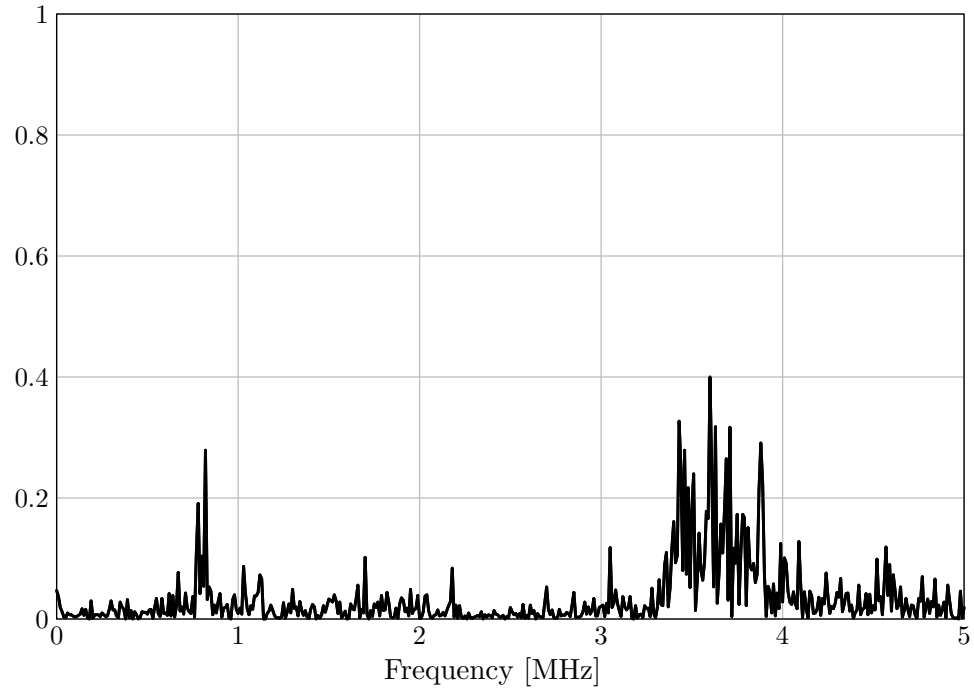


(a) Withstand event (Factor of 3.8045×10^{-6} used for normalising results).

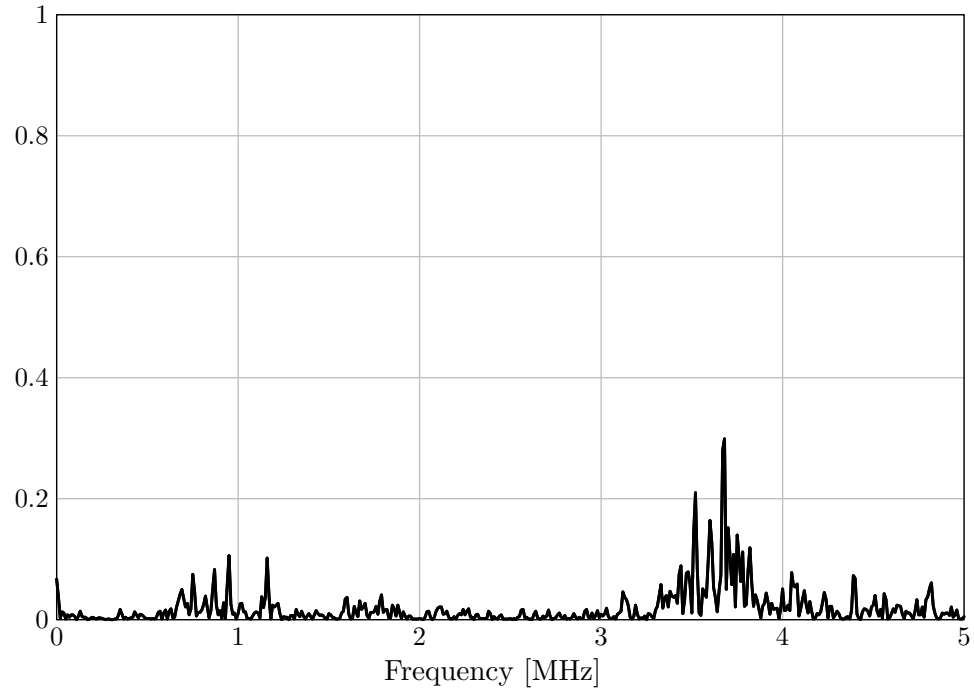


(b) Breakdown event (Factor of 5.7842×10^{-6} used for normalising results).

Figure D.6: Unitised power frequency spectrum including associated noise due to the impulse generator ($x - 10$ µs).



(a) Withstand event (Factor of 3.8045×10^{-6} used for normalising results).



(b) Breakdown event (Factor of 5.7842×10^{-6} used for normalising results).

Figure D.7: Unitised power frequency spectrum, with associated noise due to the impulse generator ($x - 10$ µs) set to zero (labelled "Imp Gen Noise" in *Figure D.5b*.

A markable decrease in the magnitudes of the peaks is seen once the initial noise from the impulse generator is removed. It is possible that the peaks are characteristics of the electromagnetic noise emitted from the currently active spark gaps and not the formation and propagation of the leader channels.

D.4 Associated difficulties and suggested solutions

D.4.1 Resolution and shunt resistor value

It is assumed that the magnitudes of the pre-breakdown currents can range from micro-amperes to an order of tens of amperes. The range of currents to be measured will guide the choice in the size of the shunt resistor used. For small currents in the order of micro and milli amperes a larger shunt resistor is required such that the volt drop across the resistor will be large enough. This ensures that the measured voltage is above the noise level. However the voltage across the resistor is directly proportional to the current flowing through it hence for larger current magnitudes larger voltages would appear across the resistor which can damage the measurement equipment (oscilloscope).

The affect of adding a large shunt resistor between the ground electrode and the ground plane or ground return path needs to be considered. The use of a large shunt resistor can offset or float the ground electrode above ground potential. This is undesirable during testing as it may lead to skewed results. The same is true for inconsistent bonding between the ground electrode and the ground return path.

A trade off between the resolution of the current measurement and the validity of the test results is necessary. It is therefore suggested that value of the shunt resistor should not exceed twice the total series resistance as measured from the ground electrode to the ground return path.

D.4.2 Coupled noise

The primary source of coupled noise in the measurement circuit was due to the firing of the spark gaps in the impulse generator. When an impulse generator is triggered the bottom spark gap is fired this in turn radiates the spark gap above it hence causing it to fire. A chain reaction occurs as each successive spark gap is fired. The

arc created across the spark gap remains active as the charge is drained from the capacitors.

This process emits large amounts of electro-magnetic radiation that induces a voltage on surrounding metallic objects. This electromagnetic radiation is incident on the coaxial cable that connects the shunt resistor to the oscilloscope. However the noise contribution from the coaxial cable is not high, as the surface area of the coaxial cable is small and runs away from the impulse generator.

The dominant cause of coupled noise in the measurement system is due to the ground electrode and shunt resistor combination. The ground electrode acts as an antenna with a large surface area. In addition the ground electrode and shunt resistor are located close to the impulse generator.

The noise seen in the initial $5 - 20$ µs of the oscillograms shown in the previous section is attributed to the impulse generator firing. The following is suggested in attempting to decrease coupled noise to the measurement circuit.

- Replace the coaxial cable with a fibre optic link. The fibre optic sender and receiver units will need to be adequately shielded.
- Shield the impulse generator from the test object using a ground plane. This typically is an impractical solution. However with the spark gaps of the impulse generator used are house in a cylinder which could be shielded on the outside.
- Move the test object further away from the impulse generator. Moving the test object further away will decrease the magnitudes of the electro-magnetic radiation as it is inversely proportional to the distance squared.
- Attempt to characterise the noise fingerprint of the spark gaps. Using Fourier analysis the dominant frequency components can be identified allowing for a filter to be applied to the measured waveforms. However due to the statistical nature of the spark gaps firing this may prove difficult to identify an exact fingerprint. Furthermore the noise footprint of the impulse generator also is dependent on the set front time.

D.5 Conclusion

The use of a shunt resistor in the ground return path allowed for current waveforms to be measured during both withstand and breakdown events. The analysis of the

current waveforms in the time domain and the frequency domain resulted in two possible conclusions respectively:

- The current waveform obtained represents a change in current flow with in the gap. Integrating the current waveform results in a continuous waveform consistent with those presented by Baldo et al. (1992).
- The frequency analysis of the current waveforms show two peaks occurring at 750 kHz and 3.5 MHz. On removal of the initial generator noise the magnitudes of the peaks were decrease substantially. The resulting peaks are possibly due to the electro-magnetic radiation emitted by the active spark gaps.

For this reason the current measurement is considered inconclusive. While the current measurements were not the focus of the presented work, future work should be aimed at reducing the noise and obtaining reliable measurements.

Appendix E

Published Paper

A paper on the work presented in the dissertation is included. The paper was presented at the 15^{th} International Symposium on High Voltage Engineering.

Flashover Performance of a Rod-rod Gap Containing a Floating Rod under Switching Surges with Critical and near Critical Times to Crest

R.A Viljoen[1*], J.P Reynders[1] and K.J Nixon[1]
[1]School of Electrical & Information Engineering, University of the Witwatersrand, Jhb, Private Bag 3, Wits, 2050, South Africa
*Email: r.viljoen@ee.wits.ac.za

Abstract: The U-curves of a 3.36 m rod-rod gap with a floating object positioned at three different positions are presented. The characteristics of the U-curves are discussed with reference to the breakdown process. Photographic evidence from high speed photography is used to support the conclusions drawn from these results. Parallels are drawn between the results, the photographs and Rizk's model for predicting the flashover voltage of a gap with a floating object present.

1 INTRODUCTION

The effect of a floating object present in a rod-rod gap is well known [1]-[3]. Furthermore, a model for determining the flashover voltage of a gap with a floating object present in the gap exists [3].

This paper discusses the breakdown mechanisms and process in light of Rizk's models for leader inception voltage and predicting the flashover voltage of an air-gap with a floating object suspended along the gap axis [3]-[5]. The work presented is unique in that the photographs obtained support the results and the model. The photographs also confirm the validity of some of the assumptions made in Rizk's model [3].

2 EXPERIMENTAL SETUP

2.1. Test Facility and Layout

The testing was conducted at the SABS-NETFA High Voltage Test Facility in the indoor laboratory. The laboratory is situated at an altitude of 1539 m above sea level. The indoor test facility is a closed system because of this, atmospheric conditions throughout the testing can be considered substantially constant. The lighting conditions within the laboratory can be controlled.

The location of the impulse generator, capacitive voltage divider, test object and camera with respect to the control room is shown in Fig. 1.

2.2. Test Object

A 3 m rod suspended via a composite insulator from a service crane forms the high voltage electrode. The ground electrode consisted of a 0.5 m rod positioned on a wooden table so as to isolate it from the ground plane. The electrode was then connected via a shunt resistor to the impulse generator's earth return path. As seen in Fig. 2.

The rod floating object was suspended along the gap axis via three diagonal guy lines attached just above the midway point of the rod. Polyethylene ropes with a 3 mm diameter were used. The floating object is positioned at three different positions along the gap. Tab. 1 lists all the lengths of the electrode dimensions. All electrodes were fitted with spherical caps to avoid any sharp edges and hence areas of higher electric field stress.

The test objects are as follows, noting that the high voltage electrode is used as reference (see Fig. 2):

- 3.36 m rod-rod gap.
- 2.6 m rod-rod gap.
- 3.36 m rod-rod gap with floating object at 25% along the gap axis (d_1 = 430 mm).
- 3.36 m rod-rod gap with floating object at 50% along the gap axis (d_1 = 1265 mm).
- 3.36 m rod-rod gap with floating object at 75% along the gap axis (d_1 = 2100 mm).

The 2.6 m rod-rod gap represents the equivalent length of the airgap when the floating object is present.

Tab. 1: Test setup parameters seen in Fig. 2.

Parameter	Description	Size [mm]
h	Length of ground electrode	500
h_g	Height above ground plane	430
l	Length of high voltage electrode	3000
d_0	Length of floating rod electrode	810
d_1	Length of primary gap	Varied
d_2	Length of secondary gap	$f(l,d_0,d_1)$
r_A	Radius of high voltage electrode	50
r_B	Radius of floating rode electrode	35
r_C	Radius of ground electrode	45

2.3. High Speed Camera

A high speed camera manufactured by *Cooke* was used to photograph any discharge or channel formation in the air gap during an applied impulse. The camera has the following specifications:

- Shutter speed range from 1 µs to 1 ms.
- 8-bit resolution.
- 752 by 286 pixel image size.
- Adjustable gain setting.
- Triggered by TTL falling edge.
- Binary or PNG output.

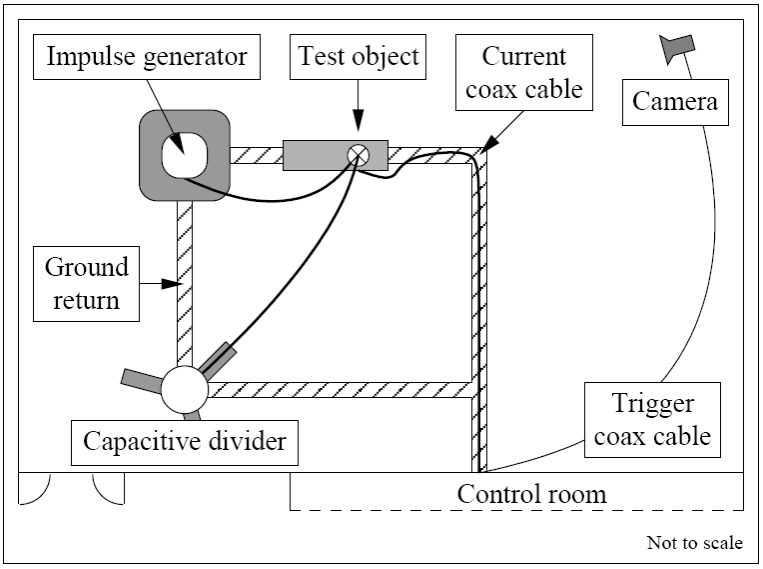


Fig. 1: Plan view of the experimental layout of indoor test facility.

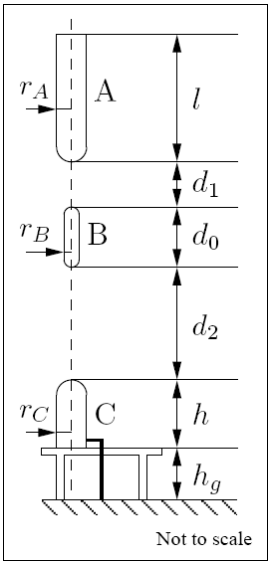


Fig. 2: Test setup
A – High voltage electrode
B – Floating object
C – Ground electrode

The field of view of the camera is approximately 1.9 m by 0.75 m in size, capturing roughly half of the test object. The location of the camera with respect to the test object and the control room is shown in Fig. 1. The camera is placed as far away from the test object as possible in order to maximize the field of view.

2.4. Triggering of Camera

A 5-stage 2.1 nF per stage, capacitor voltage divider was used to make the voltage measurements. The divider was connected to a TDA544 Tektronics Digital Storage oscilloscope via a 75 Ω coaxial cable, terminated in 75 Ω, run through cable ducts below the ground plane. The oscilloscope was set to trigger on the rising edge of the voltage waveform.

A 50 Ω coaxial cable was run from the control room to the camera. The camera is triggered by the falling edge from a TTL signal output by the oscilloscope.

3 APPROACH TAKEN

The U-curve for each test object is characterised using a selection of impulses with front times ranging from 20-200 µs. A 30-shot up-down test (U_{50} test) is completed for each waveshape and the U_{50} flashover voltage calculated. The tail time is kept constant for all waveshapes.

The high speed photographs were taken while completing the U_{50}.

3.1. Atmospheric Parameters

The atmospheric conditions were recorded during each test, however no correction factors have been applied to the results presented. The range of each parameter is listed in Tab. 2. Atmospheric correction factors cannot be successfully applied to the measured results as both streamer and leader mechanisms are present in the complete breakdown of the gap, in the presence of a floating object. Each mechanism behaves differently as atmospheric conditions change and, since the mechanisms are not fully quantified, adjustment was not attempted..

Tab. 2: Range of atmospheric conditions recorded during testing.

Parameter	Max	Min	Average	Std Dev
Temperature [ºC]	19.0	11.0	14.3	2.0%
Pressure [kPa]	86.2	84.3	85.5	0.4%
Humidity [%]	14	34	27.7	6.3%

4 RESULTS

The U-curves are plotted in Fig. 3, and the critical flashover (CFO) voltage and critical time to crest (T_{CRIT}) are listed in Tab. 3 for each test object. The results in Tab. 3 show that the CFO voltage did not always coincide with the critical time to crest, as might be expected. The corresponding time to crest (T_{C1}, T_{C2}) at which each critical time to crest and CFO occurs, respectively, are listed.

Tab. 3: Summary of critical times to crest (T_{CRIT}) and corresponding front time (T_{C1}) and CFO and corresponding front time (T_{C2}) for each test object.

Test Object	T_{C1} [µs]	T_{CRIT} [µs]	T_{C2} [µs]	CFO [kV]
3.36 m rod-rod	120	124	140	1032
2.6 m rod-rod	70	70	120	903
25% from HV	42	45	42	800
50% from HV	72	79	57	814
75% from HV	70	66	70	983

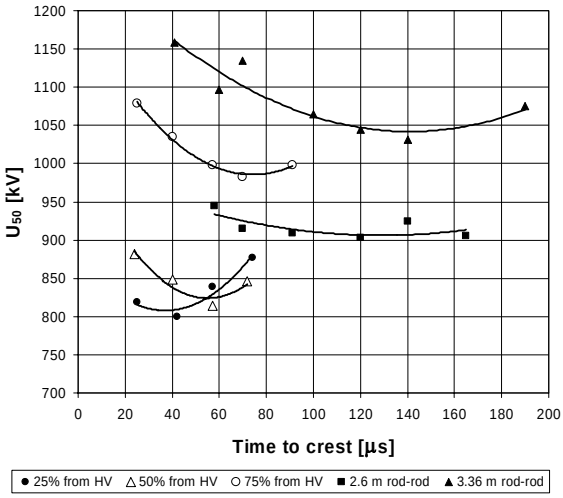


Fig. 3: U-curves plotted for each test object.

An overview of the test results:

- Test objects with the floating object along the gap show shorter critical times to crest than that of both the rod-rod test objects.
- The 3.36 m rod-rod gap resulted in the highest CFO voltage in comparison to the other test objects.
- The test object with the floating object positioned at the 25% position results in the lowest flashover voltage.
- The test object with floating object positioned at the 50% position had a similarly low flashover voltage.
- In contrast, for the floating object at the 75% position the CFO rises well above that of the 2.6m rod-rod gap.

The last bullet is of interest as the 2.6 m rod-rod gap resulted in a lower flashover voltage compared to that of the floating object positioned at 75% in the gap.

For both the 2.6 m gap and the 75% floating object position breakdown will be by leader. Initiation and early propagation of the leader channel will not be substantially affected by the remote floating object but more by the total gap length and hence the breakdown of the 75% position is expected to be higher than for the same total air gap without the floating object.

The lower critical time to crest for the 75% position can be explained due to the presence of the streamer mechanism in the secondary gap (d_2). The streamer mechanism propagates at roughly the drift velocity of electrons (~10^5 m/s), which is much greater than the propagation rate of a leader [6]. The streamer mechanism will be present in the secondary gap due to the short gap length (430 mm) and the potential of the floating object is very high.

In addition it is seen that discharges can exist simultaneously in both gaps. This is shown photographically in the next section and is also suggested by Rizk [3]. The potential of the floating object will rise as the leader channel approaches. At the point at which the potential of the floating object reaches the streamer inception voltage the secondary gap will begin to break down under the streamer mechanism. This may or may not occur before the primary gap is bridged by the leader channel [3].

The 25% and 50% positions show very similar characteristics in that their CFOs are almost identical and both exhibit very short critical times to crest (T_{C2}). In contrast the 75% position has a substantially higher CFO and a longer critical time to crest (T_{C2}).

The shorter critical time to crest (T_{C2}) and lower CFOs suggests that the streamer mechanism dominates breakdown in the 25% and 50% positions whereas the leader mechanism dominates in the 75% position.

This can be explained for the 25% test object since the short primary gap breaks down under the streamer mechanism. Once the primary gap is bridged, the effective applied voltage minus the volt drop across the channel appears at the bottom of the floating object [3]. This results in an effective shorter rod-rod gap. Given the length of the secondary gap, it will breakdown under the leader mechanism but will require a lower leader inception voltage due to it being shorter than the total gap.

The comments above are conceptually based on Rizk's model for breakdown in an air gap containing floating objects [6]. The work presented in this paper was conducted at altitude (reduced air density) and provides a platform from which the influence of air density on leader and streamer breakdown in long gaps can be investigated.

5 HIGH SPEED PHOTOGRAPHY

The high speed photographs presented have been post-processed to enhance any discharge activity. All the photographs presented were captured during unique withstands. The applied impulse front time and magnitude are recorded and listed along with the exposure time used for the relevant test object.

Fig. 4 – 25% Test object

Simultaneous discharges are seen in both the primary and secondary gap. The applied impulse front time of 57 µs is near the critical time to crest. An exposure time of 25 µs is used. As the voltage continues to increase each discharge channel will propagate further in the respective gaps.

The air in the primary gap has begun to ionise due to the high electric field. This effective ionisation "channel" has an approximate radius of 75 mm. A discharge channel has also formed and started propagating down this cylindrical zone of ionisation. Smaller discharges can also be seen on the tip of the high voltage electrode.

Fig. 5 – 25% Test Object

This photograph is similar to that of Fig. 4 however a longer exposure time is used. The primary gap is now bridged. The direct nature of the channel and the length of the primary gap (430 mm) suggest that the primary channel breaks down under the streamer mechanism.

Fig. 6 – 50% Test object

A dominant discharge channel can be seen propagating through the primary gap.

A leader channel requires a rising potential at its origin to maintain a near constant voltage at the tip of the leader channel so as to propagate [4],[5]. A streamer channel requires an electric field above that of the critical streamer electric field usually assumed to be 400 kV/m. Due to this it is assumed that what is seen is the extent of discharge activity within the gap as the applied impulse front time is the same as the exposure time and hence the applied impulse voltage begins to decrease.

Fig. 7 – 50% Test object

The enhanced photograph shows greater detail of what is occurring in the gap compared to that of Fig. 6. The enhanced photograph shows the air has started ionising but not to the same extent as seen in Fig. 4. This is due to the weaker electric field that exists between the high voltage electrode and the floating object. The effective radius of the air ionisation "channel" is approximately 100 mm. The applied voltage at the time will also affect the extent of the ionisation. There is also evidence of discharges, or corona, off the tip of the floating object seen by the concentrated area preceding the tip. The polarity of which is assumed to be negative due to the capacitive coupling between the floating object and the high voltage electrode. A positive approaching discharge induces a negative charge on the top tip of the floating object.

Fig. 8 – 75% Test object

This photograph is interesting in that there are a number of faint filaments originating from the HV electrode and no clearly dominant discharge channel extending into the gap. These filaments are short lived, based on their brightness. Furthermore it can be assumed that that is the extent of the discharge within the gap as the applied impulse front time is the same as the exposure time. The nature of the discharge can be explained by observing the final U_{50} flashover voltage (1079kV) and comparing it to the applied voltage (949 kV).

A longer dominant discharge channel is seen to propagate into the gap for impulses with magnitudes equal to or exceeding that of the U_{50} flashover voltage, during a withstand event.

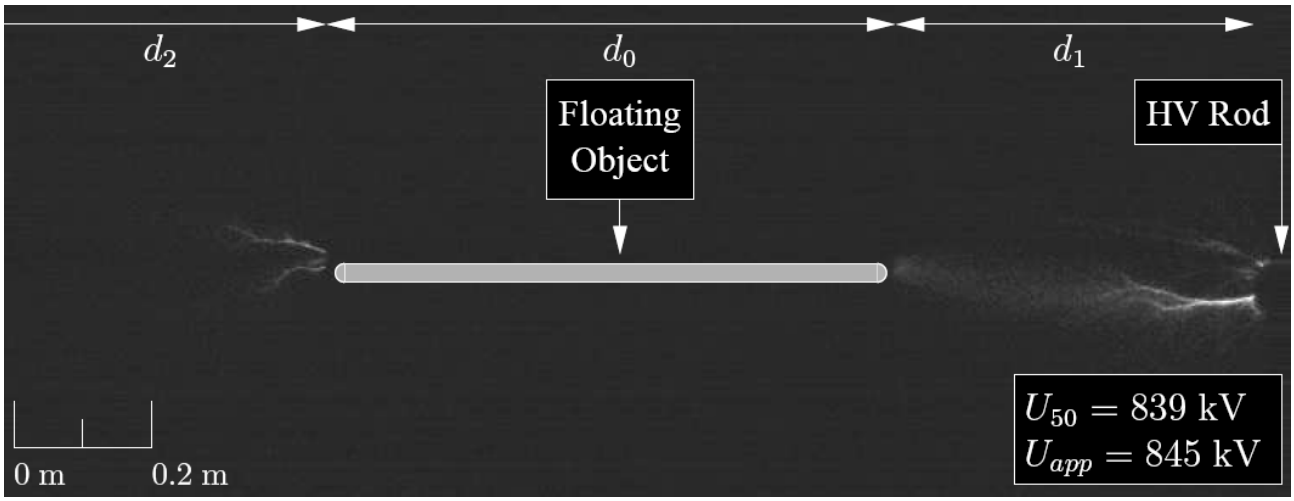


Fig. 4: High speed photograph of discharge occurring in the gap with the floating object at 25% from HV electrode resulting from a 57 µs applied impulse and 25 µs exposure time. For convenience, the location of the floating object has been indicated in this and subsequent figures by digitally superimposing an approximate representation of the object.

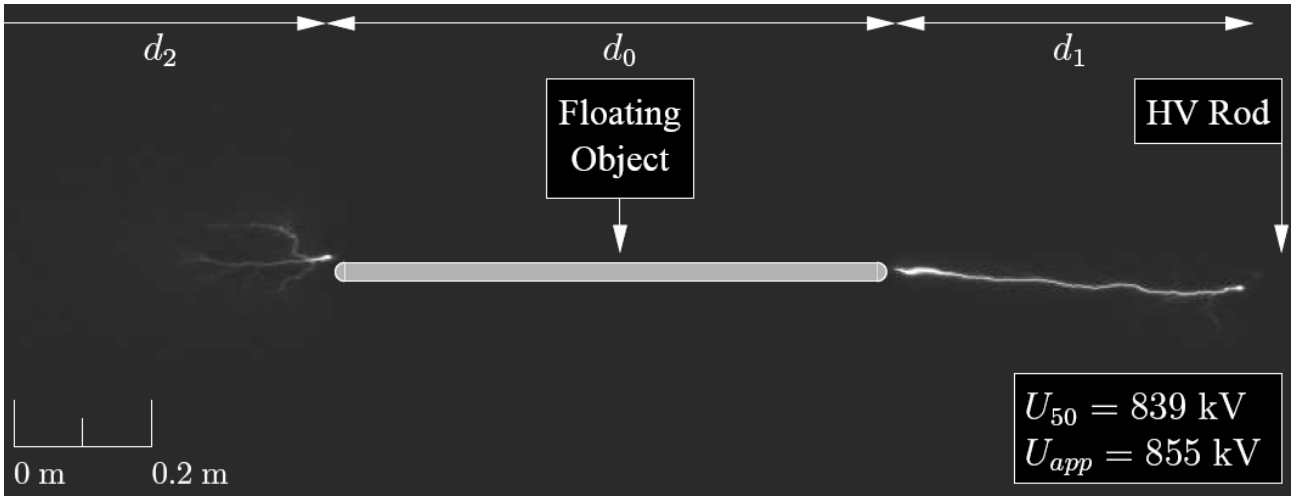


Fig. 5: High speed photograph of discharge occurring in the gap with the floating object at 25% from HV electrode resulting from a 57 μs applied impulse and 40 μs exposure time. The primary gap has been bridged.

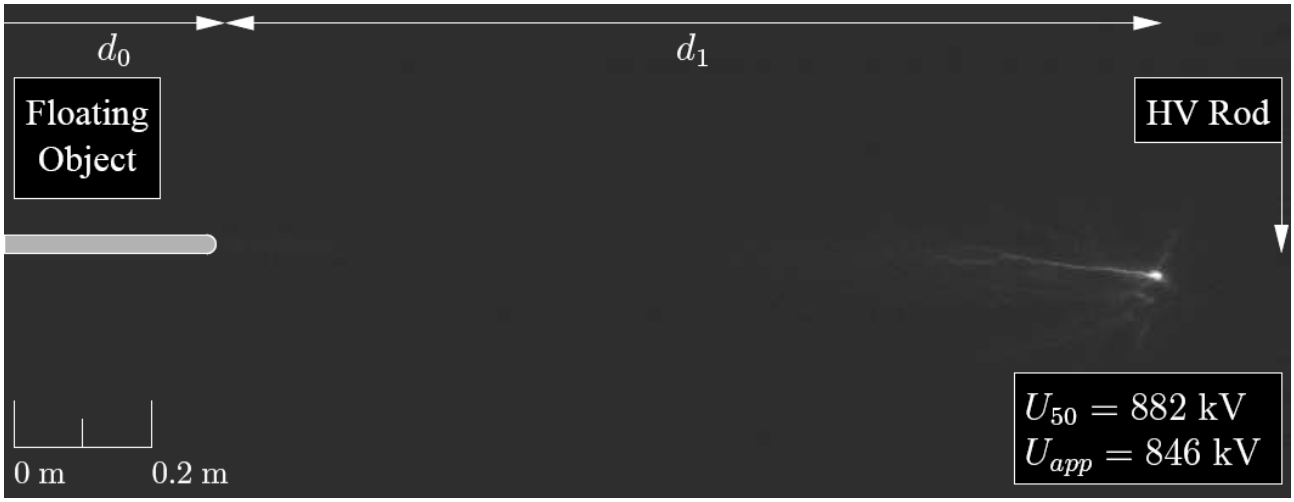


Fig. 6: High speed photograph of discharge occurring in the gap with the floating object at 50% from HV electrode resulting from a 25 μs applied impulse and 50 μs exposure time.

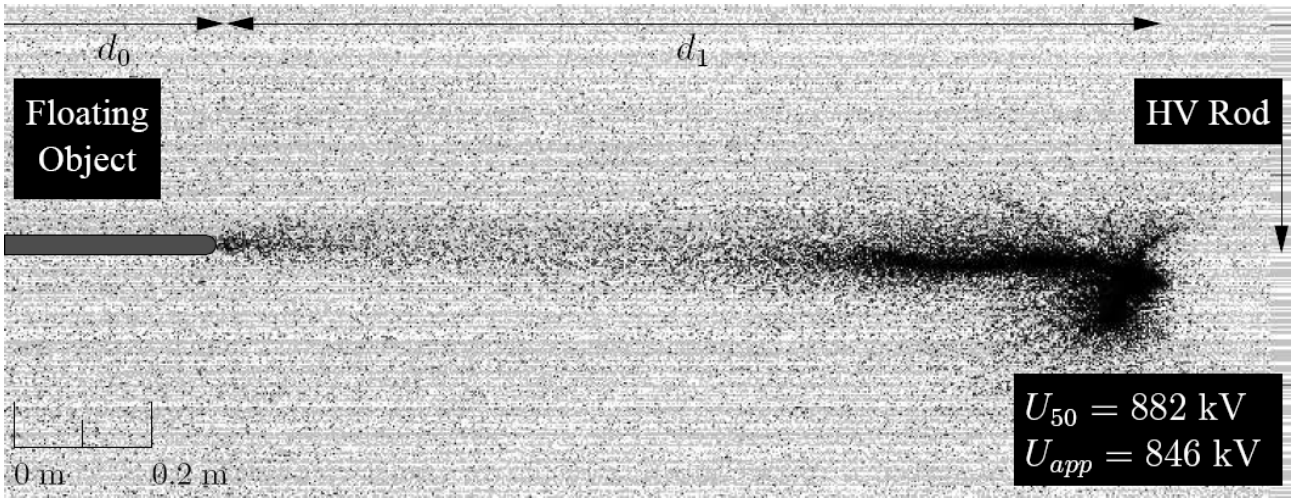


Fig. 7: Enhanced photograph of Fig. 6 show the air ionising between the floating object at 50% from the HV electrode and the HV electrode.

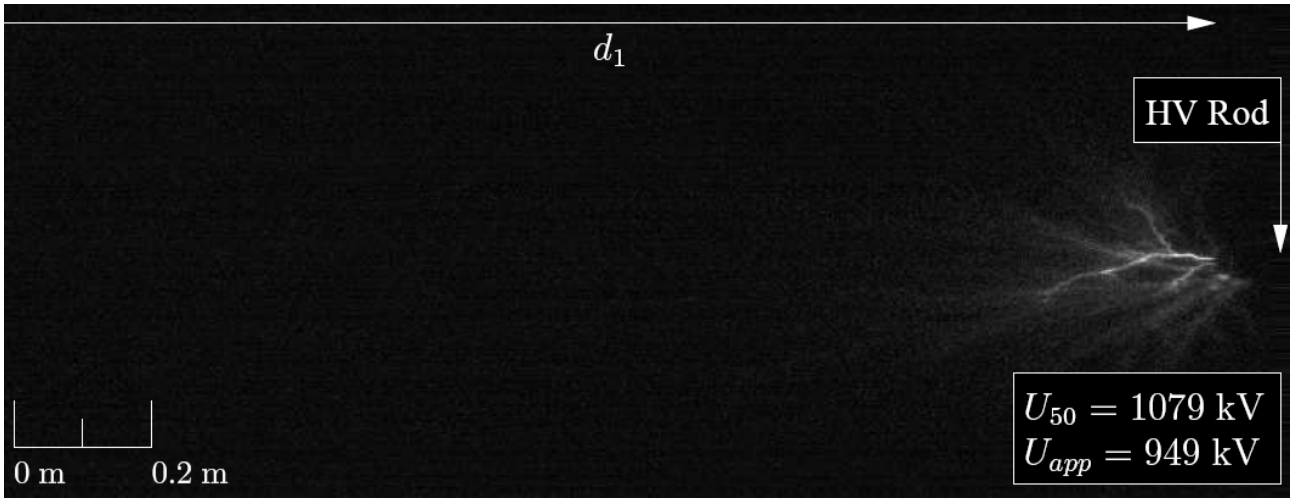


Fig. 8: High speed photograph of discharge occurring in the gap with the floating object at 75% from HV electrode resulting from a 25 µs applied impulse and 25 µs exposure time. The floating object is not visible in the photograph.

6 CONCLUSION

1. In long air gaps with floating objects both streamer and leader mechanisms may be present. When the floating object is on the high voltage side of the gap streamer breakdown will be present in the primary gap and leader in the secondary gap. When the floating object is close to earth potential, leader is present in the primary gap and streamer in the secondary gap.

2. The presence of streamer breakdown reduces the critical time to crest (T_{C2}). This means that T_{C2} for a gap with an object floating will be shorter than T_{C2} in a single air gap of equivalent air gap length.

3. The initiation and early propagation of a leader is largely dependent on the total gap length, particularly when the floating object is positioned close to the earth electrode. For this reason the breakdown voltage for a gap with a floating object in the vicinity of the earth is significantly greater than the breakdown voltage of an equivalent air gap without a floating object.

7 ACKNOWLEDGMENT

The authors would like to thank Eskom for their support of the High Voltage Engineering Research Group through TESP. They would also like to thank the Department of Trade and Industry (DTI) for THRIP funding and to the National Research Foundation (NRF) for direct funding of the research group. Furthermore, thanks are extended to SABS-NEFTA High Voltage Test Laboratory for their assistance during the testing.

8 REFERENCES

[1] B. Hutzler, “Switching impulse strength of air gaps containing a metallic body at floating potential”, in *Proc.* of *5th International Symposium on High Voltage Engineering, pp. 11.1.*

[2] G. Baldo, “Floating potential bodies and their interaction with discharge development*”, in Proc. of 6th International Symposium on High Voltage Engineering*, pp. 13–30.

[3] F. A. M. Rizk, "Effect of conducting objects on critical switching impulse breakdown of long air gaps", *CIGRE*, pp. 33-301, 1994.

[4] F. A. M. Rizk, “A model for switching impulse leader inception and breakdown of long air gaps”, *IEEE Transactions on Power Delivery*, vol. 4, no. 1, pp. 596–606.

[5] F. A. M. Rizk, ‘Switching impulse strength of air insulation: Leader inception criterion’, *IEEE Transactions on Power Delivery*, vol. 4, no. 4, pp. 2187–2195.

[6] G. Carrara and L. Thione. “Switching Surge Strength of Large Air Gaps: A Physical Approach”, *IEEE Transactions on Power Apparatus and Systems*, vol. PAS-96, no. 2, pp. 512–524, Jan 1976.

References

Baldo, G. (1989), 'Floating potential bodies and their interaction with discharge development', *6th International Symposium on High Voltage Engineering*, pp. 13–30.

Baldo, G., Hutzler, B., Pigini, A. & Rizk, F. A. M. (1992), *Guidelines for the Evaluation of the Dielectric Strength of External Insulation*, CIGRE SC 33 WG 07, chapter Fundamentals of the discharge mechanics and description of the phenomena by physical-mathematical models.

Carrara, G. & Thione, L. (1976), 'Switching surge strength of large air gaps: A physical approach', *IEEE Transactions on Power Apparatus and Systems*, vol. PAS-96, no. 2, pp. 512–524.

Gallimberti, I. (1979), 'The mechanism of the long spark formation', *Journal de Physique*, vol. 40, no. 7, pp. C7–193–C7–250.

Hochrainer, A. (1970), 'Einige bemerkungen zum stromnulldurchgang in wechselstromschaltern', *EuM*, vol. 87, no. 1, pp. 15–19.

Hutzler, B. (1987), 'Switching impulse strength of air gaps containing a metallic body at floating potential', *5th International Symposium on High Voltage Engineering*, pp. 11–11.

IEC 60060–1 (1989), 'High-voltage test techniques. Part 1: General definitions and test requirements', IEC, Geneva.

Jones, B. (1973), 'Switching surges and air insulation', *Phil. Trans. R. Soc. Lond.*, pp. 165–180.

Rizk, F. A. M. (1989*a*), 'A model for switching impulse leader inception and breakdown of long air gaps', *IEEE Transactions on Power Delivery*, vol. 4, no. 1, pp. 596–606.

Rizk, F. A. M. (1989*b*), 'Switching impulse strength of air insulation: Leader inception criterion', *IEEE Transactions on Power Delivery*, vol. 4, no. 4, pp. 2187–2195.

Rizk, F. A. M. (1994), 'Effect of conducting objects on critical switching impulse breakdown of long air gaps', *CIGRE*, pp. 33–301.

Bibliography

Akyuz, M., Gao, L. & Cooray, V. (2001), 'Streamer current in a three-electrode system', *IEEE Transactions on Dielectrics and Electrical Insulation*, vol. 8, no. 4, pp. 665–672.

Baldo, G. (1989), 'Floating potential bodies and their interaction with discharge development', *6th International Symposium on High Voltage Engineering*, pp. 13–30.

Baldo, G., Gallimberti, I., Garcia, H. N., Hutzler, B., Jouaire, J. & Simon, M. F. (1975), 'Breakdown phenomena of long air gaps under switching impulse conditions influence of distance and voltage level', *IEEE Transactions on Power Apparatus and Systems*, vol. PAS-94, no. 4, pp. 1131–1140.

Baldo, G., Hutzler, B., Pigini, A. & Rizk, F. A. M. (1992), *Guidelines for the Evaluation of the Dielectric Strength of External Insulation*, CIGRE SC 33 WG 07, chapter Fundamentals of the discharge mechanics and description of the phenomena by physical-mathematical models.

Bogdanov, O. V., Dikoj, V. P., Krylov, S. V., Ovsjannikov, A. G., Polevoj, S. V. & Timashova, L. V. (1994), 'Dielectric strength of external insulation and air gaps under live line working on EHV and UHV transmission lines', *CIGRE*, pp. 33–303.

Carrara, G. & Thione, L. (1976), 'Switching surge strength of large air gaps: A physical approach', *IEEE Transactions on Power Apparatus and Systems*, vol. PAS-96, no. 2, pp. 512–524.

CIGRE SC 33 WG 33.07 (2000), 'Guidelines for insulation coordination in live working', Section C4 - System Technical Performance.

CIGRE Task Force 33.07.02 (1990), 'Strength of external insulation during live line maintenance and repair work with special reference to transient overvoltages', *Electra No. 129*, pp. 108–131.

Gallet, G., Leroy, G., Lacey, R. & Kromer, I. (1975), 'General expression for positive switching impulse strength valid up to extra long air gaps', *IEEE Transactions on Power Apparatus and Systems*, vol. PAS-94, no. 6, pp. 1989–1993.

Gallimberti, I. (1979), 'The mechanism of the long spark formation', *Journal de Physique*, vol. 40, no. 7, pp. C7–193–C7–250.

Gao, L., Akyuz, M., Larsson, A., Cooray, V. & Scuka, V. (1999), 'Measurement of the positive streamer charge', *11th International Symposium on High Voltage Engineering*, vol. 3, pp. 35–38.

Gao, L., Cooray, V., Thottappillil, R. & Scuka, V. (1997), 'Study of cathode-directed positive streamers in air by streamer current and luminosity measurements', *IEEE Conference on Electrical Insulation and Dielectric Phenomena*, vol. 2, no. 19-22, pp. 587–590.

Geldenhuys, H. (1986), Positive streamer voltage gradient as function of atmospheric parameters, Master's dissertation, University of Pretoria.

Hochrainer, A. (1970), 'Einige bemerkungen zum stromnulldurchgang in wechselstromschaltern', *EuM*, vol. 87, no. 1, pp. 15–19.

Hutzler, B. (1987), 'Switching impulse strength of air gaps containing a metallic body at floating potential', *5th International Symposium on High Voltage Engineering*, pp. 11–11.

IEC 60060–1 (1989), 'High-voltage test techniques. Part 1: General definitions and test requirements', IEC, Geneva.

Jones, B. (1973), 'Switching surges and air insulation', *Phil. Trans. R. Soc. Lond.*, pp. 165–180.

Knutson, S. R., Abdalla, M. D. & Pixton, R. M. (1991), 'PC-Based electrostatic field calculation techniques', *12th Annual Ideas in Science and Electronics Symposium*, pp. 166–171.

Kuffel, E., Kuffel, J. & Zaengl, W. S. (2000), *High Voltage Engineering Fundamentals*, Newnes.

Landy, R. (2002), Boundary element method analysis of water droplet initiated corona on high voltage cap and pin insulator strings., Master's dissertation, University of the Witwatersrand, School of Electrical and Information Engineering.

Malik, N. H. (1989), 'A review of the charge simulation method and its applications', *IEEE Transactions on Electrical Insulation*, vol. 24, no. 1, pp. 3–20.

Marrone, G., Garbagnati, E., Valagussa, C., Perin, D., Ricca, M. & Bonzano, E. (1994), 'Investigation on the dielectric strength of damaged insulator strings of HV overhead lines during repair operations by live working', *CIGRE*, pp. 33–305.

Marshall, E. (2005), *The Fundamentals and Practice of Overhead Line Maintainence*, Crown Publications, chapter 4 - Live Maintainence as Applied to Overhead Lines.

Menemenlis, C. & Harbec, G. (1975), 'Particularities of air insulation behavior', *IEEE Transactions on Power Apparatus and Systems*, vol. PAS-94, no. 6, pp. 1814–1821.

Nielsen, S. D. (2001), A Study of Pre-Breakdown Discharge Activity in SF6 Under Impulse Conditions and the Implications for Partial Discharge Measurements, PhD thesis, University of the Witwatersrand.

Niemeyer, L., Ullrich, L. & Wiegart, N. (1989), 'The mechanism of leader breakdown in electronegative gases', *IEEE Transactions on Electrical Insulation*, vol. 24, no. 2, pp. 309–324.

Pigini, A., Rizzi, G., Garbagnati, E., Porrino, A. & Pesavento, G. (1989), 'Performance of large air gaps under lightning overvoltages: Experimental study and analysis of accuracy of predetermination methods', *IEEE Transactions on Power Delivery*, vol. 4, no. 2, pp. 1379–1391.

Rizk, F. A. M. (1989*a*), 'A model for switching impulse leader inception and breakdown of long air gaps', *IEEE Transactions on Power Delivery*, vol. 4, no. 1, pp. 596–606.

Rizk, F. A. M. (1989*b*), 'Switching impulse strength of air insulation: Leader inception criterion', *IEEE Transactions on Power Delivery*, vol. 4, no. 4, pp. 2187–2195.

Rizk, F. A. M. (1992), 'Critical switching impulse strength of long air gaps: Modelling of air density effects', *IEEE Transactions on Power Delivery*, vol. 7, no. 3, pp. 1507–1515.

Rizk, F. A. M. (1993), 'Critical switching impulse strength of phase-to-phase air insulation', *IEEE Transactions on Power Delivery*, vol. 8, no. 3, pp. 1492–1506.

Rizk, F. A. M. (1994), 'Effect of conducting objects on critical switching impulse breakdown of long air gaps', *CIGRE*, pp. 33–301.

Rizk, F. A. M. (1995), 'Effect of floating conducting objects on critical switching impulse breakdown of air insulation', *IEEE Transactions on Power Delivery*, vol. 10, no. 3, pp. 1360–1370.

Rizk, F. A. M. (1996), 'Critical switching impulse breakdown of long bundle-conductor gaps', *IEEE Transactions on Power Delivery*, vol. 11, no. 1, pp. 373–383.

Sadurski, K. J., Muftic, D. & Burger, A. A. (1995), 'Live-line maintenance on optimised 400kV lines', *International Symposium on High Voltage Engineering*, pp. 2232.

Sadurski, K. J., vd Merwe, C. W. & Muftic, D. (1994), 'Live line maintenance of EHV and UHV transmission lines - factors the dielectric strength at the work site', *CIGRE*, pp. 33–304.

Schneider, H. M. & Turner, F. J. (1975), 'Switching-surge flashover characteristics of long sphere-plane gaps for UHV station design', *IEEE Transactions on Power Apparatus and Systems*, vol. PAS-94, no. 2, pp. 551–560.

Shcherbakov, Y., Lebedev, V. B., Feldman, G. G. & Rakov, V. A. (2006), 'High-speed optical studies of upward leader and return stroke of long sparks', *International Conference on Grounding and Earthing and 2nd International Conference on Lightning Physics and Effects*, pp. 7–12.

Sung, S., Otsubo, M. & Honda, C. (2005), 'ICCD images of lazer induced streamer', *IEEE Transactions on Plasma Science*, vol. 33, no. 2, pp. 478–479.

Vidal, F., Gallimberti, I., Rizk, F. A. M., Johnston, T. W., Bondiou-Clergerie, A., Comtois, D., Kieffer, J., Fontaine, B. L., Mercure, H. P. & Pepin, H. (2002), 'Modeling of the air plasma near the tip of the positive leader', *IEEE Transactions on Plasma Science*, vol. 30, no. 3, pp. 1339–1349.